REGULATION OF ENDOTHELIAL GENE TRANSCRIPTION BY SHEAR STRESS IN A MANNER DEPENDENT ON P47PHOX-BASED NADPH OXIDASES

A Dissertation
Presented to
The Academic Faculty

by

Michelle Christine Sykes

In Partial Fulfillment
of the Requirements for the Degree
Doctor of Philosophy in
Bioengineering

Georgia Institute of Technology
August, 2008

REGULATION OF ENDOTHELIAL GENE TRANSCRIPTION

BY SHEAR STRESS IN A

MANNER DEPENDENT ON P47PHOX-BASED NADPH OXIDASES

Approved by:

Dr. Hanjoong Jo, Advisor
School of Biomedical Engineering
Georgia Institute of Technology

Dr. May Wang
School of Biomedical Engineering
Georgia Institute of Technology

Dr. Kathy Griendling
School of Medicine
Emory University

Dr. Ajit Yoganathan
School of Biomedical Engineering
Georgia Institute of Technology

Dr. David Harrison
School of Medicine
Emory University

Date Approved: □

Whatever you do, work at it with all your heart,

as working for the Lord, not for men…

Colossians 3:23 (NIV)

To My Family and Loved Ones

ACKNOWLEDGEMENTS

I would like to thank my advisor, Dr. Hanjoong Jo, and all of the former and present Jo Lab members without whom this work would not have been accomplished.

TABLE OF CONTENTS

LIST OF TABLES

LIST OF FIGURES

LIST OF SYMBOLS AND ABBREVIATIONS

ALP	alkaline phosphatase
ApoE	apolipoprotein E
BAEC	bovine aortic endothelial cells
DNA	deoxyribonucleic acid
eNOS	endothelial nitric oxide synthase
FBS	fetal bovine serum
FITC	fluorescein isothiocyanate
GC-RMA	GC robust multi-array average
GEDI	Gene Expression Dynamics Inspector
HBSS	Hank's buffered saline solution
HI-FBS	heat inactived FBS
HUVEC	human umbilical vein endothelial cells
ICAM-1	intercellular cell adhesion molecule 1
iMAEC	immortalized murine aortic endothelial cells
iMAE-p47	immortalized murine aortic endothelial cells from p47phox-/- mice
iMAE-WT	immortalized murine aortic endothelial cells from wild-type mice
IPA	Ingenuity Pathways Analysis
Jam2	junctional adhesion molecule 2
Klf2	Kruppel-like factor 2
L or LS	unidirectional laminar shear stress
LDL	low density lipoprotein
Lox	lysyl oxidase
MAEC	murine aortic endothelial cells
MAE-p47	murine aortic endothelial cells from p47phox-/- mice
MAE-WT	murine aortic endothelial cells from C57BL/6 (wild-type) mice
NADPH	nicotinamide adenine dinucleotide phosphate-oxidase
O or OS	oscillatory shear stress
PBS	phosphate-buffered saline

PCR	polymerase chain reaction
PECAM1	platelet endothelial cell adhesion molecule 1
qPCR	quantitative PCR
R	Reynolds parameter
RNA	ribonucleic acid
ROS	reactive oxygen species
rpm	revolutions per minutes
RT-PCR	reverse transcriptase polymerase chain reaction
S or ST	static
SDS-PAGE	SDS-polyacrylamide gel electrophoresis
VCAM-1	vascular cell adhesion molecule 1
VE-cadherin	vascular endothelial cell cadherin
α	cone angle
μ	dynamic viscosity
ν	kinematic viscosity
r	cone radius
τ	shear stress

SUMMARY

Atherosclerosis occurs preferentially at branches and curves in arteries exposed to disturbed flow while sparing straight portions of arteries exposed to undisturbed flow. In vivo and in vitro studies have implicated NADPH oxidases in atherosclerosis and hypertension. Shear stress can induce reactive oxygen species production in endothelial cells from a variety of sources, including NADPH oxidases. Here, we examined the hypothesis that unidirectional laminar shear (LS) and oscillatory shear (OS) would differentially regulate gene expression profiles in NADPH oxidase-dependent and -independent manners, and that these genes would provide novel molecular targets in understanding endothelial cell biology and vascular disease.

The p47phox subunit of the NADPH oxidase can be an important regulator of certain Nox isoforms, including Nox1 and Nox2 which may be responsible for shear-induced superoxide production. In order to isolate p47phox-dependent shear responses, we took advantage of the p47phox$^{-/-}$ transgenic mouse model which lacks a functional p47phox subunit. We developed a method to isolate murine aortic endothelial cells using an enzymatic digestion technique. These cells expressed characteristic endothelial markers, including VE-cadherin, PECAM1, and eNOS, and aligned in the direction of flow. We successfully isolated primary murine aortic endothelial cells from both wild-type C57BL/6 mice (MAE-WT) and p47phox$^{-/-}$ mice (MAE-p47). Furthermore, we established an immortalized cell line from each of these cell types, iMAE-WT and iMAE-p47.

We carried out microarray studies using Affymetrix Mouse Genome 430 2.0 Arrays (39,000+ transcripts) on MAE-WT and MAE-p47 that were exposed to atheroprotective LS or atherogenic OS for 24 hours. In comparison to LS, OS significantly changed the expression of 187 and 298 genes in MAE-WT and MAE-p47, respectively. Of those, 23 genes showed similar gene expression patterns in both cell

types while 462 genes showed different gene expression patterns in the two cell types, demonstrating a considerable role for p47phox-based NADPH oxidases in shear-dependent gene expression. Changes in expression of several genes, including Kruppel-like factor 2 (Klf2), endothelial nitric oxide synthase (eNOS), angiopoietin 2 (Ang2), junctional adhesion molecule 2 (Jam2), bone morphogenic receptor type II (Bmpr2), and bone morphogenic protein 4 (Bmp4) were confirmed by quantitative PCR and/or immunoblotting using both primary cells and immortalized cells. Of these genes, our data suggest that Jam2, Bmpr2, and Bmp4 may be shear-sensitive in a p47phox-dependent manner. Taken together, our studies have identified a set of shear- and p47phox-sensitive genes, including unexpected and novel targets, which may play critical roles in vascular cell biology and pathobiology.

CHAPTER ONE: INTRODUCTION

Cardiovascular Disease

The most significant cause of morbidity and mortality in developed nations is cardiovascular disease (CVD). In the United States, approximately one in three adults has some form of CVD which accounted for over a third of all deaths in 2005. It is estimated that the total cost of CVD will be almost $450 billion this year alone. [1] The incidence and subsequent cost of CVD is expected to only increase given the rapid rise of risk factors such as diabetes and obesity. [2, 3] Clearly, it is worthwhile to find ways to prevent and manage these diseases.

Cardiovascular disease encompasses conditions such as hypertension, coronary heart disease, heart failure, and stroke. In some cases, there is a genetic predisposition to developing CVD, yet there are also other potentially modifiable risk factors that contribute to its incidence. These include cigarette smoking, high cholesterol levels, hypertension, diabetes, abdominal obesity, a sedentary lifestyle, a diet poor in fruits and vegetables, alcohol overconsumption, and psychosocial indices. [1]

Hypertension, the most prevalent form of CVD, is associated with and perhaps exacerbates other forms of CVD. However, while not as prevalent, coronary heart disease accounted for half of all deaths from CVD in 2004 and is presently the single most common cause of death in the United States. Stroke is the next most common cause of death from CVD, accounting for 17% of all deaths from CVD in 2004. [1] The underlying disease process that coronary heart disease and stroke share is atherosclerosis.

Atherosclerosis is a chronic progressive disease that occurs principally in large- and medium-sized arteries. The disease may be present throughout one's lifetime. The earliest type of atherosclerotic lesion – the fatty streak – is common in young children. [4] Over time, the disease results in the buildup of a plaque which may restrict blood

flow or even occlude the blood vessel entirely, resulting in an infarction of the organ the vessel supplies. When this occurs in a coronary artery supplying the heart, it is known as myocardial infarction or, more commonly, heart attack. When this occurs in any of the arteries supplying the brain, it is known as ischemic stroke or simply stroke.

Basic Cardiovascular Anatomy

The cardiovascular system is critically responsible for transporting nutrients and removing gaseous wastes from the body. It consists of the heart, blood vessels, and blood. Blood vessels include arteries, capillaries, and veins. These different types of blood vessels differ not only with respect to size and location but also anatomical composition and function. In the systemic circulation, arteries transport oxygenated blood away from the heart to the peripheral regions of the body. Starting from the heart, the first of these arteries, including the aorta and its branches, are known as conduit arteries. They experience high cyclical pressures and, in order to accommodate this, have large diameters and thick, elastin-rich walls. Moving away from the heart, these arteries progressively divide into smaller arteries with proportionately more muscular walls. Capillaries are composed of single layers of cells to help facilitate the exchange of nutrients and waste products. Veins transport deoxygenated blood back towards the heart for gas exchange in the pulmonary circulation. They experience low pressures and as a result have thin walls and are typically more compliant than arteries.

Arteries are composed of three coaxial layers: the intima, the media, and the adventitia. The intima is the innermost layer exposed to blood and is a monolayer of endothelial cells – the endothelium – atop a single basement membrane. The endothelium serves many homeostatic roles, including regulation of vessel tone, tissue perfusion, vascular permeability, blood fluidity, anticoagulant activity, and inflammatory responses. [5] The media is the layer underlying the intima and is comprised of mostly smooth

muscle cells embedded within layers of elastic laminae. These smooth muscle cells are responsible for translating signals from the endothelium into a contraction-relaxation response. The adventitia is the outermost layer made of connective tissue, elastin, and collagen that forms a tough, protective covering. It also often houses a *vasa vasorum*, a vessel bed that supplies larger vessels with nutrients as well as a nervous supply.

Atherosclerosis

Atherosclerosis is now recognized as an inflammatory disease. [6] The vascular response-to-injury theory proposes that endothelial dysfunction (or "injury") is the first step in the disease process. Repetitive insults over time cause the disease to progress. [7] Endothelial dysfunction may be caused by hypercholesterolemia; free radicals from smoking, hypertension, or diabetes; hyperhomocysteinemia; hyperuricemia; infectious microorganisms; or combinations of these and other factors. Whatever the cause, the initial changes appear to occur in the endothelium, increasing its adhesiveness and permeability and favoring a procoagulant state. These changes include, for example, upregulation of adhesion molecules such as e-selectin, intercellular adhesion molecule (ICAM), and vascular cell adhesion molecule (VCAM). These adhesion molecules act in concert with chemotactic molecules such as MCP-1 or modified (oxidized) LDL to encourage migration of monocytes into the subendothelium. Once below the endothelium, these monocytes, now termed macrophages, take up modified LDL as well as modify LDL even further. With increased accumulation of lipids, the cells become "foam cells". T-cells also migrate to the subendothelium and amplify the inflammatory response. Together, foam cells and T-cells comprise an early fatty streak. Migration of smooth muscle cells from the media soon follows. As the process continues, the fatty streak progresses to an intermediate and then to an advanced lesion, tending to form a fibrous cap that covers a mixture of immune cells, lipid, and debris, or a necrotic core. [6]

Such lesions thicken the vessel wall, but up to a point the lumen remains patent due to gradual vessel dilation and remodeling, an observation known as the Glagov phenomenon. [8] However, this compensation is limited. Eventually the lesion will restrict the flow of blood. Advanced lesions with fibrous caps are often vulnerable to rupture or ulceration which can rapidly lead to thrombosis and occlusion of a downstream artery, if not the native artery itself. [6]

Hemodynamics

Scientists observed several decades ago that atherosclerotic lesions developed in a specific pattern within the vascular tree. Lesions were found, for instance, in the coronary and carotid arteries and in the lower abdominal aorta, all areas where the vessels curve, bifurcate, or branch. [9, 10] This suggested that a mechanical factor, specifically the hemodynamic environment, played a critical role in atherogenesis. Both flow characteristics and vessel response to flow have been intensely investigated since these initial observations were made.

The flow of blood through the branched arterial vasculature is pulsatile due to its pump-driven nature. As such, it generates various types of forces on the vessel wall, illustrated in Figure 1.1. [11] Hydrostatic pressure is the normal force exerted on the vessel wall due to the pressure of the blood and results in a compressive stress. Changes in pressure during the cardiac cycle cause the vessel wall to stretch, which results in cyclic circumferential stress on the vessel wall. Fluid shear stress is the tractive, tangential force produced by the blood passing along the luminal surface of the endothelium. [12]

We sometimes can model blood flow as a simple laminar flow in a circular cylindrical tube. We assume that blood is an incompressible Newtonian fluid, the flow is well-developed, and there is a so-called “no slip” condition at the boundary. From these

conditions, we can obtain a parabolic velocity profile – the famous Hagen-Poiseuille flow – as shown in Figure 1.2. From this solution, we can also obtain the rate of flow Q through a tube, which is the Poiseuille formula. [12]

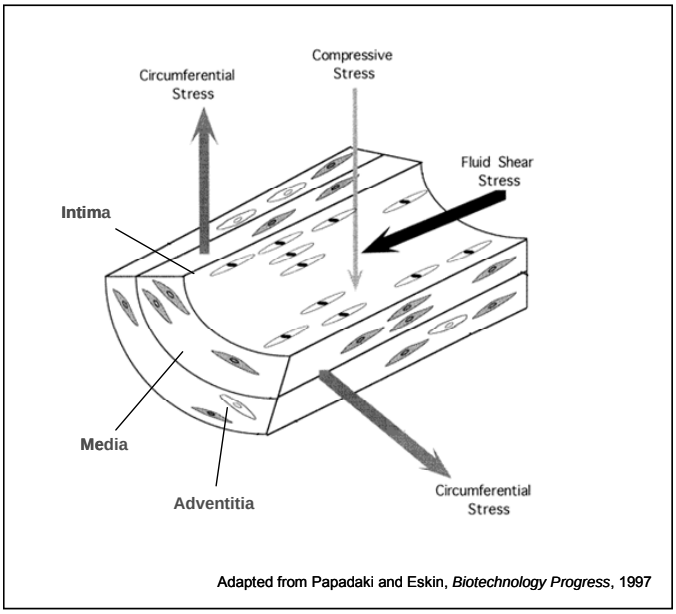

Figure 1.1. Forces acting on the vessel wall. The pump-driven nature of blood flow results in forces that result in cyclic circumferential stress, compressive stress, and fluid shear stress on the elastic vessel wall.

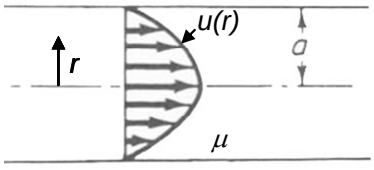

$$u = -\frac{1}{4\mu}(a^2 - r^2)\frac{dp}{dx}$$

$$\dot{Q} = -\frac{\pi a^4}{8\mu}\frac{dp}{dx}$$

Figure 1.2. Hagen-Poiseuille velocity profile in a circular cylinder.

While this model is a convenient way to understand the conceptual relationship between blood flow, properties of blood (viscosity), and vessel size, blood flow patterns can vary in complexity throughout the vasculature. There are relatively uniform, well developed laminar patterns that occur in the unbranched portions of medium-sized arteries. There are complex, disturbed flow patterns at bifurcations, branch points, and significant curves in the vasculature. These patterns involve regions of flow separation, recirculation, and reattachment that generate oscillatory wall shear stress. [13]

The importance of flow, and particularly shear stress, in vascular pathophysiology is shown by the focal development of atherosclerosis in hemodynamically defined areas of the vasculature. Regions of branches, curves, and bifurcations in the arterial tree that experience disturbed flow or unsteady, oscillatory shear stress, typically ranging from ±5 dynes/cm^2 (± indicating a change in flow direction), are prone to atherosclerotic lesion development. [6] In contrast, regions of straight arteries that experience steady, unidirectional shear stress, typically on the order of 15 dynes/cm^2, are protected from early lesion development. [6, 14]

Shear Stress and Endothelial Cells

The endothelium forms a dynamic interface between the blood and the underlying vessel wall that responds to and transduces both humoral and biomechanical stimuli. It is well established that differences in local hemodynamic environments result in phenotypically distinct endothelial cells. Under steady, unidirectional or pulsatile shear stress, endothelial cells elongate and align in the direction of flow. This has been demonstrated both *in vivo* and *in vitro*. [5, 15-17] This promotes an atheroprotective phenotype where nitric oxide (NO), a vasodilator, and other atheroprotective molecules are expressed. In contrast, under oscillatory shear stress, endothelial cells retain a

"cobblestone" appearance. This promotes an an atherogenic phenotype where apoptotic signals and inflammatory cell adhesion molecules are expressed.

How endothelial cells sense and interpret a mechanical force such as shear stress is still under debate. The simplest model of mechanotransduction suggests that it occurs when a shear-sensitive receptor is stimulated and the biochemical signal emanates from that point. A more complex, decentralized model suggests that there are multiple types of mechanoreceptors distributed throughout cell, integrated via the cytoskeleton. When an input is received, the signal is transduced to other mechanosensors as well, leading to a biochemical response from many locations having an integrated, cumulative effect on the cell. [5] Proposed mechanosensors include integrins, adherens junctions, potassium channels, receptor tyrosine kinases, and caveolae. [5, 18-22] More recently, a group identified a mechanosensory complex upstream of previously identified integrin-mediated response. This complex is comprised of VEGF receptor 2 (VEGFR2), PECAM-1, and VE-cadherin. [23]

Reactive Oxygen Species

Reactive oxygen species (ROS) include oxygen ions, free radicals, and peroxides. They are highly reactive due to the presence of unpaired valence electrons. ROS result from the sequential reduction of molecular oxygen. The first one-electron reduction produces superoxide ($O_2^{\cdot -}$). This product can be reduced again to yield hydrogen peroxide (H_2O_2) which can, in turn, be reduced to a hydroxyl radical ($OH^{\cdot}$). Each of these intermediate radicals can react with a number of other molecules to yield yet more radicals. For example, while superoxide reacts with superoxide dismutase (SOD) to yield hydrogen peroxide, it can also react with nitric oxide to form peroxynitrite ($ONOO^-$). In fact, it is reported that NO and $O_2^{\cdot -}$ react at a three-fold greater rate than the rate of reaction between SOD and $O_2^{\cdot -}$. [24]

ROS are byproducts of normal metabolism and have important functions in cell signaling. Under physiologic conditions, the cell's production of ROS is balanced by antioxidant processes. These processes include ROS scavenging by molecules such as ascorbate or glutathione or enzymatic degradation by enzymes such as superoxide dismutase, catalase, and glutathione peroxidase. [25] When this equilibrium is disturbed and ROS dominate, oxidative stress ensues. Oxidative stress plays a significant role in not only cardiovascular disease but other disorders including diabetes mellitus, neurologic diseases such as Alzheimer's or Parkinson's diseases, and cancer, among others. With regard to cardiovascular disease, ROS are important mediators of hypertension, vessel remodeling after angioplasty, atherosclerosis, myocardial infarction, and ischemic stroke.

Reactive Oxygen Species in Endothelial Cells

Endothelial cells are able to generate ROS which at moderate levels have several physiological roles, including acute and chronic oxygen sensing, regulation of vessel tone, and cell migration and proliferation during development or wound healing. An excess of endothelial ROS, however, also has pathological roles due to their cytotoxic and mutagenic properties. They have been shown to be involved in endothelial dysfunction, inflammatory activation, tissue injury, and apoptosis. Potential sources of endothelial ROS are mitochondrial respiration (via the electron transport chain), lipoxygenase, cyclooxygenase, cytochrome p450s, xanthine oxidoreductase (XOR), NADH/NADPH oxidases, uncoupled NO synthase (NOS), and peroxidases. [26] Three of these sources have been studied extensively: XOR, uncoupled NOS, and NADPH oxidase. We will briefly review the current understanding of XOR and uncoupled NOS before moving on to more closely examine the NADPH oxidase.

Xanthine Oxidoreductase

The enzyme xanthine oxidoreductase has two interconvertible forms, xanthine dehydrogenase (XDH) and xanthine oxidase (XO). XDH is the dominant form *in vivo*. Both forms catalyze the oxidation of hypoxanthine to xanthine as well as the oxidation of xanthine to uric acid, the final two reactions in the purine degradation pathway. However, XDH can reduce either NAD^+ or oxygen whereas XO can reduce only oxygen. Since XDH has a greater affinity for NAD^+, generation of $O_2^{\cdot -}$ is limited when there is ample NAD+. However, when NAD+ is converted to NADH and NAD+ levels are low, XDH can act as an NADH oxidase, generating $O_2^{\cdot -}$. [27]

XOR-generated ROS are implicated in tissue structural damage and cell signaling interference and can contribute significantly to endothelial dysfunction in cardiovascular disease. [27, 28] As such, it may play a role in hypertension, hypercholesterolemia, heart failure, and atherosclerosis. [27]

Uncoupled NO Synthase

The enzyme endothelial nitric oxide synthase (eNOS) can become a source of ROS, as demonstrated in endothelium exposed to oxidant or hemodynamic stresses. [29-31] Active eNOS is a homodimer that converts L-arginine to L-citrulline and nitric oxide (NO). When exposed to oxidant stress, particularly the radical peroxynitrite ($ONOO^-$), or when deprived of its reducing cofactor tetrahydrobiopterin (BH_4), eNOS uncouples to a monomeric form and generates $O_2^{\cdot -}$ rather than NO [30], simultaneously increasing oxidative stress and decreasing NO bioavailability. Uncoupled eNOS is considered a prominent source of endothelial ROS in hypertension, diabetes, hypercholesterolemia, and atherosclerosis. [29, 32]

NADPH Oxidase

The NADPH oxidase was first identified in the neutrophil [33] and has since been studied in great detail. In this particular setting, the enzyme generates ROS as its primary function in order to support the cell's respiratory burst-dependent antimicrobial activity. While many other NOX family members have been identified, the phagocytic NADPH oxidase is the prototypical NADPH oxidase; it is useful to discuss this enzyme first.

As shown in Figure 1.3, the phagocytic NADPH oxidase consists of two membrane-bound subunits, gp91phox (now known as Nox2) and p22phox, and several cytosolic subunits, including p47phox, p67phox, p40phox, and the small GTPase Rac. Activation is thought to be triggered by phosphorylation of p47phox which leads to conformational changes that allow its interaction with p22phox. Furthermore, it is thought that p47phox organizes the translocation of other cytosolic factors, and so it is known as an "organizer subunit." The translocation of p47phox to the membrane brings p67phox, an "activator subunit," into contact with Nox2 and also brings p40phox to the complex. Finally, Rac joins the complex, first interacting with Nox2 and then with p67phox. Once assembly is complete, the enzyme is active and Nox2-containing vesicles fuse with plasma membrane so that it can generate superoxide in the extracellular space.

Endothelial cells and other nonphagocytic cells can constitutively express superoxide-generating enzymes analogous to the neutrophil NADPH oxidase. Several isoforms of gp91phox have been identified to date – Nox1 through Nox5 and Duox1 and Duox2. Nox1, Nox2, Nox4, and Nox5 have been identified in human endothelial cells. There are also homologs to some of the cytosolic components of the NADPH oxidase. NoxO1 is known to be a p47phox homolog and NoxA1 is a p67phox homolog.

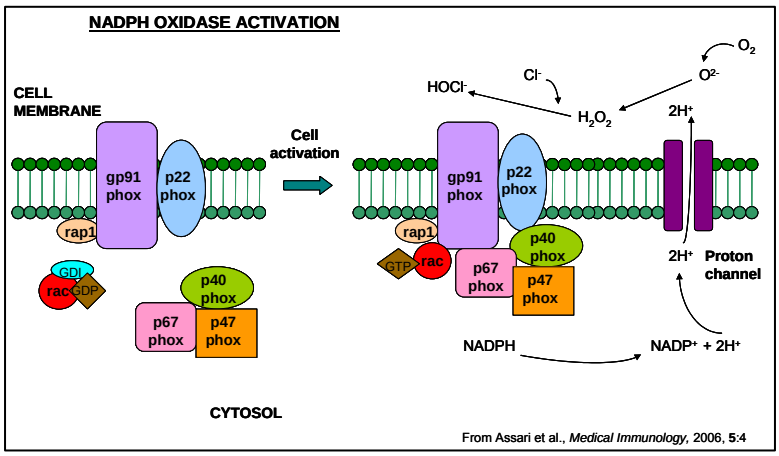

Figure 1.3. The neutrophil NADPH oxidase. The neutrophil NADPH oxidase consists of membrane-bound subunits, including gp91phox (Nox2) and p22phox, and cytosolic subunits, including p40phox, p67phox, p47phox, and rac. When activated, the cytosolic subunits join the membrane-bound proteins to form an complex that generates superoxide.

Each of the Nox isoforms appears to have tissue- and cell-specific expression and have different and possibly plastic requirements for cytosolic subunits. Nox1 is dependent on cytosolic subunits. At first, it was thought to be dependent on NoxO1 and NoxA1. However, in transfected cells, Nox1 was able to use the p47phox and p67phox subunits instead. In addition, Nox1 requires the membrane-bound subunit p22phox. Nox4 is a more distantly related Nox enzyme. While its activity is dependent on p22phox, it does not require any cytosolic subunits, though its requirement for Rac is debated. It may be constitutively active in many cell types, including endothelial cells.

The endothelial NADPH oxidase functions in a similar manner to the phagocytic NADPH oxidase, yet with some important differences. A substantial proportion of the superoxide it generates is intracellular instead of extracellular. It continuously generates a low basal level of superoxide. A substantial proportion of subunit expression and functional activity, at least in cultured endothelial cells, is intracellular and not plasma membrane bound. Furthermore, a large proportion of subunits in unstimulated cells exists in fully preassembled and functional ROS-generating complexes which are

associated with the intracellular cytoskeleton. [26] Additionally, p47phox in endothelial cells plays an essential role in activation of NADPH oxidase and superoxide production. [34, 35]

NADPH Oxidase: The p47phox Subunit

Two Nox organizer subunits of the NADPH oxidase have been identified: NoxO1 and p47phox (also known as NoxO2). For our purposes, we will focus largely on the p47phox subunit. The human p47phox gene is located on chromosome 7. To our knowledge, no splice variants of this gene exist. The gene's protein product is cytosolic and not glycosylated. [36] Approximately one-third of all cases of chronic granulomatous disease (CGD), a form of primary immunodeficiency, are caused by mutations in the p47phox gene. [37]

p47phox has several functional domains. It has a phox (PX) domain that interacts with membrane phospholipids. It has two Src homology 3 (SH3) domains that can interact with proline-rich regions in the carboxy-terminal of p22phox. p47phox also has an autoinhibitory region (AIR) that prevents interaction of the protein until it is phosphorylated and undergoes a conformational change. Finally, it has a carboxy-terminal proline-rich region that can interact with the SH3 domains in p67phox. [36]

The p47phox subunit, in particular, is thought to have a prominent role in ROS-mediated atherosclerotic development. Marschall Runge's group showed that p47phox is required for atherosclerotic lesion progression in an atherogenic mouse model. In this report, $ApoE^{-/-}/p47phox^{-/-}$ mice had less total aortic lesion area than the $ApoE^{-/-}$ mice had. Furthermore, this same group isolated smooth muscle cells from wild-type, $p47phox^{-/-}$, and $gp91^{phox-/-}$ mice, and showed that only the $p47phox^{-/-}$ cells had diminished superoxide production and decreased response to growth factors, emphasizing the role of the subunit itself and not the Nox isoform. [38] Other groups have reported conflicting results. [39]

However, Runge's group published an additional report with this model, indicating that superoxide derived from both monocytes and macrophages as well as cells within the vessel wall was critical in atherosclerotic lesion development, again demonstrating the role of the p47phox subunit. [40]

ROS and Hemodynamic Shear Stress

Various types of shear can differentially induce the formation of reactive oxygen species by the endothelium. [41] When EC are exposed to arterial levels of unidirectional steady laminar shear stress, there is a transient increase in superoxide production that peaks at about one hour and then returns to baseline within hours after that. [41, 42] The transient increase in superoxide production is most likely due to the temporal gradient in shear stress seen at the onset of flow. In contrast, when EC are exposed to oscillatory shear stress, there is a sustained increase in superoxide production compared to static or steady laminar controls. [41]

Steady laminar flow activates transcription driven by the antioxidant response element (ARE) and increases expression of ARE-regulated genes that protect against oxidative damage, including NADPH:quinine oxidoreductase 1 (NQO1) and heme oxygenase 1 (HO-1). [43] The transcription factor that binds to the ARE when activated by oxidative stresses is NF-E2-related factor 2 (Nrf2). Oscillatory flow inhibits Nrf2 binding to the ARE and thus decreases expression of antioxidant genes. [44]

The NADPH oxidase is involved in shear-mediated ROS production. [45, 46] Oscillatory shear stress has been shown to upregulate NADPH oxidase subunits including Nox1, Nox2, and Nox4. [42, 47] Furthermore, oscillatory shear stress increased NADH-dependent oxidase activity in HUVEC homogenates. [41] In particular, the p47phox subunit, possibly acting in coordination with Nox1, has been suggested to play a critical role in shear-mediated ROS production. A study by Castier et al. used transgenic animal

models to investigate vascular remodeling. This group found that shear stress induces vascular NADPH oxidase comprising p47phox but not Nox2. The ROS produced by this interacts with NO to produce peroxynitrite which affected downstream events such as MMP activation and vessel remodeling. [48]

Experimental Models

In Vitro Flow Models

To investigate the effects of hemodynamic shear stress on endothelial cells, several *in vitro* devices have been developed and characterized over the past three decades. These include the parallel-plate flow chamber as well as several modifications of a cone-and-plate viscometer. [49, 50]

The parallel-plate flow chamber was first designed to study the effects of flow on endothelial cells by Frangos and colleagues in 1985. [49] Since that time, many modifications have been made to this system in order to impart varying and complex flow profiles. The basic system consists of two critically spaced plates, between which fluid is driven by a pressure gradient. Cells are cultured on the inner surfaces of the plates and are subjected to a dragging force from the fluid moving between the plates. Overlooking the small areas affected by edge effects, the flow can be represented by plane Poiseuille flow. The shear stress is constant over the plate and can be calculated as follows where μ is dynamic viscosity, Q is the flow rate, b is the channel width, and h is the channel height.

$$\tau = \frac{6\mu Q}{bh^2}$$

An alternative to the parallel-plate flow chamber is the cone-and-plate system. This is essentially a rotational viscometer. It was first described and applied to biological systems in the early 1980's. [50] As illustrated in Figure 1.3, it consists of a stationary

plate, on which cells are grown, and a rotating cone. [51] The cone can be rotated unidirectionally to produce steady, laminar shear stress (LSS). It can also be rotated bidirectionally to produce an oscillatory shear stress (OSS). [47, 52-54]

The flow induced by the cone-and-plate model is well characterized. In conventional fluid mechanics, the Reynolds number (Re) is a measure of the ratio of inertial to viscous forces acting on a moving fluid. It can be expressed by the relationship below, where D is the characteristic length, v is velocity, and υ is the kinematic viscosity.

$$\mathrm{Re} \equiv \frac{Dv}{\upsilon}$$

When Re < 1800, laminar flow exists. When Re > 2200, turbulent flow exists. Between these two values, when 1800 < Re < 2200, a transitional flow exists. An analogous parameter has been established in cone-and-plate fluid mechanics, termed a "Reynolds like" parameter (R). This parameter is the ratio of the centrifugal force to the viscous force and is defined as follows, where r is the radial position, ω is the angular velocity, α is the cone angle, and υ is the kinematic viscosity.

$$\tilde{R} \equiv \frac{r^2 \omega \alpha^2}{12\upsilon}$$

There are three flow regimes that can be defined by this parameter. When R << 1, the viscous forces dominate and the fluid is purely azimuthal, varying linearly along the cone's radius. However, as R approaches 1, there is a tendency for the fluid to experience a centrifugal force which introduces a radial component to the flow. Fluid will move radially outward at the cone's surface and, correspondingly, will move radially inward at the plate's surface. When R > 1, the flow becomes turbulent [50].

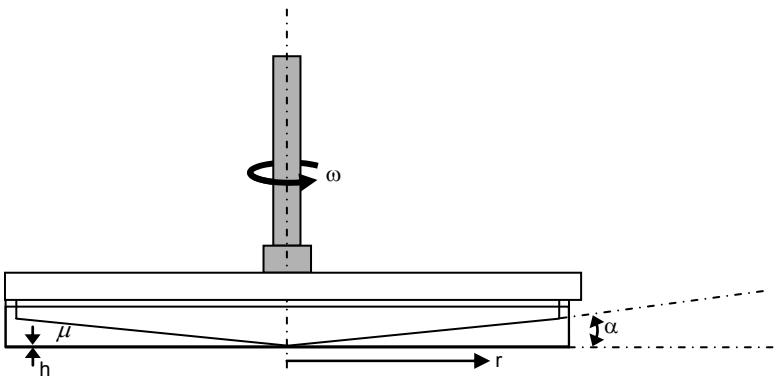

Figure 1.3. Diagram of a cone-and-plate apparatus for exposing endothelial cells to fluid shear stress. Shear stress is a function of the angular velocity (ω), cone angle (α), gap height (h), fluid viscosity (μ), and radius (r).

The shear stress on the plate surface can be calculated as follows, where μ is the dynamic viscosity, r is the radial position, ω is the angular velocity, h is the spacing between the apex of the cone and the plate, and α is the angle between the cone's surface and the plate. Therefore, one can control the level of shear stress by adjusting any of these parameters.

$$\tau = \mu \frac{\partial v}{\partial z} = \mu \frac{v}{h + r \sin \alpha} = \mu \frac{r\omega}{h + r\alpha}$$

Figure 7 shows a typical pattern of alignment by human umbilical vein endothelial cells (HUVEC) following application of 24 hours shear stress. As expected, static controls and cells exposed to oscillatory shear conditions maintained a so-called "cobblestone" appearance. Cells exposed to laminar shear conditions elongated and aligned in the direction of flow as indicated.

Animal Models

The mouse has been used extensively in the past century as one of the primary mammalian model systems for human disease. Mice share close genetic and physiologic

similarities to humans. They reproduce quickly and it is easy and economical to maintain mouse colonies. Most importantly, the mouse genome can be manipulated and analyzed with relative ease, permitting us to genetically engineer very specific strains to model various disease conditions.

A so-called "knockout" mouse is a genetically engineered mouse in which one (or more) genes have been turned off or "knocked out." By disrupting a specific gene, any differences observed between it and its wild-type counterpart can possibly be attributed to that gene and researchers can infer the gene's probable function. This technology was first demonstrated in the late 1980's by Mario Capecchi, Martin Evans, and Oliver Smithies, the work for which they were awarded the Nobel Prize in Physiology or Medicine in 2007 [55]. Currently there are thousands of different knockout mouse models in use.

We have chosen to use a p47phox-knockout mouse model which was originally created in the mid-1990's as a model for chronic granulomatous disease (CGD) [56]. The mouse p47phox gene is located on chromosome 5 and is 9.5 kilobases in length with eleven translated exons [57]. The knockout was created by targeting the 3' terminus of exon 7. A neomycin resistance cassette was inserted here to disrupt amino acid 221, a region of the protein known to be necessary for the function of both human and mouse p47phox [4, 6]. Since its establishment, this mouse model has been widely used in studies of not only CGD but also immune, cardiovascular, pulmonary, and neurologic diseases. [38, 40, 56]

CHAPTER TWO: OBJECTIVES

Atherosclerosis is an inflammatory disease that preferentially develops in regions of the arterial vasculature such as branches, curves, and bifurcations that experience low and/or unsteady, oscillating shear stress, as opposed to straight regions that experience higher, steady shear stress. Much of the disease process can be attributed to oxidative stress through reactive oxygen species generated by NADPH oxidases in these areas. It is known that endothelial cells lining the blood vessel are important modulators and indicators of vascular health. The differences between the atherogenic and atheroprotective areas in the vasculature can be reflected by gene and protein expressions of these endothelial cells. Our goal is to determine what shear responses are affected by reactive oxygen species, particularly from the p47phox-dependent NADPH oxidases.

Specific Aim 1: Isolate and characterize mouse aortic endothelial cells.

Hypothesis: Mouse aortic endothelial cells that display typical endothelial cell markers can be isolated and cultured for *in vitro* experimentation.

Specific Aim 2: Determine the effect of p47phox-dependent NADPH oxidases on shear responsive gene expression profiles in endothelial cells.

Hypothesis: p47phox-dependent NADPH oxidases alter gene expression in response to fluid shear stress.

CHAPTER THREE: MURINE AORTIC ENDOTHELIAL CELL ISOLATION AND CHARACTERIZATION

Introduction

Endothelial cells form a dynamic interface between the blood and the underlying vessel wall that responds to and transduces both humoral and biomechanical stimuli. [5] These cells are critical mediators in the development of diseases such as hypertension or atherosclerosis. Numerous transgenic mouse strains have been established to model human cardiovascular diseases, such as $ApoE^{-/-}$ mice which are hyperlipidemic and develop atherosclerotic lesions rapidly. [58, 59] Transgenic mice are particularly useful because antibodies, pharmacologic inhibitors, or newer methods such as siRNA do not preclude non-specific effects that may largely confound experimental interpretation. Non-specific effects could include cell activation, interference with intracellular signaling cascades, or altered lifespan, among others.

Whole animal models are often too complex to determine the role of a particular cell type, however. Scientists often take advantage of in vitro systems to study cell-specific responses. Although still not ideal, an in vitro experimental system allows for a clear investigation of the endothelial cell response to a well-defined stimulus. Much of the information we have gained regarding the endothelial cell response to mechanical forces or to agonists come from bovine aortic endothelial cells (BAEC) or human umbilical vein endothelial cells (HUVEC), both of which are relatively easy to isolate and culture *in vitro*.

There are relatively few reports on the isolation, in vitro characterization, and use of murine aortic endothelial cells (MAEC). [53, 60-67] The isolation methods that have been described can be categorized as either explant methods or enzymatic digestion methods. In an explant method, sections of an aorta are placed on a matrix such as

gelatin, collagen, or Matrigel in culture media. The endothelial cells are allowed to grow and expand outward from the tissue. After a number of days, the non-endothelial cells are either removed manually, through selective cell culture, or by a cell sorting technique such as fluorescence-activated cell sorting (FACS) or magnetic cell sorting (MACS). [60, 66, 67] In an enzymatic digestion method, the aorta is treated with enzymes such as collagenase, dispase, or trypsin in order to digest the extracellular matrix to achieve a single cell suspension. Only a minority of this cell suspension is endothelial cells, so it must be enriched by sorting out non-endothelial cells by FACS or MACS. [61, 65, 66]

We have developed a method to routinely isolate MAEC for use in further experiments. This allows us to combine the power of the transgenic mouse model with in vitro experimental systems to determine cell-specific responses dependent on particular genes.

Methods

Mice

Two strains of mice were used to isolate endothelial cells. C57BL/6 mice served as wild-type controls and were purchased from Jackson Laboratories on an as-needed basis. p47phox$^{-/-}$ mice, first generated and described by Steve Holland, were initially purchased from Taconic. [56] A breeding colony was established and maintained per IACUC protocols. Breeding cages were supplied with sterile water supplemented with sulfamethoxazole/trimethoprim.

Method 1: Isolation with BS-I Labeling followed by DiI-Ac-LDL Labeling

Buffers, Media, and Cell Culture Materials

All buffers and media were sterile-filtered prior to use. Cell isolation buffer consisted of HBSS with Ca^{2+} and Mg^{2+} and 1% penicillin/streptomycin. Digestion buffer consisted of HBSS without Ca^{2+} or Mg^{2+}, 0.2% collagenase type I, 0.05% collagenase type II, and 1 unit/ml dispase. Wash buffer consisted of HBSS without Ca^{2+} or Mg^{2+} and 1% penicillin/streptomycin. Labeling buffer consisted of HBSS without Ca^{2+} or Mg^{2+}, 1% penicillin/streptomycin, 1% HI-FBS, 25 mM HEPES, and 5 ug/ml FITC-labeled BS-I (Sigma). Sorting buffer consisted of HBSS without Ca^{2+} or Mg^{2+}, 1% penicillin/streptomycin, 1% HI-FBS, and 25 mM HEPES. Growth media for MAEC was MCDB 131 supplemented with 10% heat-inactivated fetal bovine serum (HI-FBS), 1% L-glutamine, 1% penicillin/streptomycin, 1% endothelial cell growth supplement (ECGS), 10 units/ml heparin sulfate, 50 ug/ml ascorbic acid, 1 ug/ml hydrocortisone, 2 ng/ml FGF, 1 ng/ml VEGF, 10 ng/ml EGF, and 2 ng/ml IGF. Unless otherwise noted, all cell culture plates and dishes were coated with 0.1% gelatin.

Isolation of Mouse Aortic Endothelial Cells

Surgical procedures and cell culture were performed under aseptic conditions. Twelve to sixteen 3-4 week old male mice were used for each isolation. The mice were sacrificed by CO_2 asphyxiation according to standard, IACUC-approved protocols. A midline incision was made from the lower abdomen to the neck. The vasculature was perfused through the left cardiac ventricle with sterile normal saline supplemented with 10 units/ml heparin sulfate. The abdominal organs, lungs, and esophagus were removed and discarded. The periadventitial fat was carefully dissected away from the aorta. Once cleaned, the thoracic aorta was removed and placed in a 35-mm culture dish with cell

isolation buffer. The aorta was bisected longitudinally to expose the endothelium, taking care to maintain the endothelial layer's integrity. All aortas were pooled and collected in 0.5 ml cell isolation buffer.

Digestion buffer was added to the pooled aortas. The aortas were digested for 30 min in a 37°C water bath, vortexing every ten minutes. After this, the mixture was passed over a sterile 100-um nylon cell filter. The filter was washed twice with 1 ml 0.25% trypsin-EDTA. The filtered suspension was centrifuged at 2000 rpm for 3 min in order to pellet the cells. The supernatant was discarded. The pellet was washed with sorting buffer. The suspension was centrifuged again at 2000 rpm for 2 min in order to pellet the cells.

The supernatant was removed and cells were then resuspended in 1 ml labeling buffer and incubated on a rocker at 4°C for 30 min. After this time, the cells were centrifuged at 2000 rpm for 3 min, washed with sorting buffer, and then centrifuged again. The cells were resuspended in a total of 1 ml sorting buffer.

FITC BS-I-labeled cells were collected by FACS using a BD FACSDiva machine. The number of positively sorted cells ranged from 5×10^3 to 10×10^4, with a typical number around 3×10^4. These cells were resuspended in growth media and then seeded into 12- or 6-well plates. The cells were kept in a humidified cell culture incubator with 5% CO_2 at 37°C. The cells were grown to confluence before passaging at a 1:2 or 1:3 ratio.

Once in a 10-cm dish, usually after 2 to 3 weeks, cells were labeled with DiI-Ac-LDL at 37°C for 4 hours. The cells were trypsinized and pelleted by centrifugation at 2000 rpm for 2 min. The cells were washed, pelleted again, and resuspended in sorting buffer. The DiI-Ac-LDL-labelled cells were collected by FACS using a BD FACSDiva machine. The number of positively sorted cells ranged from 4×10^4 to 2×10^5. The cells were resuspended in growth media and then seeded into 6-well plates. The cells were

kept in a humidified cell culture incubator with 5% CO_2 at 37°C. The cells were grown to confluence before passaging at a 1:2 or 1:3 ratio.

Method 2: Isolation with DiI-Ac-LDL Labeling Alone

Buffers, Media, and Cell Culture Materials

All buffers and media were sterile-filtered prior to use. Cell isolation buffer consisted of HBSS with Ca^{2+} and Mg^{2+} and 1% penicillin/streptomycin. Digestion buffer consisted of HBSS without Ca^{2+} or Mg^{2+} and 0.4% collagenase type II. Wash buffer consisted of HBSS without Ca^{2+} or Mg^{2+} and 1% penicillin/streptomycin. Sorting buffer consisted of HBSS without Ca^{2+} or Mg^{2+}, 1% penicillin/streptomycin, 1% HI-FBS, and 25 mM HEPES. Growth media for MAEC was MCDB 131 supplemented with 10% heat-inactivated fetal bovine serum (HI-FBS), 1% L-glutamine, 1% penicillin/streptomycin, 1% endothelial cell growth supplement (ECGS), 10 units/ml heparin sulfate, 50 ug/ml ascorbic acid, 1 ug/ml hydrocortisone, 2 ng/ml FGF, 1 ng/ml VEGF, 10 ng/ml EGF, and 2 ng/ml IGF. Unless otherwise stated, all cell culture plates and dishes were coated with 0.1% gelatin.

Isolation of Mouse Aortic Endothelial Cells

Surgical procedures and cell culture were performed under aseptic conditions. Twelve to sixteen 3-4 week old male mice were used for each isolation. The mice were sacrificed by CO_2 asphyxiation according to standard, IACUC-approved protocols. A midline incision was made from the lower abdomen to the neck. The vasculature was perfused through the left cardiac ventricle with sterile normal saline supplemented with 10 units/ml heparin sulfate. The abdominal organs, lungs, and esophagus were removed and discarded. The periadventitial fat was carefully dissected away from the aorta. Once cleaned, the thoracic aorta was removed and placed in a 35-mm culture dish with cell

isolation buffer. The aorta was bisected longitudinally to expose the endothelium, taking care to maintain the endothelial layer's integrity. All aortas were pooled and collected in 0.5 ml cell isolation buffer.

Digestion buffer was added to the pooled aortas. The aortas were digested for 20 min in a 37°C water bath, vortexing every few minutes. After this, the supernatant was removed and saved and 9 ml 0.05% trypsin was applied to the aortas. The aortas were incubated for an additional 5 min in a 37°C water bath, vortexing periodically. At the end of this incubation, 1 ml HI-FBS was added to stop the enzymatic reaction. This mixture was passed over a sterile 100-um nylon cell filter. The collagenase supernatant from earlier in the procedure was also passed over the filter as well, adding it to the cell suspension. This suspension was centrifuged at 2000 rpm for 3 min in order to pellet the cells. The supernatant was discarded. The pellet was washed with sorting buffer. The suspension was centrifuged again at 2000 rpm for 2 min in order to pellet the cells.

The cells were then resuspended in 12 ml growth media and seeded onto a 10-cm culture dish coated with 0.1% gelatin. Approximately one hour later, the unbound cells were removed and seeded onto a second 10-cm culture dish coated with 0.1% gelatin. Growth media was added to the first dish with adhered cells. Both dishes were kept in a humidified cell culture incubator with 5% CO_2 at 37°C.

Once confluent, cells were labeled with DiI-Ac-LDL at 37°C for 4 hours. The cells were trypsinized and pelleted by centrifugation at 2000 rpm for 2 min. The cells were washed, pelleted again, and resuspended in sorting buffer. The DiI-Ac-LDL-labeled cells were collected by FACS using a BD FACSDiva machine. The number of positively sorted cells ranged from 1×10^5 to 4×10^5. The cells were resuspended in growth media and then seeded into 6-well plates coated with 0.1% gelatin. The cells were kept in a humidified cell culture incubator with 5% CO_2 at 37°C. The cells were grown to confluence before passaging at a 1:2 or 1:3 ratio.

Immortalization of Primary MAEC

Primary MAEC were isolated and sorted by FACS for DiI-Ac-LDL positive cells, as described above in Method 1. Cells were immortalized by infection with a polyoma middle T (PmT) antigen, as previously described. [68] A PmT-producing packaging cell line was kindly provided by Dr. Elisabetta Dejana (FIRC Institute of Molecular Oncology, Milan, Italy). Briefly, PmT-conditioned medium was collected, 0.22 um-filtered, and stored at -80°C until use. Forty-eight hours post-seeding, cells were treated with PmT-conditioned medium along with 8 ug/ml polybrene (Sigma) for 4 hours at 37°C after which it was replaced with complete growth medium. After reaching a tight, confluent monolayer, cells were subcultured and then grown in G418-containing selective growth medium (1mg/ml). Cells were observed and regularly subcultured for over 8 weeks before complete cell selection was observed.

Reverse-Transcriptase PCR

For reverse-transcriptase polymerase chain reaction (RT-PCR) analysis, total RNA was isolated and purified using the RNeasy kit according to the manufacturer's protocols including DNase digestion (Qiagen). Quality of the RNA was ensured by both spectrophotometric analysis as well as visualization on an electrophoresis denaturing agarose gel. Quantity of the RNA was determined by spectrophotometric analysis at an absorbance of 260 nm. RNA was stored at -80°C until further use. Four micrograms of RNA from each sample were used in a reverse-transcriptase reaction with Superscript II (Invitrogen). The single-stranded cDNA was then purified using Micro-Biospin 30 chromatography columns (Bio-Rad). cDNA was stored at -20°C until further use.

Immunocytochemistry

Cells were rinsed with ice-cold PBS and fixed in 4% paraformaldehyde for 10 minutes at room temperature. Cells were then permeabilized with 0.2% Triton X-100 for

10 minutes, quenched with 50 mM ammonium chloride, and incubated in a blocking buffer of 3% BSA in PBS for one hour at room temperature. Cells were labeled with one of the following primary antibodies overnight at 4°C: VE-cadherin (1:50, Cayman Chemical) or PECAM-1 (1:50, Chemicon). Cells were washed with PBS and incubated with one of the following secondary antibodies: AlexaFluor 488-conjugatedgoat anti-rabbit (1:100, Molecular Probes) or Cy3-conjugated goat anti-hamster (1:100, Jackson Immunolabs). The samples were mounted with ProLong Gold anti-fade media, allowed to set and dry for 24 hours, and then imaged using a Zeiss Axiovert 200M fluorescent microscope.

Immunoblotting

Cells were rinsed in ice-cold PBS and lysed in RIPA buffer containing 50 mM Tris-HCl (pH 7.4), 1% NP-40, 0.25% sodium deoxycholate, 150 mM sodium chloride, 1 mM EDTA, 30 mM sodium fluoride, 40 mM ß-glycerophosphate, 10 mM sodium pyrophosphate, 2 mM sodium orthovanadate, 1 mM phenylmethylsulfonylfluoride (PMSF), and protease inhibitors (Roche). Lysates were further homogenized by brief ultrasonication on ice. Samples were centrifuged at 10,000 rpm for 10 minutes to pellet DNA and debris. The supernatant was collected and protein content was determined using a modified Lowry protein assay. Samples were mixed with Laemmeli buffer and boiled for 5-10 minutes prior to use. Aliquots of cell lysate were separated on SDS-PAGE gels. The proteins were transferred to a polyvinylidine difluoride (PVDF) membrane (Millipore). The membranes were probed with antibodies specific to eNOS (1:1000, BD Transduction), alpha smooth muscle actin (1:1000, Neomarkers), or total actin (1:5000, Santa Cruz) overnight at 4°C. The membranes were washed and then incubated with secondary antibodies for 2 hours at room temperature before chemiluminescent detection: ALP-conjugated goat anti-mouse (1:3000, Bio-Rad), ALP-

conjugated goat anti-rabbit (1:3000, Bio-Rad) or ALP-conjugated rabbit anti-goat (1:5000, Bio-Rad).

Results

Marker Specificity

We used two markers for identifying and sorting endothelial cells: a lectin from Bandeiraea Simplicifolia (BS-I) and acetylated LDL (Ac-LDL). BS-I has been characterized to specifically bind to arterial endothelial cells. [69] In order to ensure that this was the case in the mouse aorta, we incubated a whole aorta with FITC-conjugated BS-I under the same conditions as we used for labeling our cell isolates and observed the marker's specificity with a confocal microscope. As shown in Figure 3.2(a), BS-I labeled the endothelial cell junctions and was largely confined to the intima.

DiI-conjugated acetylated LDL (DiI-Ac-LDL) is an established endothelial cell marker. It is routinely used to identify endothelial cells in mixed cell populations. It does not label smooth muscle cells, fibroblasts, pericytes, or epithelial cells. It labels endothelial cells and also monocytes (and macrophages). However, monocytes can still be differentiated from endothelial cells by either cell morphology or signal intensity since they are more brightly labeled. [70] Shown in Figure 3.2(b) is an example of DiI-Ac-LDL labeling of BAEC. These cells exhibit typical cobblestone endothelial morphology and are uniformly and intensely labeled with DiI-Ac-LDL.

(a)

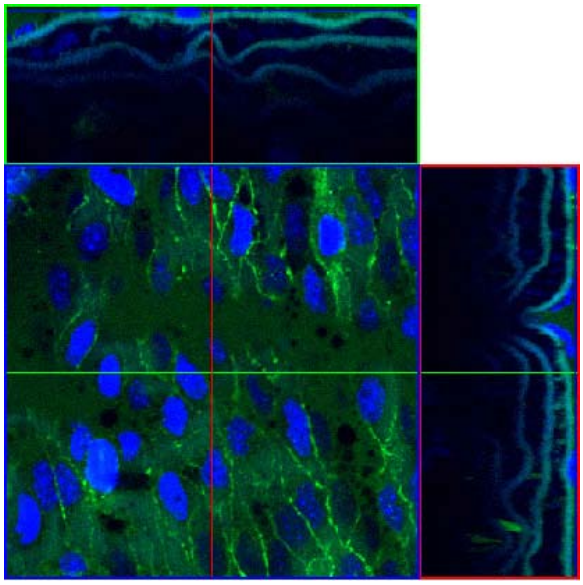

(b)

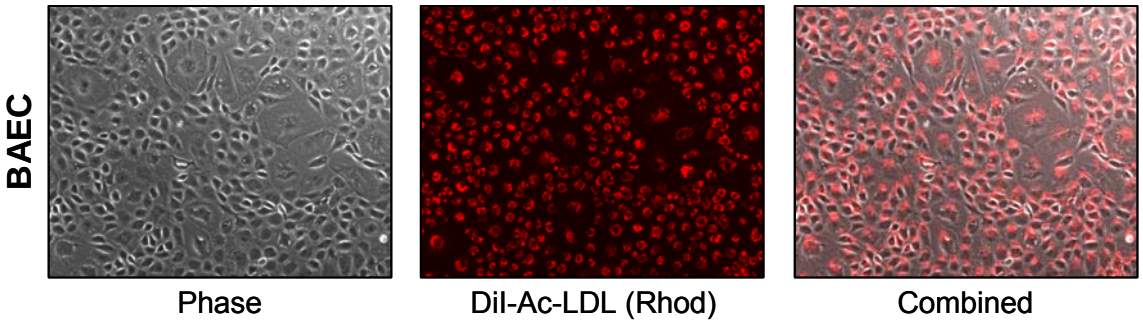

Figure 3.1. Markers used to identify and sort endothelial cells. (a) Lectin BS-I specifically labels endothelial cells in the mouse aorta. The thoracic aorta was cleaned, excised, and opened longitudinally. The aorta was then incubated with 5 ug/ml FITC-conjugated BS-I for 30 min at 4°C. The aorta was carefully washed to remove excess BS-I without disturbing the endothelium and mounted on a standard microscope slide with VectaShield with Dapi. The sample was imaged immediately on a Zeiss LSM 510 confocal microscope. Shown is an orthogonal view with three different orientations. The FITC-BS-I can be distinguished from green autofluorescence because the signal is more intense and localized to the cell-cell junctions. The signal is almost exclusively in the intima. (b) DiI-Ac-LDL efficiently labels endothelial cells. Bovine aortic endothelial cells were grown to confluence. Standard growth media was replaced with growth media containing 1 ug/ml DiI-Ac-LDL and incubated for 4 hours at 37°C. The cells were then washed twice with HBSS with Ca^{2+} and Mg^{2+} to remove excess DiI-Ac-LDL and imaged with a Zeiss Axiovert 200M fluorescent microscope.

Primary Cell Cultures Contain Multiple Cell Types

We initially based our isolation method on that of Kevil and Bullard, as shown in Figure 3.1(a). [61] One major difference is that we did not perform an external digestion of the aortas to remove the adventitial cells; this is because in a pilot experiment (not described) we found that this significantly compromised the architecture of the vessel and made it difficult to manipulate in later steps while still preserving the endothelial cell layer.

Even after sorting with BS-I, however, we found that there were multiple cell morphologies in our cultures. Shown in Figure 3.3(a) are the cells several hours after sorting with BS-I. The cells were sparse but adhered to the culture dish. After several days, the cells proliferated and were mostly confluent, as shown in Figure 3.3(b). We were able to observe multiple cell morphologies at this point. There were slightly elongated, spindle-shaped cells, as seen on the left and in the middle of the picture. There were narrow, stringy cells, shown mainly to the left and lower-left of the picture. There were also compact, cobblestone cells, apparent on the right of the picture. While these displayed a prototypic endothelial cell "cobblestone" morphology, they do not display endothelial cell markers as we will show later.

Primary Endothelial Cells are Rapidly Lost

Since we observed multiple cell morphologies in our BS-I sorted cell cultures, we used a second marker, DiI-Ac-LDL, to identify which cells were actually endothelial cells. Figure 3.4 shows DiI-Ac-LDL labeling of primary cells. At passage 2, there are a significant number of LDL-positive cells. Note that the positively labeled cells are not those with cobblestone morphology; instead, they are the slightly elongated, spindle-shaped cells. As passage 4, there are fewer LDL-positive cells. And by passage 14, there are practically no LDL-positive cells remaining in the culture. Whether this loss is due to dedifferentiation of the endothelial cells initially present in the culture or due to a

(a)

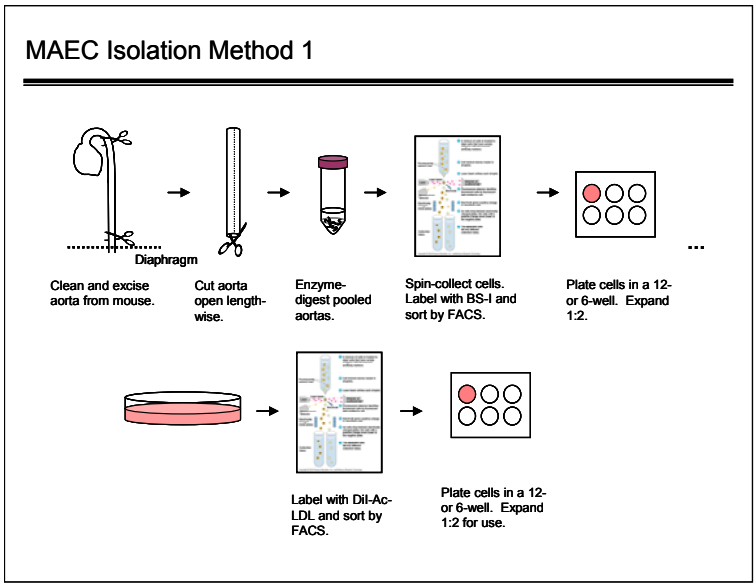

(b)

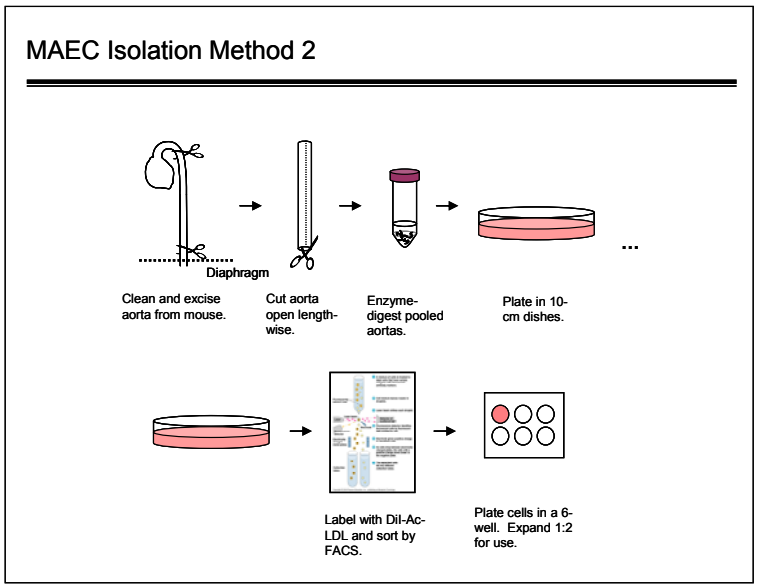

Figure 3.2. Methods for isolating primary MAEC. MAEC are isolated using an enzyme digestion technique. In Method 1, the cells are first sorted by BS-I, cultured, and then later sorted by DiI-Ac-LDL. In Method 2, the cells are initially cocultured and then sorted by DiI-Ac-LDL before use.

(a)

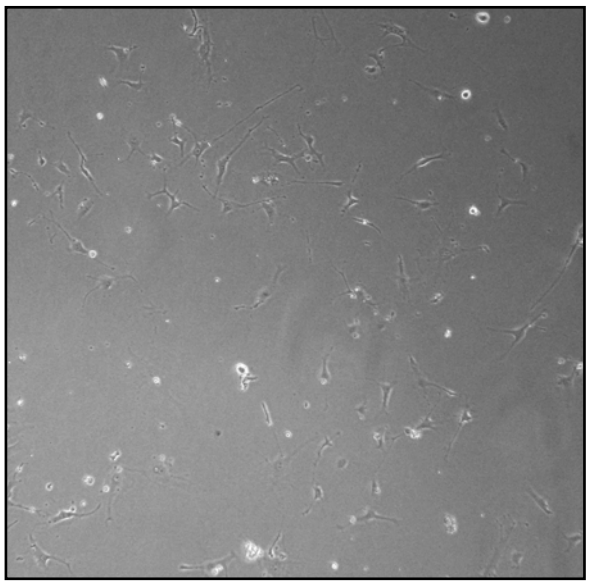

Day 0

(b)

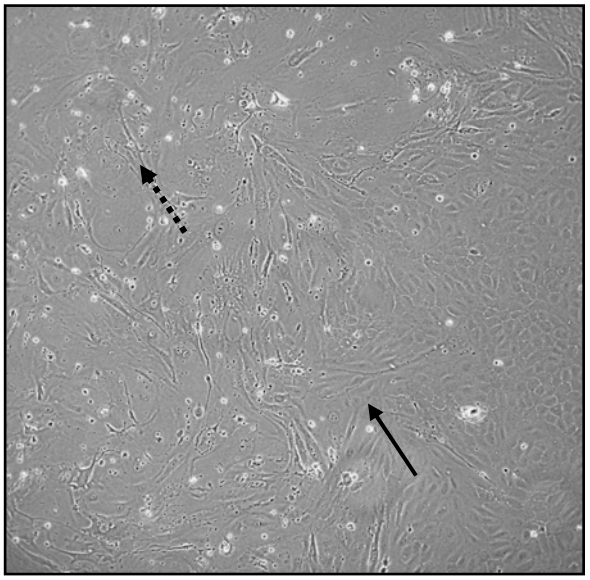

Day 4

Figure 3.3. Primary cell cultures contain multiple cell types. As described in the methods, primary mouse aortic cells were isolated using enzymatic digestion, labeled with FITC-BS-I, and then sorted using a BD FACSDiva machine. The positively sorted cells were plated in a 6-well. As shown in (a), the cells were sparse but adhered to the plate. Four days later, as shown in (b), the cells were confluent but displayed multiple cell types as distinguished by their differing morphologies. We can see thin, stringy cells, such as those marked with a dashed arrow. We can also see slightly elongated, spindle-shaped cells, such as those marked with a solid arrow. We can also see a large patch of cobblestone-shaped cells to the right (unmarked).

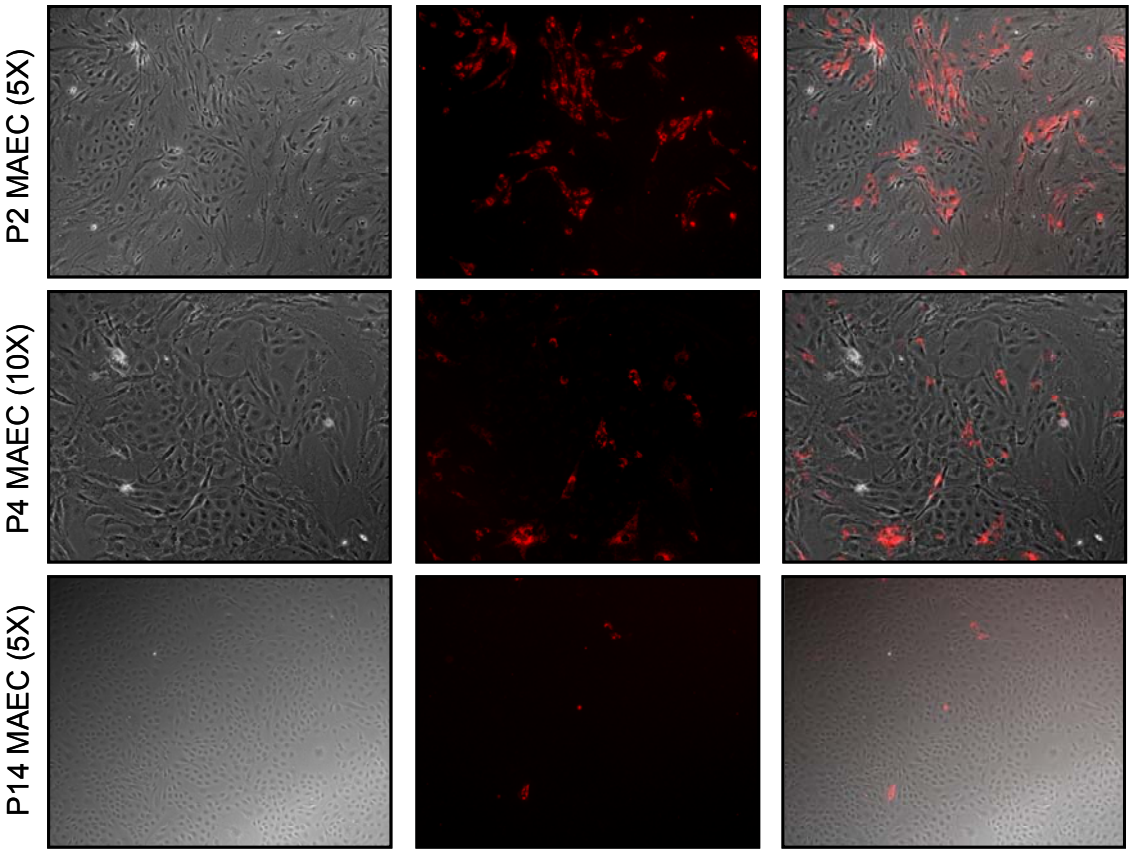

Figure 3.4. Primary endothelial cells are rapidly lost in culture. Primary mouse aortic cells were isolated using enzymatic digestion, labeled with FITC-BS-I, and then sorted using a BD FACSDiva machine. The cells were initially plated in a 6-well and then passaged upon confluence at a ratio of 1:2 to 1:4. At the indicated passages, the cells were incubated with 1 ug/ml DiI-Ac-LDL for 4 hours at 37°C. The cells were rinsed twice with HBSS with Ca^{2+} and Mg^{2+} to remove excess DiI-Ac-LDL and then immediately imaged with a Zeiss Axiovert 200M fluorescent microscope. The relative number of LDL-positive cells decreased with each passage, apparent even at P4. Note the presence of "daughter cells," circled, at P14.

contaminating, hyperproliferative cell type such as fibroblasts, we are still not sure. Yet we can still gain valuable information from this exercise. First, we know that primary endothelial cells proliferate slowly. Low-passage cultures take at least two or more days to become confluent, even when passaged at a conservative ratio of 1:2. High-passage cultures grow more rapidly and take less time to become confluent. We were able to make an interesting observation since the LDL-positive cells were sparsely distributed across the cell culture dishes at this point. Approximately three days after passaging, we could see "daughter cells" appear in the culture – where there had been one, there were two, meaning that it took that amount of time for the cell to divide. This suggests the "doubling time" for primary MAEC is quite long at two to three days, compared to one or two days for most conventional endothelial cell cultures such as HUVEC or BAEC.

Sorting with DiI-Ac-LDL Alone Improves Yield

We also pursued a variation on our initial cell isolation method, shown in Figure 3.1(b). After enzymatic digestion of the pooled aortas, we simply seeded all of the cells in one 10-cm dish. After approximately one hour, the non-adhered cells were transferred to a second 10-cm dish. The majority of the LDL-positive cells remained in the first dish (data not shown), indicating that they adhered relatively rapidly to the gelatin coating. These LDL-positive cells continued to proliferate and expand in the coculture. As shown in Figure 3.5, these LDL-positive cells, as before, had an elongated appearance. We were able to enrich the LDL-positive cell population by selectively removing LDL-negative cells from the dish by trypsinization since the LDL-positive cells were relatively resistant to removal. LDL-positive cells from C57BL/6 mice (MAE-WT) formed a matrix across the entire dish, with cells migrating and growing towards one another, as shown in Figure 3.5(a). LDL-positive cells from p47phox-/- mice (MAE-p47) behaved somewhat differently; they grew primarily in isolated clusters, as shown in Figure 3.5(b). After

approximately one or two weeks, the cells were sorted using DiI-Ac-LDL. We were able to obtain yields an order of magnitude higher than with our previous method.

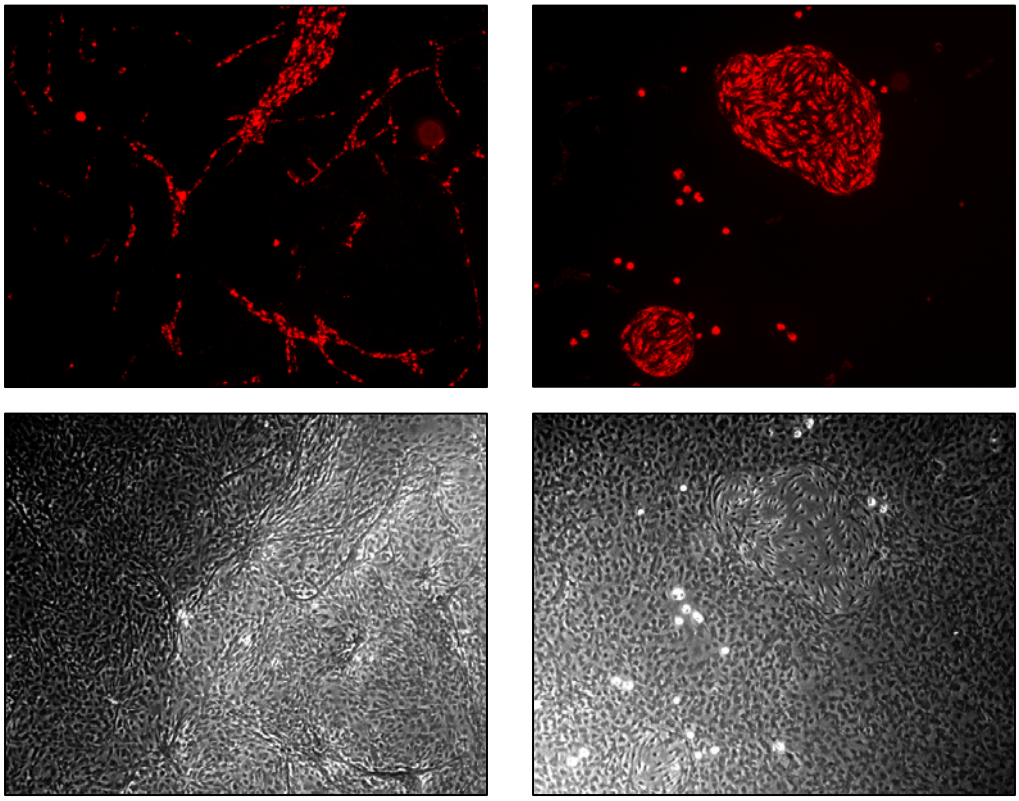

Figure 3.5. Sorting with DiI-Ac-LDL alone improves yield. Primary mouse aortic cells were isolated using enzymatic digestion and then immediately seeded onto a 10-cm dish in growth media. Approximately one hour later, unbound cells were transferred to a second dish and the initial dish was replenished with fresh growth media. Upon reaching confluence, cells were incubated with 1 ug/ml DiI-Ac-LDL for 4 hours at 37°C. The cells were rinsed twice with HBSS with Ca^{2+} and Mg^{2+} to remove excess DiI-Ac-LDL and then immediately imaged with a Zeiss Axiovert 200M fluorescent microscope. The majority of LDL-positive cells could be found in the initial dish, where the cells had adhered first. Pictures of these cells are shown above. On the left are primary aortic cells from wild-type (C57BL/6) mice and on the right are primary aortic cells from p47phox$^{-/-}$ mice.

Characterization of Primary Endothelial Cells

From our observation early on that cells sorted with BS-I alone were comprised of multiple cell types, we implemented a second round of cell sorting with DiI-Ac-LDL. However, even after this second round of selection, we still observed a contaminating cell type after several passages as shown in Figure 3.3. Attempts to minimize this other cell type through cell culture techniques or media supplements were not successful (data not shown). We decided that in the interest of time, the most practical strategy to achieve our goal was to maximize our initial cell yield and to use these cells for experiments as early as possible in order to have a predominantly endothelial cell culture.

LDL-positive primary cells exhibited an endothelial phenotype. As shown in Figure 3.6, these cells expressed VE-cadherin and PECAM1, two endothelial cell markers. Furthermore, as shown in Figure 3.7, MAE-WT and MAE-p47 both express another characteristic endothelial cell marker, eNOS, by PCR (a) and by Western (b). While we know there is a small percentage of "contaminating" LDL-negative cells in our cultures, the absence of alpha-smooth muscle actin indicates that the LDL-negative cells are at least not smooth muscle cells.

Characterization of Immortalized Endothelial Cells

As described in the methods, LDL-positive primary cells were infected with a retrovirus containing a PmT antigen. After two months in selection media, we were able to observe cell cultures that were almost entirely LDL-positive.

LDL-positive immortalized endothelial cells exhibit an endothelial phenotype. As shown in Figure 3.7, these cells express VE-cadherin and PECAM1, two endothelial cell markers. Furthermore, the immortalized wild-type cells (iMAE-WT) and the immortalized p47phox-/- cells (iMAE-p47) both express eNOS by PCR (a) and by Western (b). These cell cultures do not contain smooth muscle cells, as indicated by the absence of alpha-smooth actin.

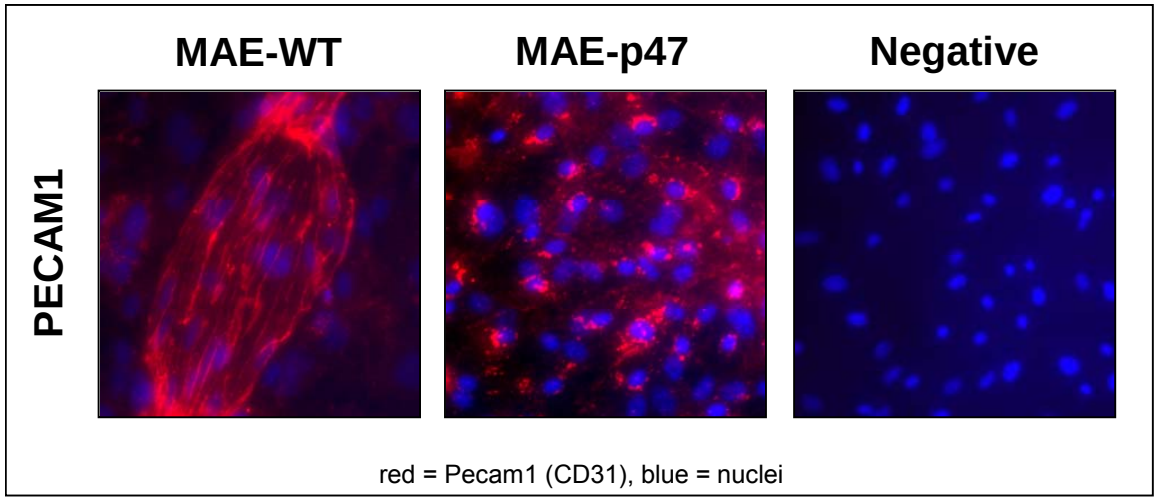

Figure 3.6. Primary MAEC exhibit the characteristic endothelial cell marker PECAM1. Primary cells were isolated as described in methods. Once confluent, the cells were rinsed with PBS, fixed with 4% paraformaldehyde, and incubated with an antibody to PECAM1. A Zeiss Axiovert 200M fluorescent microscope was used to image the results. Pictures depict PECAM1 staining in MAE-WT and MAE-p47 with a negative control. There is non-uniform staining due to the cells growing in coculture and being stained prior to sorting.

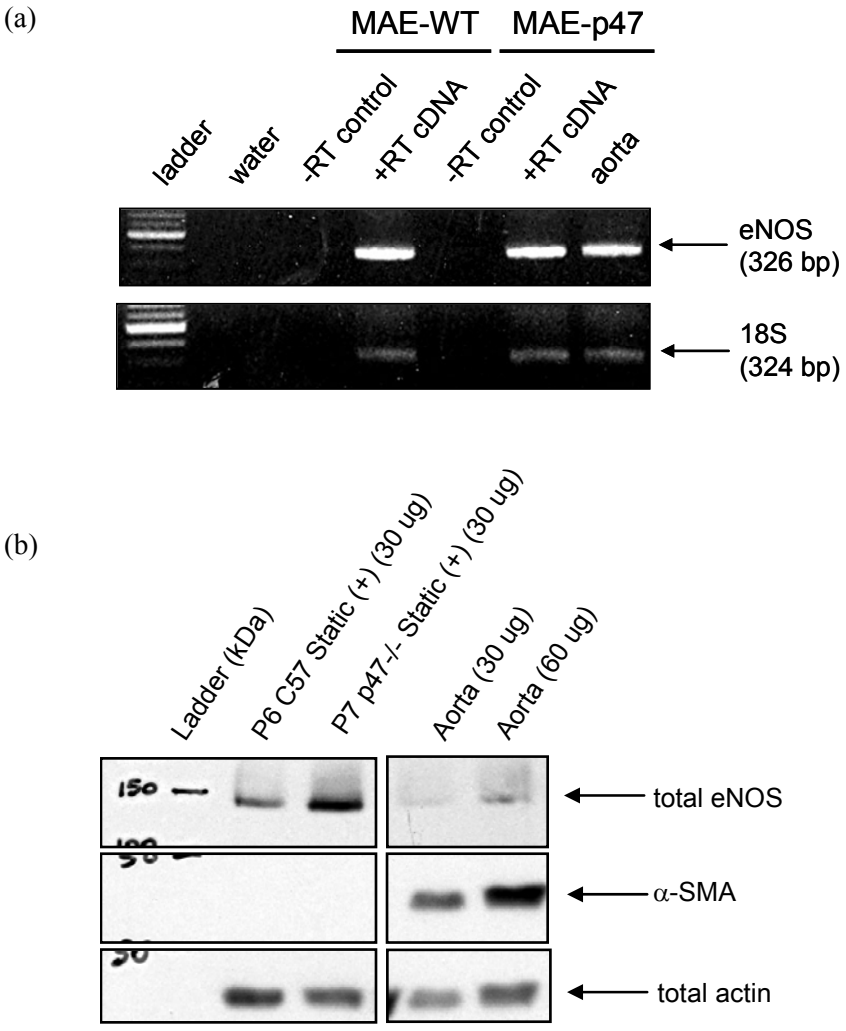

Figure 3.7. LDL-positive primary MAEC express the endothelial gene eNOS. Primary cells were sorted first with FITC-BS-I and then with DiI-Ac-LDL. Cell lysates were collected in either RLT buffer for mRNA analysis or RIPA buffer for protein analysis. As described in the methods section, RNA was isolated and reverse transcribed to yield single-stranded cDNA. Conventional PCR was used to analyze expression of eNOS using gene-specific primers. The results are shown in the top panel (a). Both MAE-WT and MAE-p47 expressed eNOS mRNA. Water and –RT controls were used to demonstrate that no extragenomic or genomic contamination was present. (b) Protein lysates were run on a denaturing SDS-PAGE gel, transferred to a PVDF membrane, and blotted with a monoclonal eNOS antibody. Additionally, the membrane was blotted with an alpha-smooth muscle actin (α-SMA) antibody in order to show that the cell cultures were not contaminated with smooth muscle cells. Wild-type aorta lysate was used as a positive control. Both MAE-WT and MAE-p47 expressed eNOS protein and did not express α-SMA.

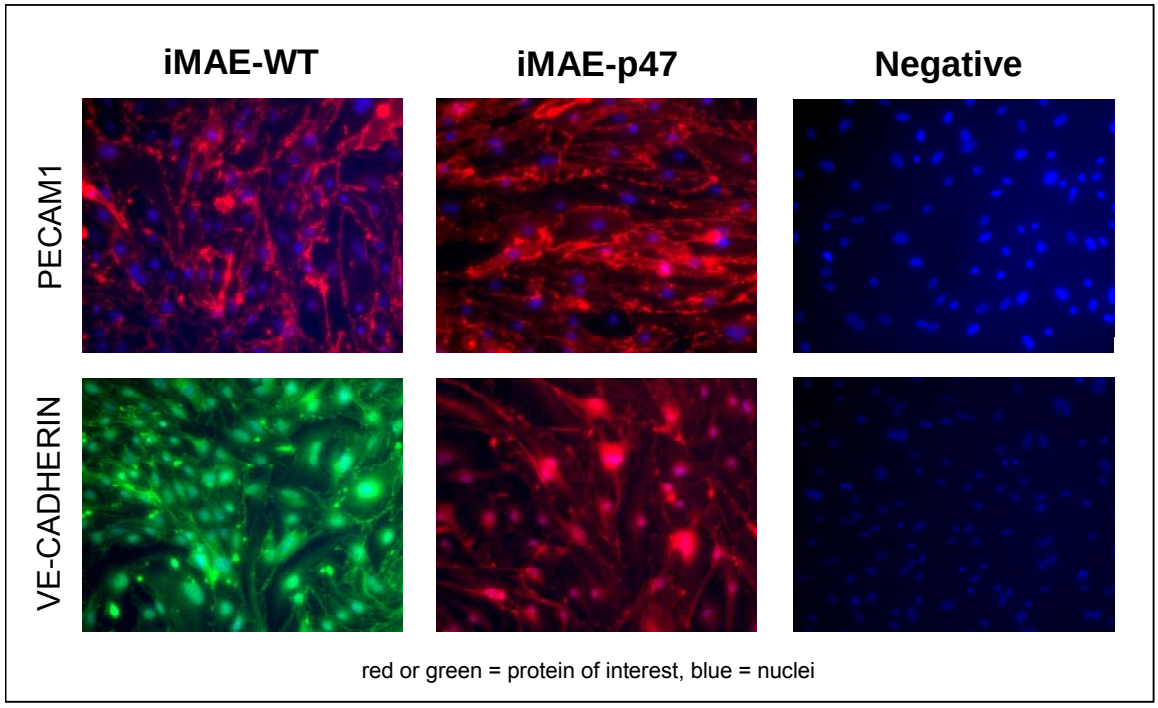

Figure 3.8. Immortalized MAEC exhibit characteristic endothelial cell markers, including PECAM1 and VE-cadherin. Primary cells were isolated and immortalized as described in methods. Once confluent, the cells were rinsed with PBS, fixed with 4% paraformaldehyde, and incubated with antibodies to PECAM1 and VE-cadherin. A Zeiss Axiovert 200M fluorescent microscope was used to image the results. The top row of pictures depicts PECAM1 staining in iMAE-WT and iMAE-p47 with a negative control. The bottom row of pictures depicts VE-cadherin staining in iMAE-WT and iMAE-p47 with a negative control.

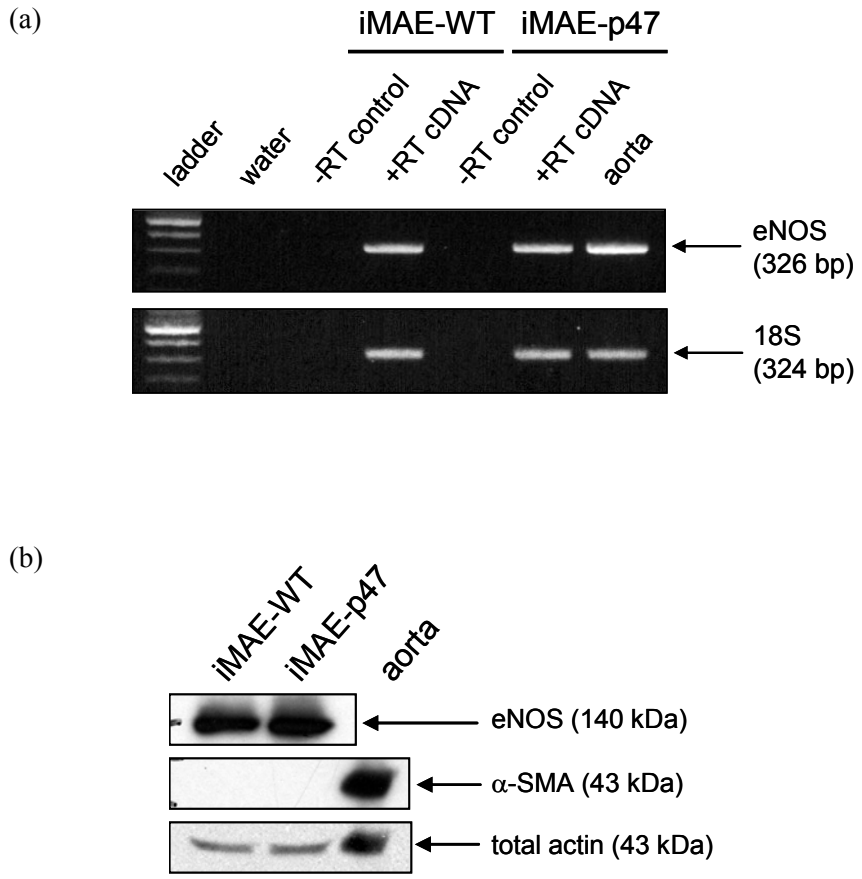

Figure 3.9. LDL-positive immortalized MAEC express the endothelial gene eNOS. Immortalized cells were cultured as described in the methods section. RNA was isolated using an RNeasy Mini Kit and reverse transcribed using Superscript III to yield single-stranded cDNA. Conventional PCR was used to analyze expression of eNOS using gene-specific primers. The results are shown in the top panel (a). Both iMAE-WT and iMAE-p47 immortalized cells expressed eNOS mRNA. Water and –RT controls were used to demonstrate that no extragenomic or genomic contamination was present. (b) Protein lysates were run on a denaturing SDS-PAGE gel, transferred to a PVDF membrane, and blotted with a monoclonal eNOS antibody. Additionally, the membrane was blotted with an alpha-smooth muscle actin (α-SMA) antibody in order to show that the cell cultures were not contaminated with smooth muscle cells. Wild-type aorta lysate was used as a positive control. Both iMAE-WT and iMAE-p47 immortalized cells expressed eNOS protein and did not express α-SMA.

Discussion

The isolation and culture of mouse aortic endothelial cells is a challenge on many levels. Initial yield from each mouse is quite low given the size of each aorta. We have estimated that there are just a few thousand endothelial cells in one thoracic aorta, so even with maximum efficiency and after pooling many aortas together, we begin with perhaps 50,000 endothelial cells. These cells are mature, terminally differentiated cells and do not readily proliferate in culture.

There is some question as to how to define an endothelial cell. Endothelial cells display remarkable heterogeneity *in vivo* which likely carries over into the *in vitro* setting. [71-73] Ultrastructural features such as Weibel-Palade bodies are not expressed uniformly throughout the vascular system and many genes associated with endothelial cells, such as eNOS, are not exclusive to only these cells. The only consistent definition for an endothelial cell is its anatomic definition – a cell that lines the inner wall of a blood vessel. With this in mind, we used several different markers of endothelial cells in optimizing our cell isolation method. We initially used BS-I lectin as it was shown to be specific for endothelial cells *in vivo*, as reported by other and shown by us in Figure 3.2. [69] However, we were not sure as to its specificity *in vitro*. As our cells lost their ability to take up DiI-Ac-LDL, they often maintained their ability to bind BS-I. We continued to use DiI-Ac-LDL since it is a more widely accepted marker for endothelial cells and we were able to correlate it with typical endothelial cell characteristics and behavior. LDL-positive cells expressed eNOS at both the mRNA and protein levels, as shown in Figures 3.7 and 3.9, while LDL-negative cells did not express eNOS (data not shown). Furthermore, LDL-positive cells aligned in the direction of flow (data shown in Chapter 4) while LDL-negative cells did not (data not shown). We concluded that uptake of DiI-Ac-LDL was the most important marker for indicating an endothelial phenotype.

Once in monoculture, LDL-positive cells alone did not proliferate rapidly. It is possible that MAEC require autocrine and paracrine factors from both other endothelial cells and other cell types in order to proliferate. This has been reported for hepatic sinusoidal endothelial cells cultured from rat. [74] We observed that when we subcultured LDL-positive cells into separate small dishes, as opposed to a larger dish of equivalent surface area, they were rapidly lost (data not shown). Perhaps they require signals from one another to maintain a differentiated state. Furthermore, we observed that LDL-positive cells proliferated more readily under coculture conditions. We could see large patches of LDL-positive cells, shown in Figure 3.5, that proliferated and yielded far greater cell numbers than when grown under monoculture conditions.

Not only did LDL-positive cells not proliferate, but these cell cultures were eventually overtaken by LDL-negative cells. Whether this was due to an invading cell type, such as fibroblasts, which proliferate rapidly, or dedifferentiation of the LDL-positive cells, we are still not sure. If it was due to an invading cell, the possible cell types would include smooth muscle cells, pericytes, monocytes/macrophages, adipocytes, or fibroblasts, all cells that could be present in the aorta as we removed it. We did not detect alpha-smooth muscle actin by Western (shown in Figure 3.7), however, indicating that the "invading cells" were not smooth muscle cells or pericytes. By PCR, we detected one of two fibroblast markers – fibroblast specific protein (Fsp) but not thymus cell antigen 1 (Thy1) – and one of two adipocyte markers – lipoprotein lipase (Lpl) but not adiponectin (Adipoq) (data not shown). We could not conclude anything from these results. The only definitive method to answer this question would be to perform a genetic lineage tracing experiment, as has been described with murine pancreatic cells. This report concluded that cultured β-cells both dedifferentiate and stop proliferating, eventually being eliminated from cell cultures by non-β-cells. [75] A similar experiment could be done with MAEC; however, this would be a significant undertaking and, in the interest of time, it was not done for the present study.

Despite these challenges, we were able to successfully isolate small populations of LDL-positive cells which have many characteristics of endothelial cells. These small populations were used in further experiments, as will be described in the following chapter. Furthermore, these cells were successfully immortalized with a PmT virus which yielded highly proliferative LDL-positive cell cultures that exhibited endothelial cell markers such as eNOS, VE-cadherin, and PECAM1. We are aware that the immortalization process may have impacted intracellular signaling pathways and thus may affect certain phenotypic responses. However, with proper screening, these cells lines can potentially be used indefinitely to study endothelial responses.

CHAPTER FOUR:
p47PHOX-DEPENDENT SHEAR RESPONSES IN ENDOTHELIAL CELLS

Introduction

Endothelial cells form a dynamic interface between the blood and the underlying vessel wall that responds to and transduces both humoral and biomechanical stimuli. Blood flow imparts a shearing stress on these cells that has been shown to affect cell morphology and function including regulation of vascular tone, vessel wall remodeling, hemostasis, and inflammatory responses. [5] The importance of this shear stress in vascular pathophysiology is shown by the focal development of atherosclerosis in regions of branches, curves, and bifurcations in the arterial tree that experience disturbed flow or unsteady, oscillating shear stress and low mean shear stress. In contrast, straight regions of arteries that experience steady, unidirectional shear stress are protected from early lesion development. [76] The mechanisms by which different types of flow and shear stress exert atheroprotective or atherogenic effects have been the subject of intense investigation for many years. These opposite effects may be determined by the differential expression of genes and proteins which ultimately induce these different phenotypes. In the past few years, several studies have addressed these opposite effects by using the high-throughput method of microarray analysis to determine expression profiles of mechanosensitive genes. [54, 77-85] The functional importance of those genes, including Klf2 and Bmp4, is currently being established.

Reactive oxygen species (ROS) have been shown to play a role in atherosclerotic development. [24] Specifically, oxidative stress is an important cause of endothelial cell dysfunction. [86] For example, ROS signaling is associated with increased expression of endothelial adhesion molecules such as e-selectin, ICAM1, and VCAM1, all of which play essential roles in the recruitment of monocytes to the subintimal layer, a critical step

in the progression of atherosclerosis. [6, 24, 42, 53] An important source of endothelial cell-derived ROS is the NADPH oxidase. Five NADPH oxidases have been cloned: Nox1, Nox2, Nox3, Nox4, and Nox5. [87] Nox1 is expressed in endothelial cells and smooth muscle cells; Nox2 is expressed in endothelial cells and adventitial fibroblasts; Nox4 is found in endothelial cells, smooth muscle cells, and fibroblasts. [26, 88, 89] p47phox is a cytosolic component of the NADPH oxidases that is necessary for optimum activation of Nox1 and Nox2. [90] Shear stress can induce ROS production in endothelial cells from a variety of sources, including NADPH oxidases. [28, 42, 53, 91]

Despite the role of ROS produced from NADPH oxidases in shear-dependent responses including inflammation, systematic investigation of which genes are regulated by shear in an NADPH oxidase-dependent manner has not been addressed. We hypothesized that LS and OS differentially regulate gene expression profiles in NADPH oxidase-dependent and -independent manners and these mechanosensitive and NADPH oxidase-sensitive genes would play critical roles in endothelial biology and atherosclerosis. Here, we examined the initial part of this hypothesis by carrying out DNA microarray studies using mouse aortic endothelial cells (MAEC) obtained from wild-type and p47phox$^{-/-}$ mice exposed to unidirectional laminar shear (LS) and oscillatory shear (OS) conditions.

Methods

Cell Culture

MAEC were isolated as described in the previous chapter. Cells were cultured at 37°C and 5% CO_2 in growth media of MCDB 131 supplemented with 10% heat-inactivated fetal bovine serum (HI-FBS), 1% L-glutamine, 1% penicillin/streptomycin, 1% endothelial cell growth supplement (ECGS), 10 units/ml heparin sulfate, 50 ug/ml ascorbic acid, 1 ug/ml hydrocortisone, 2 ng/ml FGF, 1 ng/ml VEGF, 10 ng/ml EGF, and

2 ng/ml IGF. For shear stress experiments, MAEC were seeded onto 35-mm culture dishes coated with 0.1% gelatin and grown to confluence. Media were changed to growth media containing 5% (v/v) Hyskon approximately one hour prior to experiments.

Immortalized MAEC (iMAEC) were developed as described in the previous chapter. Cells were cultured at 37°C and 5% CO_2 in growth media of DMEM supplemented with 10% HI-FBS, 1% penicillin/streptomycin, and 1% ECGS. For shear stress experiments, iMAEC were seeded onto 10-cm culture dishes coated with 0.1% gelatin and grown to confluence. Media were changed one day prior to experiments.

Human umbilical vein endothelial cells (HUVEC) were purchased (Emory Dermatology) and grown to confluence at 37°C and 5% CO_2 in growth media of M199 supplemented with 20% heat-inactivated fetal bovine serum (HI-FBS), 1% penicillin/streptomycin, 10 units/ml heparin sulfate, and 1% endothelial cell growth supplement (isolated by us). For shear stress experiments, HUVEC were seeded onto either 35-mm culture dishes or 10-cm culture dishes coated with 0.1% gelatin and grown to confluence. Media were changed one day prior to experiments. Cells from passages 4 to 6 were used.

Cone-and-Plate Shear Apparatus

Cells were exposed to an arterial level of unidirectional laminar shear stress (L or LS) (~15-20 dyn/cm^2) or oscillatory shear stress (O or OS) (±5 dyn/cm^2 with directional changes of flow at 1 Hz) for 24 hours in growth media using a cone-and-plate shear apparatus, as described previously. [51, 53] The apparatus was maintained in a tissue culture incubator at 37°C and 5% CO_2.

RNA Isolation

Total RNA was isolated and purified using the RNeasy kit according to the manufacturer's protocols including DNase digestion (Qiagen). Quality of the RNA was

ensured by both spectrophotometric analysis as well as visualization on an electrophoresis denaturing agarose gel. Quantity of the RNA was determined by spectrophotometric analysis at an absorbance of 260 nm. RNA was stored at -80°C until further use.

Microarray Procedures

RNA QC: RNA integrity is critical to the quality of microarray data. The integrity of total RNA for each sample was assessed using an RNA 6000 Nano Lab Chip on a Agilent 2100 Bioanalyzer. We used RNA samples with 260/280 ratios between 1.8 and 2.0, RNA Integrity Number (RIN) values of 10, and 28S:18S ratios of 1.5 and higher. This is shown in Figure 4.1.

Arrays: Gene expression profiling was measured using Affymetrix reagents kits and Affymetrix Mouse 430v2 Genechip Arrays comprised of over 45,000 probe sets representing over 34,000 well-substantiated mouse genes. Target labeling, hybridization and post-hybridization processing were performed as described in the Affymetrix GeneChip Expression Analysis manuals. 100 ng of total RNA was reverse transcribed using T7-oligo(dT) primers and SuperScript II in the first-strand cDNA synthesis reaction. Following RNase H-mediated second-strand cDNA synthesis, the double-stranded cDNAs were purified with a GeneChip sample clean-up module and served as templates in the generation of complementary RNAs (cRNAs) by an *in vitro* transcription (IVT) reaction. The biotinylated cRNAs were then cleaned up, fragmented, and hybridized to the mouse expression arrays at 45°C for 16 h with constant rotation at 60 rpm. The microarrays were then washed and stained on an Affymetrix fluidics station and scanned on Affymetrix 3000 scanner. The images were processed to collect raw data (.CEL and .CHP files) with the GeneChip Operating Software (GCOS).

Microarray Data Analysis: The Affymetrix CEL files were imported into GeneSpring 7.3 and normalized by the GC-Robust Multichip Average (GC-RMA) method. The data was normalized to the 50th percentile of the measurements taken from

(a)

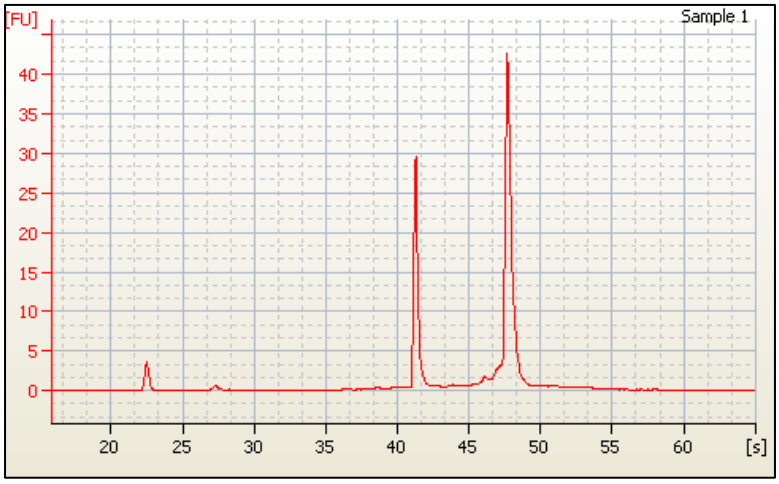

(b)

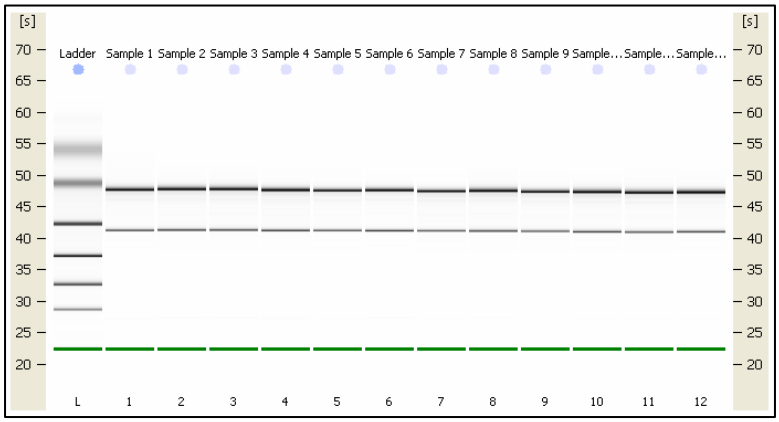

Figure 4.1. RNA quality for samples submitted for microarray analysis. The integrity of total RNA for each sample was assessed using an Agilent 2100 Bioanalyzer and RNA 6000 Nano Lab Chip. Shown in (a) is a representative electropherogram. The 18S and 28S peaks are strong and distinct, indicating intact RNA. Shown in (b) is the gel image of all twelve samples. RNA samples were all of high quality with 260/280 ratios between 1.8 and 2.0, RNA Integrity Number (RIN) values of 10, and 28S:18S ratios of 1.5 and higher.

the chip to reduce chip-wide variations in intensity. Each gene was normalized to the average measurement of the gene throughout the experiment to enable comparison of relative changes in gene expression levels between different conditions. We removed genes with absent signals in all arrays and then computed the fold change (O/L) between oscillatory shear (O) and laminar shear (L) for each batch. The average fold change for each gene in each cell type, either MAE-WT or MAE-p47, was calculated. Statistical significance of the average fold change was calculated using a two-tailed t-test. Genes were filtered out that had $p < 0.03$. The remaining genes were filtered by fold change. We included genes that were downregulated < 0.66-fold or upregulated > 1.52-fold. This is schematically described in Figure 4.2.

Genes identified by GeneSpring were uploaded into the Ingenuity Pathways Analysis tool as well as GOMiner to further analyze the gene ontology, including biological processes, cellular components, molecular functions and genetic networks and signaling pathways.

GEDI Analysis

Expression fold changes (O/L) for each batch of cells were loaded into the Gene Expression Dynamics Inspector (GEDI). After organization by a self-organizing map (SOM) algorthim, expression fold changes were averaged for each cell type and represented graphically in mosaics.

Quantitative PCR

Four micrograms of RNA from each sample were used in a reverse-transcriptase reaction with Superscript II (Invitrogen). The single-stranded cDNA was then purified using Micro-Biospin 30 chromatography columns (Bio-Rad). cDNA was stored at -20°C until further use.

Quantitative PCR (qPCR), or "real-time" PCR, was carried out for several genes. Primer sequences are shown in Table 5.1. Standards for each gene of interest were generated using conventional PCR. PCR products were separated on and extracted from an agarose gel using a Qiaquick gel extraction kit (Qiagen). Pure cDNA was eluted and quantified, and standards of known concentrations were generated. qPCR was conducted using standards and cDNA from samples (in triplicate) on a Roche LightCycler 2 real-time PCR machine. mRNA copy numbers were determined based on standard curves generated with murine experimental templates and normalized to GAPDH.

Table 5.1 Primer Sequences for qPCR

Gene	Forward	Reverse
eNOS	GGCTTCAGGAAGTGGAGGCTGAGGT	CTGCTGCCTATAGCCCGCATAGCGTAT
Klf2	CCAACTGCGGCAAGACCTAC	AGTCGACCCAGGCTACATGTG
Jam2	GGGTCGGAGTGTCTCCTTTG	ACGATATTTCCCCGCATCAC
Bmpr2	GGGAGAGAAACAAGTCTGTGAGC	AAGCAGACAGGGGTTGGCCC
Bmp4	CTGCGGGACTTCGAGGCGACACTTCT	TCTTCCTCCTCCTCCTCCCCAGACTG
Ang2	AGATCCAACAGAATGTGGTGC	TGTTGACGGTCTCCATTAGG
GAPDH	TGCACCACCAACTGCTTAG	GATGCAGGGATGATGTTC

Immunoblotting

Cells were rinsed in ice-cold PBS and lysed in RIPA buffer containing 50 mM Tris-HCl (pH 7.4), 1% NP-40, 0.25% sodium deoxycholate, 150 mM sodium chloride, 1 mM EDTA, 30 mM sodium fluoride, 40 mM ß-glycerophosphate, 10 mM sodium pyrophosphate, 2 mM sodium orthovanadate, 1 mM phenylmethylsulfonylfluoride (PMSF), and protease inhibitors (Roche). Lysates were further homogenized by brief ultrasonication on ice. Samples were centrifuged at 10,000 rpm for 10 minutes to pellet DNA and debris. The supernatant was collected and protein content was determined using a modified Lowry protein assay. Samples were mixed with Laemmeli buffer and

boiled for 5-10 minutes prior to use. Aliquots of cell lysate were separated on SDS-PAGE gels. The proteins were transferred to a polyvinylidine difluoride (PVDF) membrane (Millipore). The membranes were probed with antibodies specific to Klf2, total eNOS (1:1000, BD Transduction), phospho-eNOS (Ser1177) (1:1000, Cell Signaling), Bmpr2 (1:1000, BD Transduction), Bmp4 (1:1000, Santa Cruz) or total actin (1:5000, Santa Cruz) overnight at 4°C. The membranes were washed and then incubated with secondary antibodies for 2 hours at room temperature before chemiluminescent detection: ALP-conjugated goat anti-rabbit (1:3000, Bio-Rad), ALP-conjugated rabbit anti-mouse (1:3000, Bio-Rad), or ALP-conjugated rabbit anti-goat (1:5000, Bio-Rad).

Partial Ligation Model

Wild-type (C57Bl/6) and p47phox-/- mice were bred and housed according to standard IACUC protocols. Partial ligation of only the left carotid was performed on each experimental animal. The external carotid, internal carotid, and occipital arteries were ligated, leaving only the superior thyroid artery patent. One day following this procedure, animals were sacrificed by CO_2 asphyxiation. The vasculature was perfused and fixed with formalin. Aortas were excised and incubated with a primary antibody toward Bmp4 and then appropriate secondary antibodies. Fluorescent *en face* images were taken using a Zeiss LSM 510 confocal microscope.

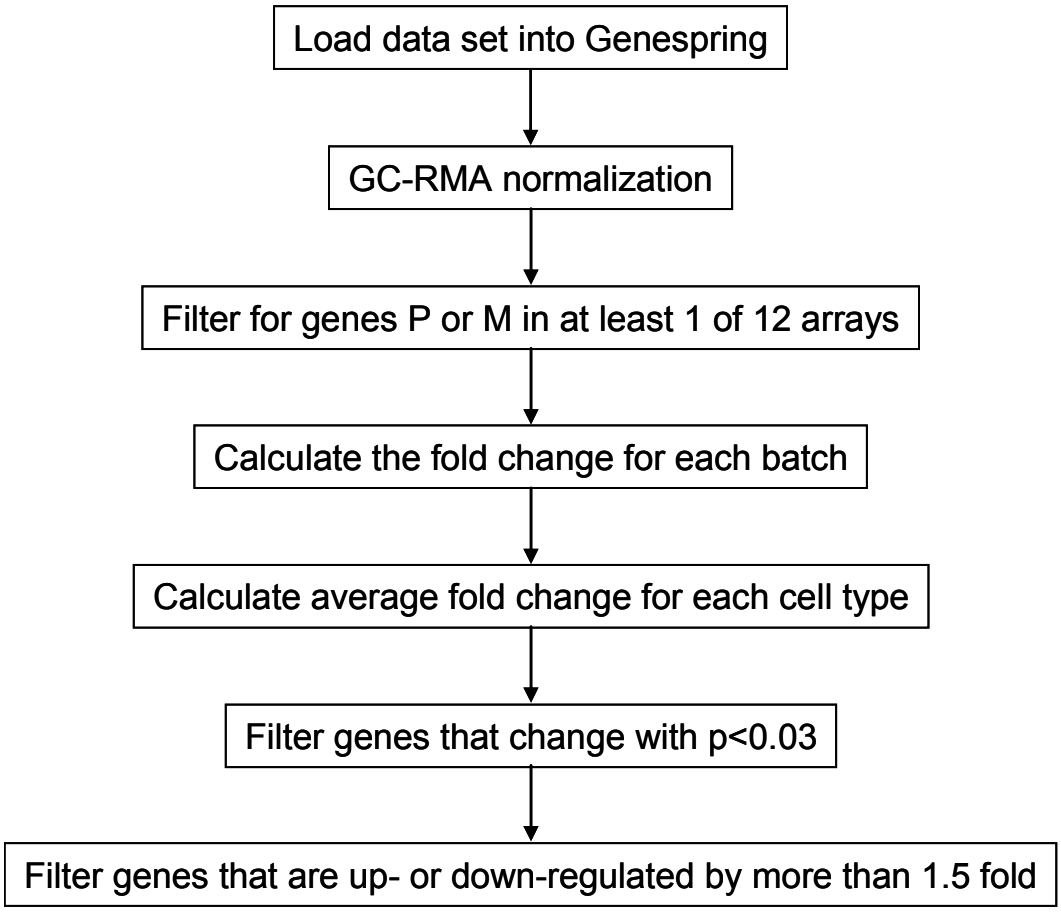

Figure 4.2. Schematic of gene expression analysis.

Results

Murine Aortic Endothelial Cells Align in the Direction of Flow

As described in the introductory chapter, the Reynolds-like number and shear stress values are two important parameters that characterize the flow environment with this model. We typically use a cone-and-plate apparatus equipped for 10-cm culture dishes. Shown in Figure 4.3 are typical values for both unidirectional flow and oscillatory flow in this system. As noted before, the Reynolds-like parameter, shown in (a), varies radially. While towards the outer portion of the plate, we show only that $R < 1$ for laminar flow, our experimental observations that endothelial cells continue to align towards the outer edge of the cone support the assumption that viscous forces are still dominant and in an azimuthal direction. Shear stress also varies radially, as depicted in (b). In unidirectional laminar flow, the majority of cells see a physiologic level of shear stress of 15-20 dyn/cm^2. In oscillatory flow, most cells see a maximum shear stress of 5 dyn/cm^2 during each 1 Hz cycle.

It is important to note that the oscillatory flow is also laminar. As you can see, at the outer edge of the plate, the Reynolds parameter is an order of magnitude less than 1, indicating that the viscous forces are dominating and there is little if any secondary flow. Hence, this flow can be considered laminar. This is supported by the observation that after adding a drop of India ink to the shear fluid, the ink maintained a circumferential path and did not disperse, as it would be prone to doing under less laminar and more turbulent conditions (data not shown).

In order to accommodate the small MAEC populations, we used 35-mm dishes to shear these cells. In order to do this, we had to find a way to scale down our typical cone-and-plate system. To achieve the same level of shear stress in smaller dishes, we needed to increase the rotational velocity of the cones; however, there is a limit to how fast we can rotate the cones due to not only possible secondary flows as our Reynolds

(a)

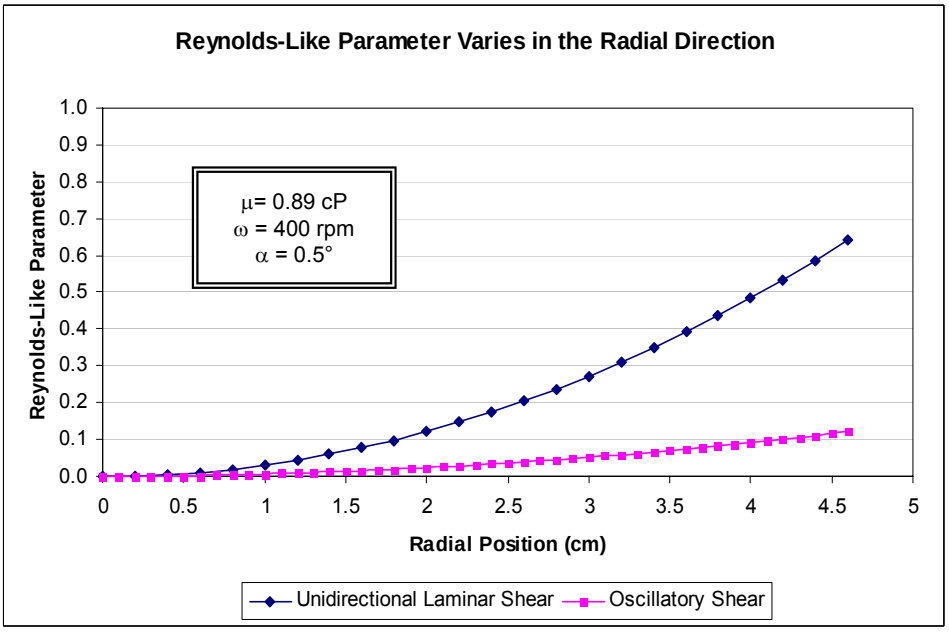

(b)

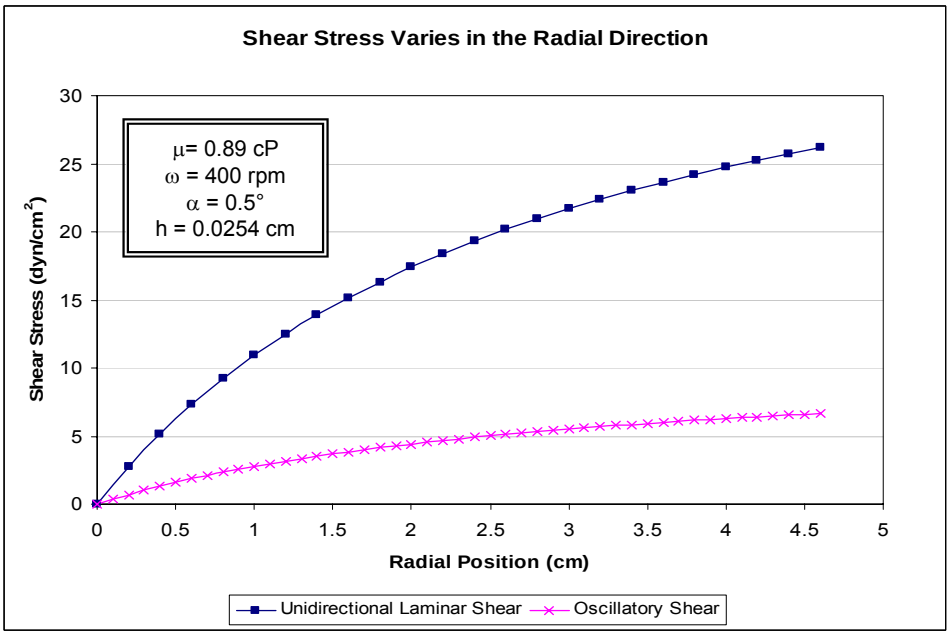

Figure 4.3. Reynolds-like parameter and shear stress distribution in a 10-cm cone-and-plate apparatus. (a) Reynolds-like parameter, an indicator of the relative dominance of viscous forces, varies along the radius and can be calculated from the media's viscosity (μ), the angular velocity (ω), cone angle (α) and radius (r). Values typically used by us are boxed. (b) Shear stress varies along the radius and can be calculated from the media's viscosity (μ), the angular velocity (ω), cone angle (α), gap height (h), and radius (r). Values typically used by us are boxed.

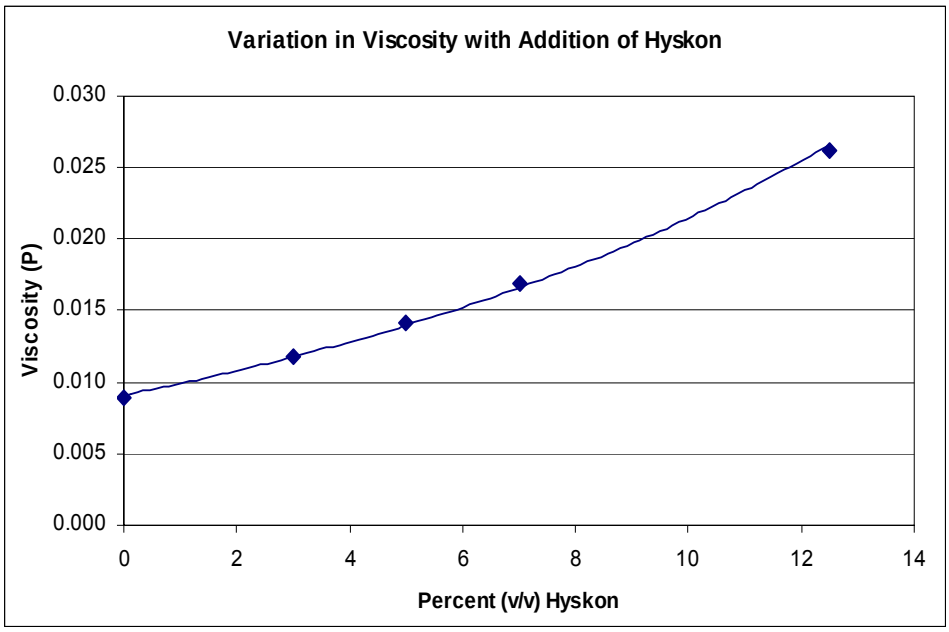

Figure 4.4. Addition of Hyskon increases the viscosity of shear media. Varying percentages of Hyskon were added to shear media and the viscosity of each solution was measured. (Contributed by Sarah E. Coleman)

parameter increases, but also practical reasons such as media evaporation. Our other option was to increase the viscosity of the shear media. Hyskon, a solution of 32% dextran-70 in 10% dextrose, has been used previously to do this. As shown in Figure 4.4, Hyskon increases the viscosity of the shear media significantly. We chose to use 5% (v/v) Hyskon which increased the viscosity of the shear media by roughly 50%.

Shown in Figure 4.5 are values for both unidirectional flow and oscillatory flow in the 35-mm system. As noted before, the Reynolds-like parameter, shown in (a), varies radially and is much less than 1 for both types of flow, indicating the predominance of viscous forces in the azimuthal direction. Shear stress also varies radially, as depicted in (b). In unidirectional laminar flow, the majority of cells see a physiologic level of shear stress of 15-20 dyn/cm^2. In oscillatory flow, most cells see a maximum shear stress of 5 dyn/cm^2 during each 1 Hz cycle.

To validate the use of the 35-mm system, we looked at both cell morphology and protein expression of HUVEC which are widely used in shear stress studies. Endothelial cells characteristically align in the direction of flow. As shown in 4.6(a), a typical cobblestone pattern can be seen in the static and oscillatory shear conditions for both the 10-cm and 35-mm systems. Under laminar shear, the cells aligned in the direction of flow for both systems. eNOS is phosphorylated at serine 1177 by laminar shear stress. [52] We detected this phosphorylation by laminar shear stress in both the 10-cm and 35-mm shear systems, as shown in Figure 4.6(b).

(a)

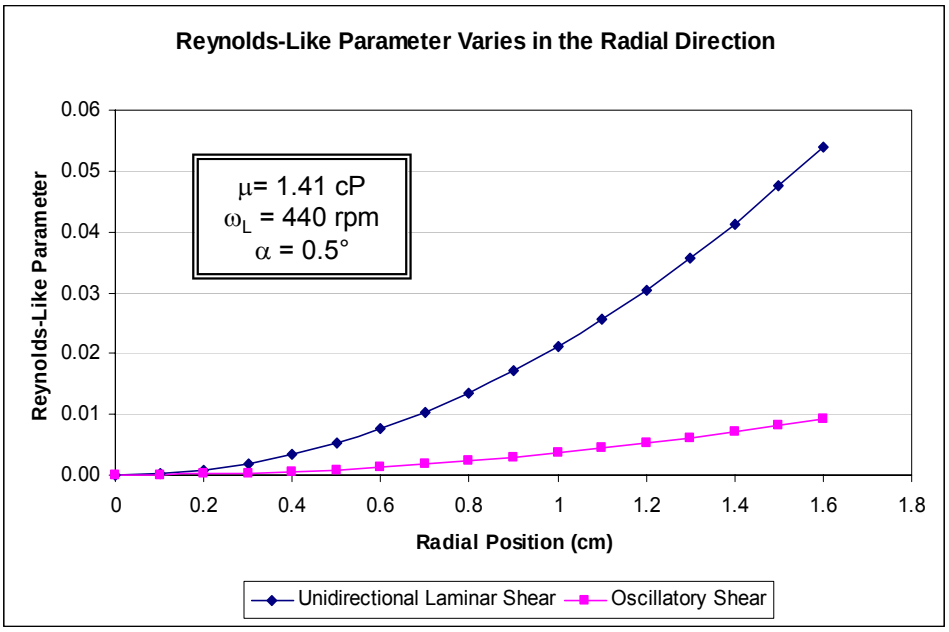

(b)

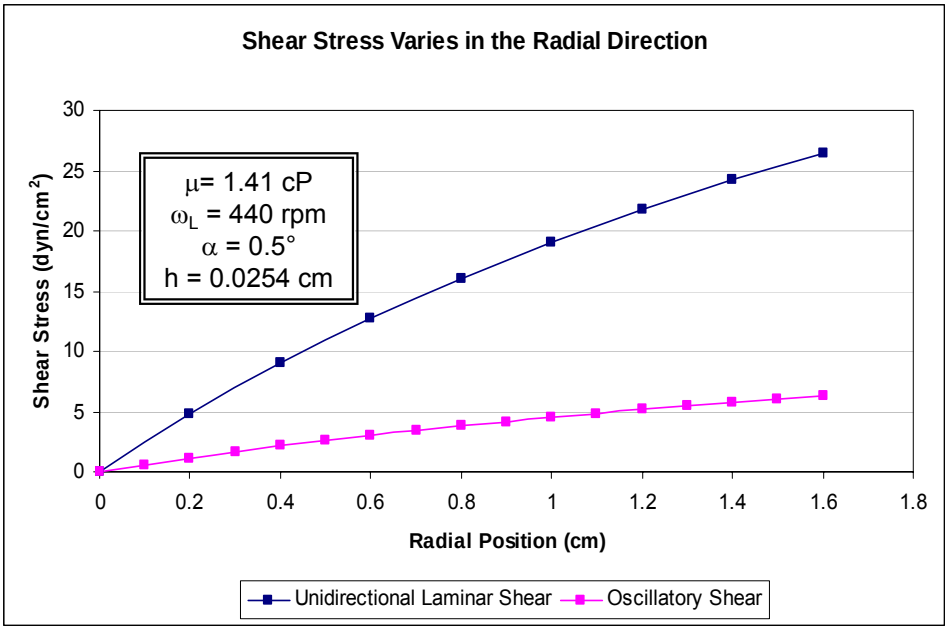

Figure 4.5. Reynolds-like parameter and shear stress distribution in a 35-mm cone-and-plate apparatus. (a) Reynolds-like parameter, an indicator of the relative dominance of viscous forces, varies along the radius and can be calculated from the media's viscosity (μ), the angular velocity (ω), cone angle (α) and radius (r). Values typically used by us are boxed. (b) Shear stress varies along the radius and can be calculated from the media's viscosity (μ), the angular velocity (ω), cone angle (α), gap height (h), and radius (r). Values typically used by us are boxed.

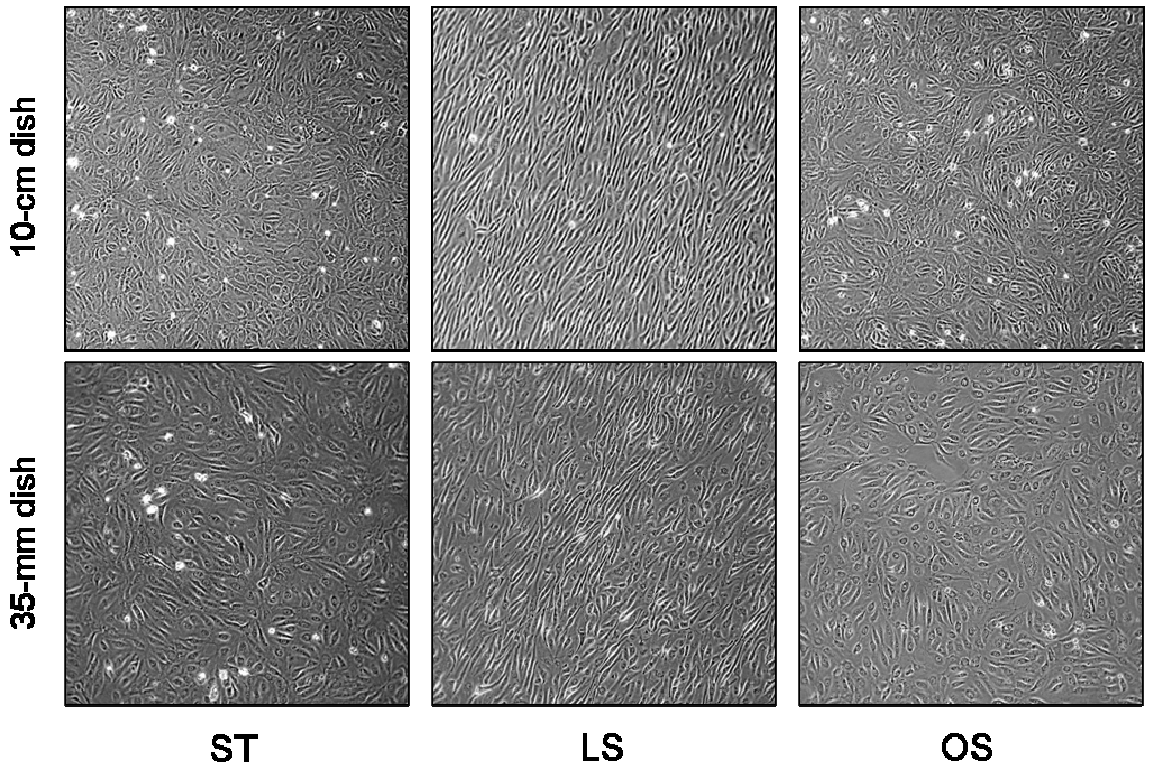

(b)

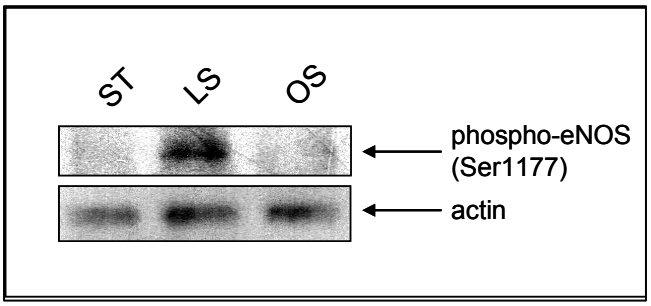

Figure 4.6. HUVEC respond to laminar shear in both 10-cm and 35-mm cone-and-plate systems. (a) HUVEC were grown to confluent monolayers in either 10-cm or 35-mm culture dishes. They were then exposed to either static conditions (ST), unidirectional laminar shear (LS), or oscillatory shear (OS) for 24 hours. 5% Hyskon was added to the media for cells in 35-mm dishes to achieve an equivalent shear stress level. Following shear exposure, the cells were photographed under a phase contrast microscope. A typical cobblestone pattern can be seen in the static and oscillatory shear conditions. Under laminar shear, however, HUVEC aligned in the direction of flow in both the 10-cm and 35-mm dishes. Furthermore, as shown in (b), the cells eNOS was phosphorylated after shear exposure in 35-mm dishes.

We next exposed both types of LDL-positive primary MAEC, MAE-WT and MAE-p47, to shear in the 35-mm system. Both cell types aligned under laminar shear stress but did not align under oscillatory shear stress. This is shown in Figure 4.7. Given batch-to-batch variability in cell purity, samples used in further analyses, including microarray analyses, were screened by real-time PCR for down-regulation by OS of Kruppel-like factor 2 (Klf2) and eNOS, two well-established shear-sensitive genes.

We also exposed both types of LDL-positive immortalized MAEC, iMAE-WT and iMAE-p47, to shear in the 10-cm system. Both cell types aligned under laminar shear stress but not under oscillatory shear stress, as shown in Figure 4.8.

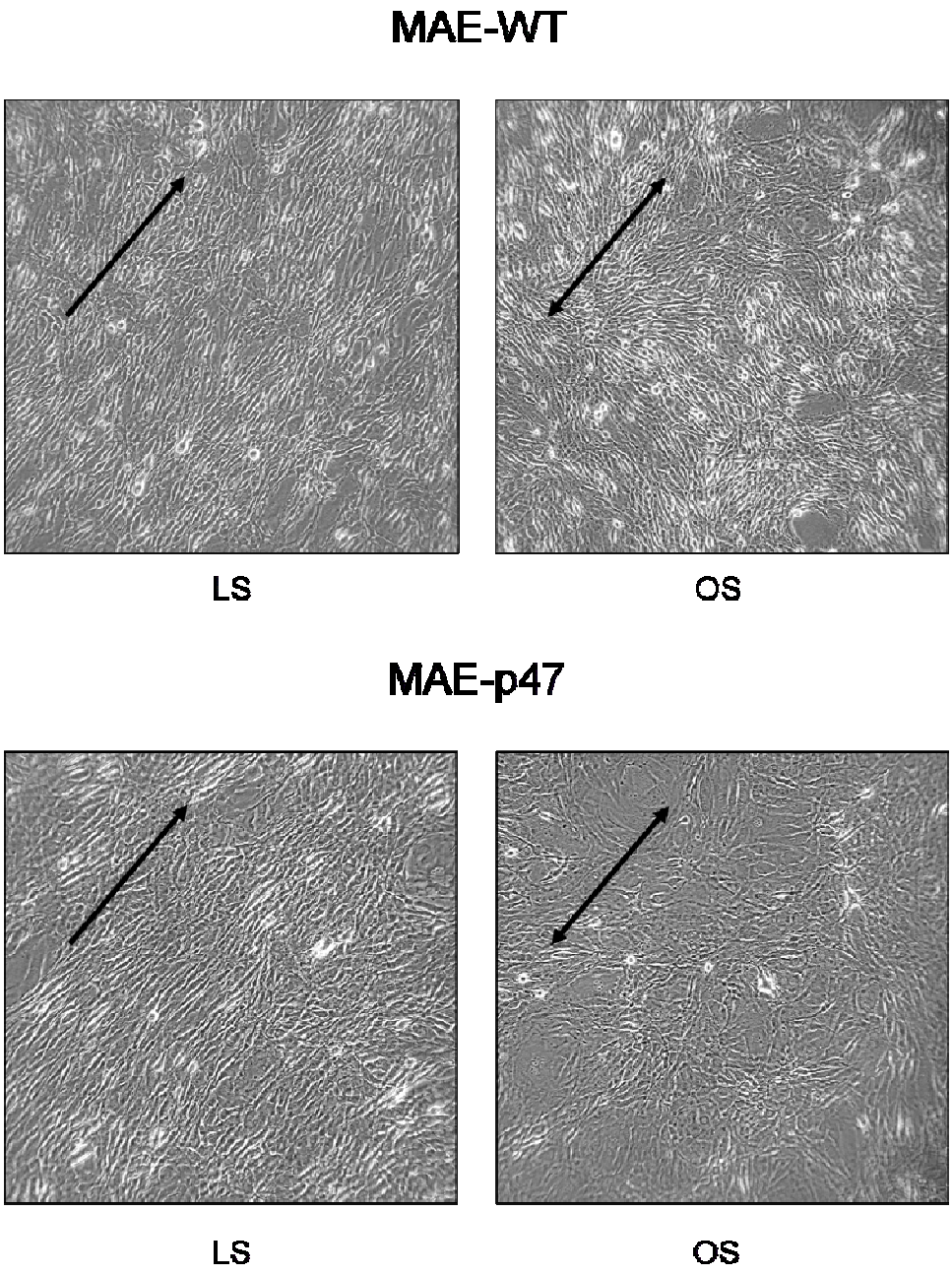

Figure 4.7. MAEC align in the direction of laminar shear but not oscillatory shear. MAE-WT and MAE-p47 were grown to confluence in 35-mm culture dishes. They were then exposed to either laminar shear (LS) or oscillatory (OS) for 24 hours. 5% Hyskon was added to the media to achieve average laminar shear stress values of 15-20 dyn/cm^2 and oscillatory shear stress values of ±5 dyn/cm^2.

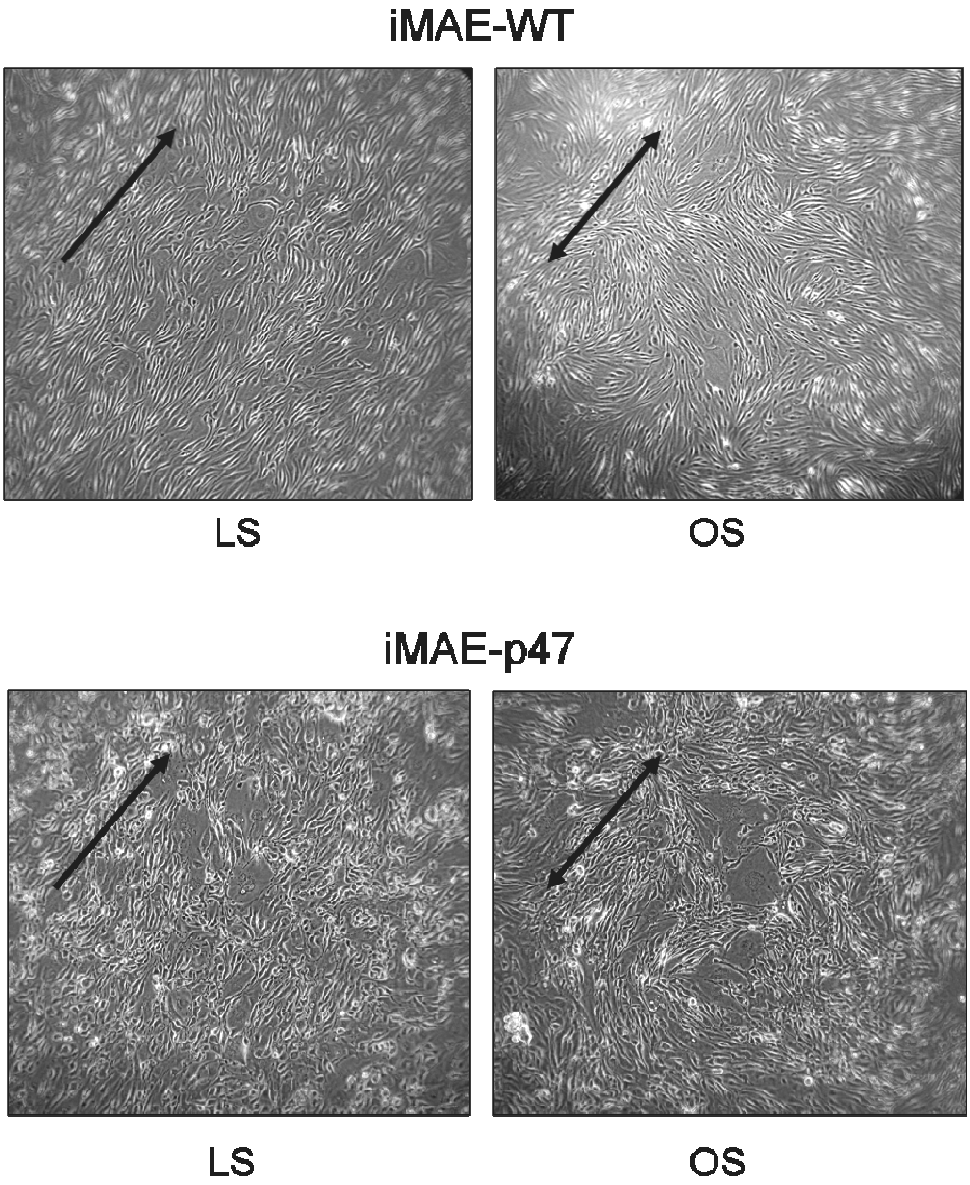

Figure 4.8. iMAEC align in the direction of laminar shear but not oscillatory shear. iMAE-WT and iMAE-p47 were grown to confluence in 10-cm culture dishes. They were then exposed to either laminar shear (LS) or oscillatory (OS) for 24 hours. Both cell types aligned in the direction of flow with LS but did not align with OS.

Shear Stress Alters Global Gene Expression Profiles of MAE-WT and MAE-p47

To determine which shear responses were p47phox-dependent, we analyzed total RNAs obtained from MAE-WT and MAE-p47 that were exposed to LS or OS for 1 day each by using Affymetrix microarrays. In our statistical analysis we used the following criteria: p-value < 0.03 and fold change (O/L) ≤ 0.66 or ≥ 1.52. We determined the number of mechanosensitive genes in each cell type, as shown in Figure 4.9, which shows the number of genes up- or down-regulated by OS in comparison to LS in MAE-WT and MAE-p47. 126 genes were down-regulated in only MAE-WT but not MAE-p47. 211 genes were down-regulated in only MAE-p47 but not MAE-WT. 22 genes were down-regulated in both MAE-WT and MAE-p47. 38 genes were up-regulated in only MAE-WT but not MAE-p47. 64 genes were up-regulated in only MAE-p47 but not MAE-WT. One gene was up-regulated in both MAE-WT and MAE-p47.

The Gene Expression Dynamics Inspector (GEDI) was used to analyze the global gene expression patterns. This program uses a self-organizing map (SOM) algorithm to identify clusters of genes and to group them into tiles within a mosaic. We used GEDI to analyze gene expression data from MAE-WT and MAE-p47. The resulting mosaics or maps are shown in Figure 4.10. The map on the left represents gene expression changes in MAE-WT. The map to the right of this represents gene expression changes in MAE-p47. There are similar patterns of global gene expression across the mosaics. However, there are distinct areas that are more or less intense in one of the two cell types, indicating genes whose shear response may be p47phox-dependent.

Established genes that were shear-sensitive in MAEC are shown in Tables 5.2 through 5.4. Table 5.2 lists genes that were changed by OS significantly in both cell types. Note that one gene, Rest, was changed by OS significantly but in opposite directions in MAE-WT and MAE-p47. Table 5.3 lists genes that were changed by OS significantly in only MAE-WT. Table 5.4 lists genes that were changed by OS significantly in only MAE-p47.

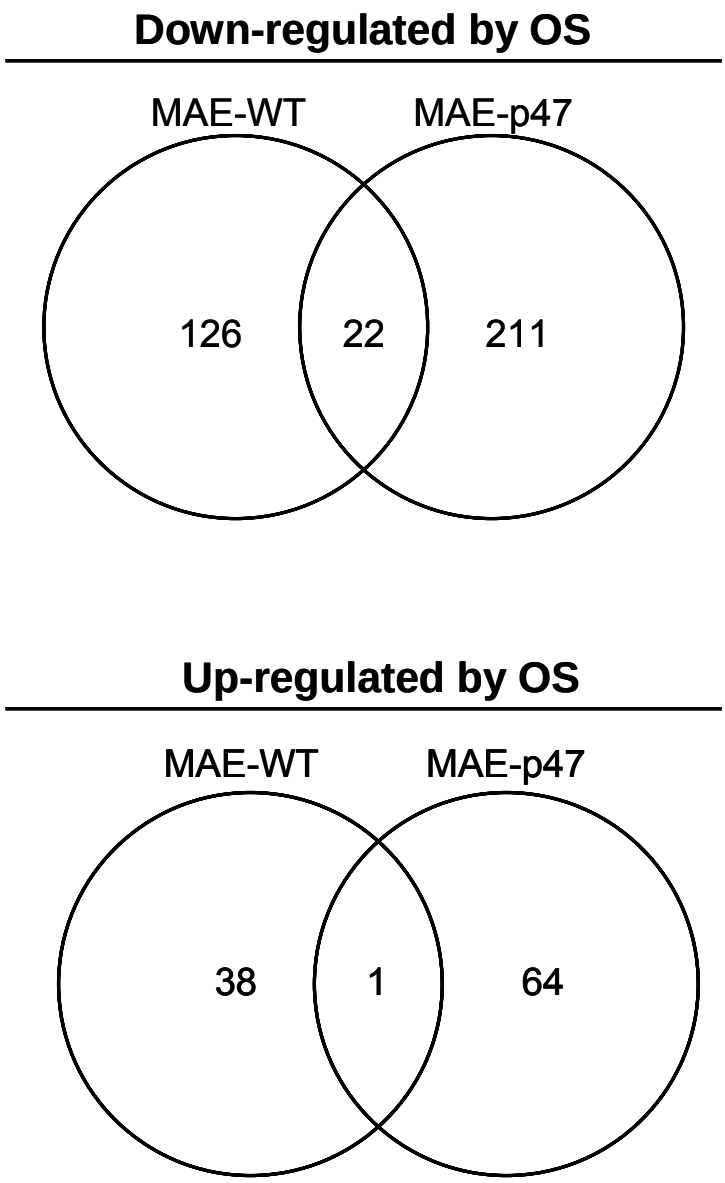

Figure 4.9. Genes regulated by OS in MAE-WT and MAE-p47. Shown above are Venn diagrams representing the number of genes changing in response to OS (compared to LS). The top Venn diagram depicts genes that were down-regulated by OS. 126 genes were down-regulated in only MAE-WT but not MAE-p47. 211 genes were down-regulated in only MAE-p47 but not MAE-WT. 22 genes were down-regulated in both MAE-WT and MAE-p47. The bottom Venn diagram depicts genes that were up-regulated by OS. 38 genes were up-regulated in only MAE-WT but not MAE-p47. 64 genes were up-regulated in only MAE-p47 but not MAE-WT. One gene was up-regulated in both MAE-WT and MAE-p47.

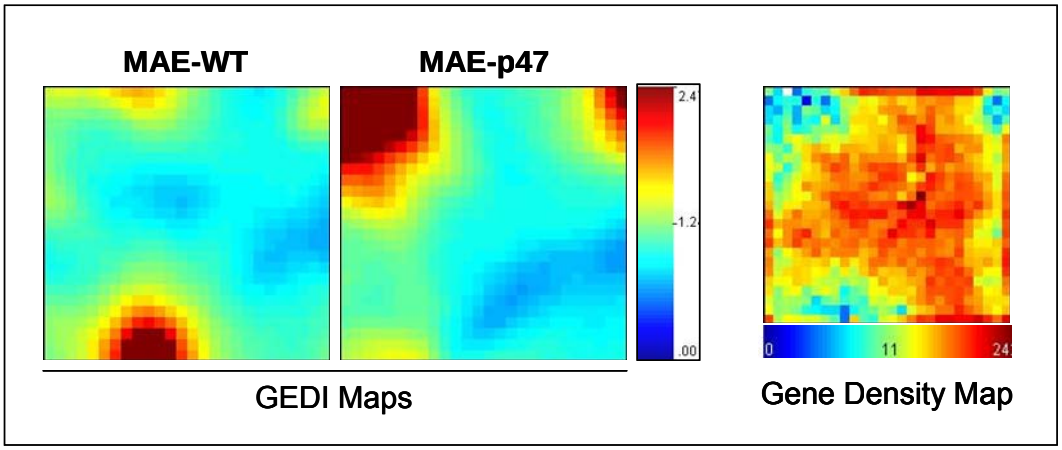

Figure 4.10. GEDI analysis of microarray results. Expression fold changes (O/L) for each batch of cells were loaded into the Gene Expression Dynamics Inspector (GEDI). After organization by a self-organizing map (SOM) algorthim, expression fold changes were averaged for each cell type, MAE-WT and MAE-p47. Shown on the left is the mosaic for MAE-WT. To the right of this is the mosaic for MAE-p47. Each tile in these mosaics is identical between MAE-WT and MAE-p47 and represents a cluster of genes. The color of each tile indicates the average fold change in response to OS, corresponding to the scale to the right of these maps. To the far right of the figure is the gene density map which indicates how many genes are located in each tile of the mosaic.

Table 5.2. Genes changing significantly by OS in both MAE-WT and MAE-p47

		MAE-WT		MAE-p47	
Accession No.	Gene Description	O/L	p-value	O/L	p-value
NM_008452	Kruppel-like factor 2 (lung) (Klf2)	0.24	0.00	0.31	0.00
NM_007483	ras homolog gene family, member B (Rhob)	0.35	0.00	0.50	0.00
NM_007553	bone morphogenetic protein 2 (Bmp2)	0.37	0.01	0.35	0.00
NM_019471	matrix metallopeptidase 10 (Mmp10)	0.41	0.00	0.40	0.01
NM_009063	regulator of G-protein signaling 5 (Rgs5)	0.41	0.01	0.38	0.00
NM_018781	early growth response 3 (Egr3)	0.42	0.02	0.31	0.00
NM_177715	potassium channel tetramerisation domain containing 12 (Kctd12)	0.43	0.02	0.64	0.01
NM_019496	Alport syndrome, mental retardation, midface hypoplasia and elliptocytosis chromosomal region gene 1 (Ammecr1)	0.48	0.03	0.57	0.00
NM_015806	mitogen-activated protein kinase 6 (Mapk6)	0.51	0.00	0.56	0.00
NM_053169	tripartite motif protein 16 (Trim16)	0.51	0.01	0.42	0.00
NG_001395	high mobility group AT-hook 2, pseudogene 1 (Hmga2-ps1)	0.51	0.02	0.65	0.03
NM_013657	semaphorin 3C (Sema3c)	0.52	0.00	0.34	0.00
NM_001037987	EGF-like repeats and discoidin I-like domains 3 (Edil3)	0.53	0.00	0.36	0.01
NM_001002268	G protein-coupled receptor 126 (Gpr126)	0.54	0.01	0.38	0.02
NM_010016	CD55 antigen (Cd55)	0.56	0.00	0.60	0.01
NM_013458	adducin 2 (beta) (Add2)	0.57	0.00	0.56	0.03
NM_008982	protein tyrosine phosphatase, receptor type J (Ptprj)	0.58	0.01	0.65	0.00
NM_001025570	paired related homeobox 1 (Prrx1)	0.64	0.01	0.52	0.00
NM_018869	G protein-coupled receptor kinase 5 (Gprk5)	0.65	0.01	0.61	0.00
NM_011738	tyrosine 3-monooxygenase/tryptophan 5-monooxygenase activation protein, eta polypeptide (Ywhah)	0.65	0.01	0.64	0.01
NM_173739	UDP-N-acetyl-alpha-D-galactosamine:polypeptide N-acetylgalactosaminyltransferase-like 4 (Galntl4)	0.65	0.01	0.36	0.00
NM_011200	protein tyrosine phosphatase 4a1 (Ptp4a1)	0.66	0.03	0.60	0.00
NM_031843	dipeptidylpeptidase 7 (Dpp7)	1.58	0.01	1.59	0.00
NM_011263	RE1-silencing transcription factor (Rest)	0.55	0.00	1.73	0.03

Table 5.3. Genes changing significantly by OS in only MAE-WT

		MAE-WT	
Accession No.	Gene Description	O/L	p-value
NM_013473	annexin A8 (Anxa8)	0.30	0.00
NM_007974	coagulation factor II (thrombin) receptor-like 1 (F2rl1)	0.30	0.00
NM_023653	wingless-related MMTV integration site 2 (Wnt2)	0.36	0.01
NM_007722	chemokine (C-X-C motif) receptor 7 (Cmkor1)	0.38	0.02
NM_198247	SERTA domain containing 4 (Sertad4)	0.39	0.02
NM_010200	fibroblast growth factor 13 (Fgf13)	0.41	0.01
NM_026639	ADP-ribosyltransferase 4 (Art4)	0.43	0.00
NM_010929	Notch gene homolog 4 (Drosophila) (Notch4)	0.44	0.00
NM_021389	SH3-domain kinase binding protein 1 (Sh3kbp1)	0.45	0.00
NM_023844	junction adhesion molecule 2 (Jam2)	0.45	0.01
NM_007743	collagen, type I, alpha 2 (Col1a2)	0.46	0.03
NM_010217	connective tissue growth factor (Ctgf)	0.46	0.01
NM_007389	cholinergic receptor, nicotinic, alpha polypeptide 1 (Chrna1)	0.47	0.00
NM_007626	chromobox homolog 5 (Drosophila HP1a) (Cbx5)	0.48	0.00
NM_028712	RAP2B, member of RAS oncogene family (Rap2b)	0.49	0.01
NM_011782	a disintegrin-like and metallopeptidase with thrombospondin type 1 motif, 5 (Adamts5)	0.49	0.01
NM_145962	pantothenate kinase 3 (Pank3)	0.49	0.02
NM_007735	collagen, type IV, alpha 4 (Col4a4)	0.50	0.03
NM_010728	lysyl oxidase (Lox)	0.50	0.00
NM_013496	cellular retinoic acid binding protein I (Crabp1)	0.50	0.02
NM_054043	Musashi homolog 2 (Drosophila) (Msi2)	0.50	0.01
NM_010476	hydroxysteroid (17-beta) dehydrogenase 7 (Hsd17b7)	0.51	0.01
NM_001043355	microtubule-associated protein 6 (Mtap6)	0.51	0.00
NM_054044	G protein-coupled receptor 124 (Gpr124)	0.51	0.01
NM_145611	ankyrin repeat domain 25 (Ankrd25)	0.52	0.01
NM_015776	microfibrillar associated protein 5 (Mfap5)	0.52	0.00
NM_010637	Kruppel-like factor 4 (gut) (Klf4)	0.52	0.01
NM_008441	kinesin family member 1B (Kif1b)	0.53	0.01
NM_023279	tubulin, beta 3 (Tubb3)	0.53	0.01
NM_130450	ELOVL family member 6, elongation of long chain fatty acids (yeast) (Elovl6)	0.53	0.02
NM_054042	CD248 antigen, endosialin (Cd248)	0.53	0.00
NM_145360	isopentenyl-diphosphate delta isomerase (Idi1)	0.53	0.02
NM_009338	acetyl-Coenzyme A acetyltransferase 2 (Acat2)	0.54	0.02
NM_026784	phosphomevalonate kinase (Pmvk)	0.54	0.00
NM_019552	ATP-binding cassette, sub-family B (MDR/TAP), member 10 (Abcb10)	0.54	0.01
XM_619639	tensin 1 (Tns1)	0.55	0.00
XM_001004940	ATP-binding cassette, sub-family A (ABC1), member 13 (Abca13)	0.55	0.01
NM_026772	CDC42 effector protein (Rho GTPase binding) 2 (Cdc42ep2)	0.55	0.01
NM_146006	Lanosterol synthase (Lss)	0.55	0.03
NM_010516	cysteine rich protein 61 (Cyr61)	0.56	0.01
NM_010941	NAD(P) dependent steroid dehydrogenase-like (Nsdhl)	0.56	0.02
NM_007477	ADP-ribosylation factor 2 (Arf2)	0.56	0.00
NM_001033713	similar to Myocyte enhancer factor 2A (Mef2a)	0.56	0.01
NM_026743	tetraspanin 11 (Tspan11)	0.56	0.01
NM_026416	S100 calcium binding protein A16 (S100a16)	0.57	0.00
NM_009260	spectrin beta 2 (Spnb2)	0.57	0.01
NM_020010	cytochrome P450, family 51 (Cyp51)	0.57	0.01
NM_173440	nuclear receptor interacting protein 1 (Nrip1)	0.57	0.01
NM_027164	leucine rich repeat containing 27 (Lrrc27)	0.58	0.00
NM_145942	3-hydroxy-3-methylglutaryl-Coenzyme A synthase 1 (Hmgcs1)	0.58	0.03
NM_015800	cysteine rich transmembrane BMP regulator 1 (chordin like) (Crim1)	0.58	0.01
NM_028778	NUAK family, SNF1-like kinase, 2 (Nuak2)	0.58	0.01
NM_010448	Alanine-glyoxylate aminotransferase 2-like 2 (Hnrpab)	0.58	0.03
NM_010700	low density lipoprotein receptor (Ldlr)	0.58	0.02
NM_008433	potassium intermediate/small conductance calcium-activated channel, subfamily N, member 4 (K	0.58	0.03
NM_138741	serum deprivation response (Sdpr)	0.58	0.00
NM_009338	acetyl-Coenzyme A acetyltransferase 2 (Acat2)	0.59	0.02
NM_019819	dual specificity phosphatase 14 (Dusp14)	0.59	0.01
NM_013668	jumonji, AT rich interactive domain 1C (Rbp2 like) (Jarid1c)	0.59	0.02
NM_007496	zinc finger homeobox 3 (Atbf1)	0.59	0.00
NM_172769	sterol-C5-desaturase (fungal ERG3, delta-5-desaturase) homolog (S. cerevisae) (Sc5d)	0.59	0.02
NM_178615	RGM domain family, member B (Rgmb)	0.59	0.03
NM_029569	ankyrin repeat and SOCs box-containing protein 5 (Asb5)	0.59	0.02
NM_007715	circadian locomoter output cycles kaput (Clock)	0.59	0.01
NM_133774	StAR-related lipid transfer (START) domain containing 4 (Stard4)	0.59	0.03
NM_009154	semaphorin 5A (Sema5a)	0.59	0.00
NM_007413	adenosine A2b receptor (Adora2b)	0.59	0.01
NM_008396	integrin alpha 2 (Itga2)	0.60	0.02
NM_019827	glycogen synthase kinase 3 beta (Gsk3b)	0.60	0.00
NM_022023	glia maturation factor, beta (Gmfb)	0.60	0.03
NM_011052	programmed cell death 6 interacting protein (Pdcd6ip)	0.60	0.01

Table 5.3. continued

		MAE-WT	
Accession No.	**Gene Description**	**O/L**	**p-value**
NM_007896	microtubule-associated protein, RP/EB family, member 1 (Mapre1)	0.60	0.03
NM_008813	ectonucleotide pyrophosphatase/phosphodiesterase 1 (Enpp1)	0.60	0.03
NM_001039373	mature T-cell proliferation 1 (Mtcp1)	0.60	0.00
NM_007841	DEAD (Asp-Glu-Ala-Asp) box polypeptide 6 (Ddx6)	0.61	0.03
XM_001000931	ring finger and CCCH-type zinc finger domains 2 (Mnab)	0.61	0.00
NM_010284	growth hormone receptor (Ghr)	0.61	0.00
NM_028870	clathrin, light polypeptide (Cltb)	0.61	0.00
NM_019765	CAP-GLY domain containing linker protein 1 (Rsn)	0.61	0.02
NM_021881	quaking (Qk)	0.62	0.00
NM_172266	lysophosphatidylglycerol acyltransferase 1 (Lpgat1)	0.62	0.02
NM_001025372	adenylate cyclase activating polypeptide 1 receptor 1 (Adcyap1r1)	0.62	0.01
NM_009128	stearoyl-Coenzyme A desaturase 2 (Scd2)	0.62	0.00
NM_177282	microtubule associated monoxygenase, calponin and LIM domain containing 2 (Mical2)	0.62	0.01
NM_013635	synaptophysin-like protein (Sypl)	0.62	0.01
NM_009616	a disintegrin and metallopeptidase domain 19 (Adam19)	0.62	0.01
NM_029891	NF-kappaB repressing factor (Nkrf)	0.62	0.02
NM_028493	Rho-related BTB domain containing 3 (Rhobtb3)	0.62	0.02
NM_019978	doublecortin-like kinase 1 (Dcamkl1)	0.62	0.01
NM_009457	ubiquitin-like modifier activating enzyme 1 (Ube1x)	0.62	0.01
NM_146001	huntingtin interacting protein 1 (Hip1)	0.62	0.01
NM_146191	leucine-rich repeat kinase 1 (Lrrk1)	0.62	0.03
NM_015771	large tumor suppressor 2 (Lats2)	0.62	0.00
NM_025629	ADAMTS-like 5 (Adamtsl5)	0.63	0.00
NM_133656	v-crk sarcoma virus CT10 oncogene homolog (avian) (Crk)	0.63	0.03
NM_028454	transmembrane 7 superfamily member 2 (Tm7sf2)	0.63	0.00
NM_028785	dedicator of cytokinesis 8 (Dock8)	0.63	0.01
NM_024436	RAB22A, member RAS oncogene family (Rab22a)	0.64	0.00
NM_022410	myosin, heavy polypeptide 9, non-muscle (Myh9)	0.64	0.01
NM_144530	zinc finger CCCH type containing 11A (Zc3h11a)	0.64	0.02
NM_016780	integrin beta 3 (Itgb3)	0.64	0.00
NM_018807	pleiomorphic adenoma gene-like 2 (Plagl2)	0.64	0.01
NM_001025163	zinc finger protein 78 (Zfp78)	0.64	0.01
NM_010124	eukaryotic translation initiation factor 4E binding protein 2 (Eif4ebp2)	0.64	0.01
NM_198702	latrophilin 3 (Lphn3)	0.64	0.03
NM_001013833	protein kinase, cGMP-dependent, type I (Prkg1)	0.65	0.00
NM_199476	ribonucleotide reductase M2 B (TP53 inducible) (Rrm2b)	0.65	0.01
XM_283153	polymerase (RNA) III (DNA directed) polypeptide G (Polr3g)	0.65	0.00
NM_029810	5'-nucleotidase, cytosolic II (Nt5c2)	0.65	0.02
NM_198023	REST corepressor 1 (Rcor1)	0.65	0.02
NM_008453	Kruppel-like factor 3 (Klf3)	0.65	0.01
NM_145979	chromodomain helicase DNA binding protein 4 (Chd4)	0.65	0.03
NM_027504	PR domain containing 16 (Prdm16)	0.65	0.01
NM_013720	MAX gene associated (Mga)	0.65	0.00
NM_030249	CTTNBP2 N-terminal like (Cttnbp2nl)	0.65	0.00
NM_007561	bone morphogenic protein receptor, type II (serine/threonine kinase) (Bmpr2)	0.65	0.00
NM_010271	glycerol-3-phosphate dehydrogenase 1 (soluble) (Gpd1)	0.66	0.00
NM_001039179	bicaudal D homolog 2 (Drosophila) (Bicd2)	0.66	0.01
NM_019699	fatty acid desaturase 2 (Fads2)	0.66	0.03
NM_010129	epithelial membrane protein 3 (Emp3)	0.66	0.00
NM_207659	hook homolog 3 (Drosophila) (Hook3)	0.66	0.00
NM_023233	tripartite motif protein 13 (Trim13)	0.66	0.02
NM_009730	attractin (Atrn)	0.66	0.01
NM_153143	potassium channel tetramerisation domain containing 11 (Kctd11)	0.66	0.03
NM_145624	zinc finger protein 709 (Zfp709)	0.66	0.00
NM_177806	PRP39 pre-mRNA processing factor 39 homolog (yeast) (Prpf39)	1.53	0.03
NM_026573	UPF3 regulator of nonsense transcripts homolog B (yeast) (Upf3b)	1.53	0.03
NM_172668	low density lipoprotein receptor-related protein 4 (Lrp4)	1.53	0.03
NM_030714	deltex 3 homolog (Drosophila) (Dtx3)	1.53	0.01
NM_001039515	ADP-ribosylation factor-like 4A (Arl4a)	1.54	0.01
NM_177368	transmembrane and tetratricopeptide repeat containing 2 (Tmtc2)	1.55	0.01
XM_133655	autophagy related 16 like 2 (S. cerevisiae) (Atg16l2)	1.56	0.03
NM_029688	sulfiredoxin 1 homolog (S. cerevisiae) (Srxn1)	1.58	0.03
NM_001033954	calcitonin/calcitonin-related polypeptide, alpha (Calca)	1.59	0.03
NM_028002	dihydrouridine synthase 4-like (S. cerevisiae) (Dus4l)	1.61	0.01
/// NM_133723	aspartate-beta-hydroxylase (Asph)	1.61	0.01
NM_011158	protein kinase, cAMP dependent regulatory, type II beta (Prkar2b)	1.61	0.01
NM_177462	zinc finger, MYM-type 6 (Zmym6)	1.62	0.02
NM_011665	ubiquitin-conjugating enzyme E2I	1.62	0.00
NM_013931	mitogen-activated protein kinase 8 interacting protein 3 (Mapk8ip3)	1.63	0.03
NM_175121	solute carrier family 38, member 2 (Slc38a2)	1.64	0.01
NM_027184	inositol polyphosphate multikinase (Ipmk)	1.64	0.00

Table 5.3. continued

		MAE-WT	
Accession No.	**Gene Description**	**O/L**	**p-value**
NM_009863	cell division cycle 7 (S. cerevisiae) (Cdc7)	1.66	0.00
NM_008902	placental protein 11 related (Pp11r)	1.70	0.00
NM_145429	arrestin, beta 2 (Arrb2)	1.72	0.03
NM_011229	RAB5B, member RAS oncogene family (Rab5b)	1.74	0.03
NM_181391	Coiled-coil-helix-coiled-coil-helix domain containing 7 (Chchd7)	1.75	0.02
NM_027057	WD repeat and FYVE domain containing 1 (Wdfy1)	1.76	0.01
NM_018881	flavin containing monooxygenase 2 (Fmo2)	1.79	0.01
NM_030203	TSPY-like 4 (Tspyl4)	1.82	0.02
NM_009458	ubiquitin-conjugating enzyme E2B, RAD6 homology (S. cerevisiae) (Ube2b)	1.83	0.03
NM_010724	proteasome subunit, beta type 8 (large multifunctional peptidase 7) (Psmb8)	1.84	0.02
NM_026574	INO80 complex homolog 1 (S. cerevisiae) (Inoc1)	1.86	0.03
NM_016906	Sec61 alpha 1 subunit (S. cerevisiae) (Sec61a1)	1.90	0.03
NM_020271	pyridoxal (pyridoxine, vitamin B6) phosphatase (Pdxp)	1.92	0.00
NM_001033178	transmembrane protein 181 (Tmem181) (Gpr178)	1.94	0.00
XM_487363	filamin, beta (Flnb)	1.97	0.02
NM_019926	X-linked myotubular myopathy gene 1 (Mtm1)	1.99	0.03
NM_001040686	zinc finger protein 692 (Zfp692)	2.05	0.02
NM_053177	mucolipin 1 (Mcoln1)	2.08	0.02
NM_019511	receptor (calcitonin) activity modifying protein 3 (Ramp3)	2.10	0.03
NM_011018	sequestosome 1 (Sqstm1)	2.33	0.03
NM_178697	chloride channel calcium activated 5 (Clca5)	2.35	0.01
NM_009655	activated leukocyte cell adhesion molecule (Alcam)	2.97	0.03

Table 5.4. Genes changing significantly by OS in only MAE-p47

		MAE-p47	
Accession No.	Gene Description	O/L	p-value
NM_028122	solute carrier family 14 (urea transporter), member 1 (Slc14a1)	0.27	0.00
NM_019867	neuronal guanine nucleotide exchange factor (Ngef)	0.33	0.00
NM_021367	thymic stromal lymphopoietin (Tslp)	0.35	0.00
NM_008940	kallikrein related-peptidase 8 (Klk8)	0.35	0.00
NM_011990	solute carrier family 7 (cationic amino acid transporter, y+ system), member 11 (Slc7a11)	0.35	0.00
NM_010112	Embryonal Fyn-associated substrate (Efs)	0.36	0.01
NM_008115	glial cell line derived neurotrophic factor family receptor alpha 2 (Gfra2)	0.37	0.01
NM_011146	peroxisome proliferator activated receptor gamma (Pparg)	0.37	0.00
NM_008397	integrin alpha 6 (Itga6)	0.37	0.01
NM_008706	NAD(P)H dehydrogenase, quinone 1 (Nqo1)	0.39	0.01
NM_177794	transmembrane protein 26 (Tmem26)	0.39	0.00
NM_153546	membrane bound O-acyltransferase domain containing 1 (Mboat1)	0.40	0.00
NM_009510	ezrin /// hypothetical protein LOC100044177 (Vil2)	0.40	0.00
NM_173731	3-hydroxymethyl-3-methylglutaryl-Coenzyme A lyase-like 1 (Hmgcll1)	0.41	0.00
NM_009912	chemokine (C-C motif) receptor 1 (Ccr1)	0.42	0.00
NM_001025602	interleukin 1 receptor-like 1 (Il1rl1)	0.42	0.00
NM_026993	dimethylarginine dimethylaminohydrolase 1 (Ddah1)	0.42	0.01
NM_001033336	ATP-binding cassette, sub-family C (CFTR/MRP), member 4 (Abcc4)	0.43	0.00
NM_009112	S100 calcium binding protein A10 (calpactin) (S100a10)	0.43	0.00
NM_008576	ATP-binding cassette, sub-family C (CFTR/MRP), member 1 (Abcc1)	0.43	0.01
NM_011213	protein tyrosine phosphatase, receptor type, F (Ptprf)	0.44	0.00
NM_008181	glutathione S-transferase, alpha 1	0.44	0.03
NM_023256	keratin 20 (Krt20)	0.44	0.01
NM_177343	calcium/calmodulin-dependent protein kinase ID (Camk1d)	0.45	0.00
NM_001033149	tetratricopeptide repeat domain 9 (Ttc9)	0.45	0.00
NM_010607	potassium channel, subfamily K, member 2 (Kcnk2)	0.45	0.01
NM_013723	podocalyxin-like (Podxl)	0.45	0.03
NM_010577	integrin alpha 5 (fibronectin receptor alpha) (Itga5)	0.46	0.00
NM_010403	hydroxyacid oxidase 1, liver (Hao1)	0.47	0.00
NM_172621	chloride intracellular channel 5 (Clic5)	0.47	0.00
NM_010234	FBJ osteosarcoma oncogene (Fos)	0.48	0.01
NM_011807	discs, large homolog 2 (Drosophila) (Dlgh2)	0.48	0.02
NM_016969	myeloid-associated differentiation marker (Myadm)	0.49	0.03
NM_016719	growth factor receptor bound protein 14 (Grb14)	0.50	0.00
NM_001038621	RAB GTPase activating protein 1-like (Rabgap1l)	0.51	0.00
XM_355205	Ras association (RalGDS/AF-6) and pleckstrin homology domains 1 (Raph1)	0.51	0.00
XM_111244	cerebellar degeneration-related protein 2-like (Cdr2l)	0.51	0.01
NM_023117	cell division cycle 25 homolog B (S. pombe) (Cdc25b)	0.51	0.01
XM_001000829	tetratricopeptide repeat, ankyrin repeat and coiled-coil containing 2 (Tanc2)	0.51	0.02
NM_033444	Chloride intracellular channel 1 (Clic1)	0.51	0.02
NM_001033406	mutated in colorectal cancers (Mcc)	0.51	0.00
NM_031999	G protein-coupled receptor 137B (Gpr137b)	0.51	0.02
NM_153552	THO complex 1 (Thoc1)	0.51	0.03
NM_011518	spleen tyrosine kinase (Syk)	0.52	0.03
NM_025303	staufen (RNA binding protein) homolog 2 (Drosophila) (Stau2)	0.52	0.00
NM_018764	protocadherin 7 (Pcdh7)	0.52	0.02
NM_026647	zinc finger, DHHC domain containing 21 (Zdhhc21)	0.52	0.03
NM_178685	protocadherin 20 (Pcdh20)	0.52	0.01
XM_001000944	ATPase type 13A3 (Atp13a3)	0.52	0.03
NM_010617	kinesin family member 13A (Kif13a)	0.53	0.03
NM_029879	Regulator of G-protein signalling 7 binding protein (D13Bwg1146e)	0.53	0.00
NM_175502	transmembrane protein 74 (Tmem74)	0.53	0.01
NM_008967	prostaglandin I receptor (IP) (Ptgir)	0.53	0.03
NM_029595	phosphatidylethanolamine binding protein 2 (Pbp2)	0.53	0.03
NM_183315	cortexin 1 (Ctxn1)	0.53	0.01
NM_198114	diacylglycerol lipase, alpha (Nt5dc3)	0.53	0.00
XM_485383	protein tyrosine phosphatase, non-receptor type 3 (Ptpn3)	0.53	0.01
XM_001003344	protocadherin 9 (Pcdh9)	0.54	0.03
NM_008924	protein kinase, cAMP dependent regulatory, type II alpha (Prkar2a)	0.54	0.01
NM_178644	OAF homolog (Drosophila) (D9Ucla1)	0.54	0.00
NM_001003719	GTPase activating RANGAP domain-like 1 (Garnl1)	0.54	0.00
NM_133955	ras homolog gene family, member U (Rhou)	0.54	0.01
NM_008486	alanyl (membrane) aminopeptidase (Anpep)	0.54	0.00
NM_001024851	ankyrin repeat domain 34 (Ankrd34)	0.55	0.03
NM_016811	diacylglycerol kinase, alpha (Dgka)	0.55	0.00
NM_008708	N-myristoyltransferase 2 (Nmt2)	0.55	0.00
NM_011670	ubiquitin carboxy-terminal hydrolase L1 (Uchl1)	0.55	0.00
NM_009289	STE20-like kinase (yeast) (Slk)	0.55	0.01
NM_013472	annexin A6 (Anxa6)	0.55	0.02
NM_009477	uridine phosphorylase 1 (Upp1)	0.56	0.00
NM_019914	myeloid/lymphoid or mixed-lineage leukemia translocated to 11 (Mllt11)	0.56	0.01

Table 5.4. continued

		MAE-p47	
Accession No.	**Gene Description**	**O/L**	**p-value**
NM_153542	leucine rich repeat containing 20 (Lrrc20)	0.56	0.02
NM_026998	sorting nexin 6 (Snx6)	0.56	0.00
	mirror-image polydactyly gene 1 homolog (human) (Mipol1)	0.56	0.01
NM_173781	RAB6B, member RAS oncogene family (Rab6b)	0.56	0.01
NM_027641	sperm flagellar 1 (Spef1)	0.56	0.00
NM_007436	aldehyde dehydrogenase family 3, subfamily A1 (Aldh3a1)	0.56	0.03
NM_010664	keratin 18 (Krt18)	0.56	0.02
NM_009254	serine (or cysteine) peptidase inhibitor, clade B, member 6a (Serpinb6a)	0.56	0.00
NM_013871	mitogen-activated protein kinase 12 (Mapk12)	0.56	0.02
NM_021273	creatine kinase, brain (Ckb)	0.56	0.01
NM_001039194	apoptosis-inducing factor, mitochondrion-associated 2 (Amid)	0.56	0.01
NM_011607	tenascin C (Tnc)	0.57	0.00
NM_001001999	glycoprotein Ib, beta polypeptide (Gp1bb)	0.57	0.03
NM_001024716	TRIO and F-actin binding protein (Triobp)	0.57	0.01
NM_011843	membrane bound C2 domain containing protein (Mbc2)	0.57	0.00
NM_007855	twist homolog 2 (Drosophila) (Twist2)	0.57	0.03
NM_008380	inhibin beta-A (Inhba)	0.57	0.00
NM_011535	T-box 3 (Tbx3)	0.58	0.00
NM_011756	zinc finger protein 36 (Zfp36)	0.58	0.00
NM_028030	RNA binding protein with multiple splicing 2 (Rbpms2)	0.58	0.00
NM_008702	nemo like kinase (Nlk)	0.58	0.01
NM_029352	dual specificity phosphatase 9 (Dusp9)	0.58	0.01
NM_001033439	leucine-rich repeats and calponin homology (CH) domain containing 1 (Lrch1)	0.58	0.03
NM_009285	stanniocalcin 1 (Stc1)	0.58	0.01
NM_013813	erythrocyte protein band 4.1-like 3 (Epb4.1l3)	0.58	0.00
XM_897426	rhotekin 2 (Plekhk1)	0.58	0.02
NM_001042513	thioredoxin reductase 1 (Txnrd1)	0.58	0.02
NM_026331	solute carrier family 25, member 37 (Slc25a37)	0.58	0.01
NM_013569	potassium voltage-gated channel, subfamily H (eag-related), member 2 (Kcnh2)	0.59	0.00
NM_021454	CDC42 effector protein (Rho GTPase binding) 5 (Cdc42ep5)	0.59	0.02
NM_007929	epithelial membrane protein 2 (Emp2)	0.59	0.03
NM_008258	hematological and neurological expressed sequence 1 (Hn1)	0.60	0.01
NM_001039103	RAS p21 protein activator 4 (Rasa4)	0.60	0.00
NM_153552	THO complex 1 (Thoc1)	0.60	0.02
NM_007763	cysteine-rich protein 1 (intestinal) (Crip1)	0.60	0.00
NM_016900	caveolin 2 (Cav2)	0.60	0.03
NM_011923	angiopoietin-like 2 (Angptl2)	0.60	0.03
XM_126489	forkhead box K2 (Foxk2)	0.60	0.01
NM_009072	Rho-associated coiled-coil containing protein kinase 2 (Rock2)	0.60	0.00
NM_013641	prostaglandin E receptor 1 (subtype EP1) (Ptger1)	0.60	0.00
NM_008851	phosphatidylinositol membrane-associated 1 (Pitpnm1)	0.60	0.00
NM_175274	tweety homolog 3 (Drosophila) (Ttyh3)	0.60	0.00
NM_008113	Rho GDP dissociation inhibitor (GDI) gamma (Arhgdig)	0.60	0.00
NM_153162	thioredoxin reductase 3 (Txnrd3)	0.60	0.03
NM_172684	rosbin, round spermatid basic protein 1 (Rsbn1)	0.60	0.01
NM_017368	CUG triplet repeat, RNA binding protein 1 (Cugbp1)	0.61	0.00
NM_173414	LanC lantibiotic synthetase component C-like 3 (bacterial) (Lancl3)	0.61	0.03
NM_020493	serum response factor (Srf)	0.61	0.02
NM_010344	glutathione reductase 1 (Gsr)	0.61	0.01
NM_134122	nurim (nuclear envelope membrane protein) (Nrm)	0.61	0.02
NM_009047	rad and gem related GTP binding protein 1 (Rem1)	0.61	0.01
NM_001035228	ST3 beta-galactoside alpha-2,3-sialyltransferase 5 (St3gal5)	0.61	0.00
NM_133348	acyl-CoA thioesterase 7 (Acot7)	0.61	0.00
NM_020593	F-box protein 3 (Fbxo3)	0.61	0.00
NM_016856	cleavage and polyadenylation specific factor 2 (Cpsf2)	0.62	0.03
NM_001017968	zinc finger, DHHC domain containing 18 /// similar to ribosomal protein L29 (Zdhhc18)	0.62	0.01
NM_013565	integrin alpha 3 (Itga3)	0.62	0.00
NM_008442	kinesin family member 2A (Kif2a)	0.62	0.00
NM_013476	androgen receptor (Ar)	0.62	0.00
NM_153103	kinesin family member 1C (Kif1c)	0.62	0.00
XM_486103	sorbin and SH3 domain containing 2 (Sorbs2)	0.62	0.01
NM_019654	suppressor of cytokine signaling 5 (Socs5)	0.62	0.00
NM_008761	FXYD domain-containing ion transport regulator 5 (Fxyd5)	0.63	0.02
NM_176832	spire homolog 1 (Drosophila) (Spire1)	0.63	0.01
NM_080448	SLIT-ROBO Rho GTPase activating protein 3 (Srgap3)	0.63	0.00
NM_080553	inositol 1,4,5-triphosphate receptor 3 (Itpr3)	0.63	0.01
NM_001040690	RAP1, GTP-GDP dissociation stimulator 1 (Rap1gds1)	0.63	0.00
NM_008869	phospholipase A2, group IVA (cytosolic, calcium-dependent) (Pla2g4a)	0.63	0.01
NM_138752	pleckstrin homology domain containing, family G (with RhoGef domain) member 2 (Plekhg2)	0.63	0.02
NM_144881	hedgehog acyltransferase (Hhat)	0.63	0.01
NM_001043322	formin 1 (Fmn1)	0.63	0.00

Table 5.4. continued

		MAE-p47	
Accession No.	**Gene Description**	**O/L**	**p-value**
NM_080287	engulfment and cell motility 2, ced-12 homolog (C. elegans) (Elmo2)	0.63	0.03
NM_007616	caveolin, caveolae protein 1 (Cav1)	0.63	0.01
XM_485202	zinc finger and BTB domain containing 10 (Zbtb10)	0.63	0.02
NM_025999	ring finger protein 141 (Rnf141)	0.63	0.00
NM_009794	calpain 2 (Capn2)	0.63	0.01
NM_020559	aminolevulinic acid synthase 1 (Alas1)	0.63	0.00
NM_009504	vitamin D receptor (Vdr)	0.63	0.00
NM_013777	aldo-keto reductase family 1, member C12 (Akr1c12)	0.63	0.01
NM_172992	putative homeodomain transcription factor 2 (Phtf2)	0.63	0.01
NM_130863	adrenergic receptor kinase, beta 1 (Adrbk1)	0.63	0.00
NM_021469	dysferlin /// fer-1-like 3, myoferlin (C. elegans) (Dysf /// Fer1l3)	0.63	0.00
XM_908334	ethanolamine kinase 1 (Etnk1)	0.63	0.00
NM_133167	parvin, beta (Parvb)	0.63	0.00
NM_026514	CDC42 effector protein (Rho GTPase binding) 3 (Cdc42ep3)	0.63	0.03
XM_140308	DCP2 decapping enzyme homolog (S. cerevisiae) (Dcp2)	0.64	0.01
NM_026700	dopey family member 2 (Dopey2)	0.64	0.01
NM_011803	Kruppel-like factor 6 (Klf6)	0.64	0.01
NM_198161	basic helix-loop-helix domain containing, class B9 (Bhlhb9)	0.64	0.02
NM_001038642	E26 avian leukemia oncogene 1, 5' domain (Ets1)	0.64	0.02
XM_001002526	interferon regulatory factor 2 binding protein 2 (Irf2bp2)	0.64	0.00
NM_145136	myocardin (Myocd)	0.64	0.00
NM_144513	maternally expressed 3 (Gtl2 /// Lphn1)	0.64	0.01
NM_011212	protein tyrosine phosphatase, receptor type, E (Ptpre)	0.64	0.00
NM_011379	signal-induced proliferation associated gene 1 (Sipa1)	0.64	0.02
NM_011528	transaldolase 1 (Taldo1)	0.64	0.02
NM_021531	coactivator-associated arginine methyltransferase 1 (Carm1)	0.64	0.02
NM_144792	sphingomyelin synthase 1 (Tmem23)	0.64	0.02
NM_022320	G protein-coupled receptor 35 (Gpr35)	0.64	0.01
NM_133198	liver glycogen phosphorylase (Pygl)	0.64	0.00
NM_181821	host cell factor C1 regulator 1 (XPO1-dependent) (Hcfc1r1)	0.64	0.02
NM_030241	SET domain containing (lysine methyltransferase) 8 (Setd8)	0.65	0.01
NM_001040111	centaurin, delta 2 (Centd2)	0.65	0.01
NM_146073	zinc finger, DHHC domain containing 14 (Zdhhc14)	0.65	0.00
NM_175003	expressed sequence AU040829 (AU040829)	0.65	0.01
NR_001592	H19 fetal liver mRNA (H19)	0.65	0.02
NM_010135	enabled homolog (Drosophila) (Enah)	0.65	0.01
NM_019572	histone deacetylase 7A (Hdac7a)	0.65	0.01
NM_001037762	zinc finger, DHHC domain containing 12 (Zdhhc12)	0.65	0.03
NM_008783	RIKEN cDNA 4833414E09 gene (Pbx1)	0.65	0.00
NM_018736	meiotic recombination 11 homolog A (S. cerevisiae) (Mre11a)	0.65	0.00
NM_007600	calpain 1 (Capn1)	0.65	0.02
NM_011276	ring finger protein 12 (Rnf12)	0.65	0.02
XM_125637	Rho-related BTB domain containing 1 (Rhobtb1)	0.65	0.03
NM_010305	guanine nucleotide binding protein (G protein), alpha inhibiting 1 (Gnai1)	0.65	0.01
NM_011303	dehydrogenase/reductase (SDR family) member 3 (Dhrs3)	0.65	0.02
NM_026697	RAB14, member RAS oncogene family (Rab14)	0.65	0.01
XM_001001143	SET binding factor 2 (Sbf2)	0.65	0.00
NM_011446	SRY-box containing gene 7 (Sox7)	0.65	0.00
NM_172945	ankyrin repeat domain 13b (Ankrd13b)	0.65	0.02
NM_001012450	ankyrin repeat domain 6 (Ankrd6)	0.65	0.00
NM_007765	collapsin response mediator protein 1 (Crmp1)	0.65	0.02
NM_001002011	lamin A (Lmna)	0.66	0.01
NM_013484	complement component 2 (within H-2S) (C2)	0.66	0.02
NM_181074	leucine rich repeat and Ig domain containing 1 (Lrrn6a)	0.66	0.00
XM_194040	microtubule-associated protein 1 A (Mtap1a)	0.66	0.02
NM_022980	regulator of calcineurin 3 (Dscr1l2)	0.66	0.01
XM_128781	lysocardiolipin acyltransferase (Lycat)	0.66	0.01
NM_016765	dimethylarginine dimethylaminohydrolase 2 (Ddah2)	0.66	0.01
NM_029348	zinc finger and BTB domain containing 4 (Zbtb4)	0.66	0.01
NM_010820	multiple PDZ domain protein (Mpdz)	0.66	0.01
NM_133687	CXXC finger 5 (Cxxc5)	0.66	0.02
XM_001000816	SLIT-ROBO Rho GTPase activating protein 2 (Srgap2)	0.66	0.00
NM_008862	protein kinase inhibitor, alpha (Pkia)	0.66	0.02
NM_001025261	tumor protein D52 (Tpd52)	0.66	0.01
NM_010720	lipase, endothelial (Lipg)	0.66	0.01
NM_011774	solute carrier family 30 (zinc transporter), member 4 (Slc30a4)	0.66	0.00
NM_025569	microsomal glutathione S-transferase 3 (Mgst3)	0.66	0.02
NM_011898	sprouty homolog 4 (Drosophila) (Spry4)	0.66	0.02
NM_001037841	chemokine-like factor (Cklf)	0.66	0.01
NM_023042	RecQ protein-like (Recql)	1.52	0.02
NM_028381	coiled-coil domain containing 94 (Ccdc94)	1.52	0.03

Table 5.4. continued

		MAE-p47	
Accession No.	Gene Description	O/L	p-value
NM_013763	transducin (beta)-like 2 (Tbl2)	1.52	0.02
NM_011285	retinitis pigmentosa GTPase regulator (Rpgr)	1.53	0.01
NM_016690	heterogeneous nuclear ribonucleoprotein D-like (Hnrpdl)	1.53	0.01
NM_021326	RB-associated KRAB repressor (Rbak)	1.53	0.03
NM_026494	phosphopantothenoylcysteine synthetase (Ppcs)	1.53	0.02
NM_011937	glucosamine-6-phosphate deaminase 1 (Gnpda1)	1.54	0.02
NM_028923	GLE1 RNA export mediator (yeast) (Gle1l)	1.54	0.01
NM_030684	tripartite motif protein 34 (Trim34)	1.55	0.03
NM_001039388	WD repeat domain 37 (Wdr37)	1.55	0.03
NM_148941	elongation of very long chain fatty acids-like 4 (Elovl4)	1.56	0.03
NM_175009	enhancer of yellow 2 homolog (Drosophila) (Eny2)	1.56	0.02
NM_019823	cytochrome P450, family 2, subfamily d, polypeptide 22 (Cyp2d22)	1.56	0.03
NM_146151	testis-specific kinase 2 (Tesk2)	1.56	0.01
XM_001000094	importin 8 (Ipo8)	1.57	0.01
NM_145353	Yip1 domain family, member 3 (Yipf3)	1.58	0.00
NM_144546	zinc finger protein 119 (Zfp119)	1.59	0.03
NM_001042671	preimplantation protein 4 (Prei4)	1.60	0.01
NM_011704	vanin 1 (Vnn1)	1.60	0.00
NM_009104	ribonucleotide reductase M2 (Rrm2)	1.61	0.00
NM_026162	plexin domain containing 2 (Plxdc2)	1.61	0.00
NM_026554	nuclear cap binding protein subunit 2 (Ncbp2)	1.62	0.03
NM_053196	sideroflexin 2 (Sfxn2)	1.64	0.02
NM_145520	TruB pseudouridine synthase homolog 2 (E. coli) (Trub2)	1.64	0.00
NM_019963	signal transducer and activator of transcription 2 (Stat2)	1.65	0.01
NM_023048	ankyrin repeat and SOCS box-containing protein 4 (Asb4)	1.66	0.01
NM_011511	ATP-binding cassette, sub-family C (CFTR/MRP), member 9 (Abcc9)	1.67	0.03
NM_153543	aldehyde dehydrogenase 1 family, member L2 (Aldh1l2)	1.68	0.00
NM_173762	centromere protein E (Cenpe)	1.70	0.03
NM_207245	cDNA sequence BC066107 (BC066107)	1.73	0.03
NM_010228	FMS-like tyrosine kinase 1 (Flt1)	1.74	0.00
NM_144808	solute carrier family 39 (zinc transporter), member 14 (Slc39a14)	1.75	0.01
NM_178877	Na+/H+ exchanger domain containing 2 (C80638)	1.77	0.02
XM_619244	chromodomain helicase DNA binding protein 8 (Chd8)	1.77	0.00
NM_029665	importin 11 (Ipo11)	1.77	0.03
NM_013852	ATP-binding cassette, sub-family F (GCN20), member 3 (Abcf3)	1.78	0.03
NM_178804	slit homolog 2 (Drosophila) (Slit2)	1.78	0.02
NM_029763	polymerase (RNA) III (DNA directed) polypeptide F (Polr3f)	1.79	0.00
NM_172578	expressed sequence C79407 (C79407)	1.81	0.00
XM_907983	hect domain and RLD 5 (Herc5)	1.81	0.00
NM_030684	Predicted gene, EG667823 (Trim34)	1.82	0.01
NM_001033851	copine VIII (Cpne8)	1.82	0.02
NM_008555	Mannan-binding lectin serine peptidase 1 (Masp1)	1.85	0.01
NM_080857	ankyrin repeat and SOCS box-containing protein 13 (Asb13)	1.85	0.03
NM_013584	leukemia inhibitory factor receptor (Lifr)	1.86	0.01
NM_007691	checkpoint kinase 1 homolog (S. pombe) (Chek1)	1.90	0.01
NM_008977	protein tyrosine phosphatase, non-receptor type 2 (Ptpn2)	1.92	0.01
NM_011117	plectin 1 (Plec1)	1.93	0.03
NM_011150	lectin, galactoside-binding, soluble, 3 binding protein (Lgals3bp)	1.98	0.00
XM_356065	DDHD domain containing 2 (Ddhd2)	2.06	0.03
NM_008796	phosphatidylcholine transfer protein (Pctp)	2.07	0.00
NM_008446	kinesin family member 4 (Kif4)	2.10	0.00
NM_133832	retinol dehydrogenase 10 (all-trans) (Rdh10)	2.13	0.00
NM_172893	poly (ADP-ribose) polymerase family, member 12 (Parp12)	2.28	0.01
XM_891672	peptidylprolyl isomerase (cyclophilin)-like 6 (Ppil6)	2.30	0.01
NM_019440	interferon inducible GTPase 2 (Iigp2)	2.38	0.02
NM_018738	interferon gamma induced GTPase (Igtp)	2.48	0.02
NM_009283	signal transducer and activator of transcription 1 (Stat1)	2.55	0.00
NM_030253	poly (ADP-ribose) polymerase family, member 9 (Parp9)	2.61	0.01
NM_001013371	deltex 3-like (Drosophila) (Dtx3l)	2.67	0.00
NM_009605	adiponectin, C1Q and collagen domain containing (Adipoq)	2.74	0.01
NM_026301	ring finger protein 125 (Rnf125)	3.90	0.03

Shear Stress-Sensitive Genes Were Grouped by Biologic Function

Next, we examined which biological responses are regulated by shear stress in p47phox-dependent manner in endothelial cells. To this end, we compared the shear-dependent biological responses in MAE-WT and MAE-p47 cells by using Ingenuity Pathways Analysis (IPA) and GOMiner. IPA identified several significant functional categories of shear-sensitive genes in both cell types, as shown in Figure 4.11. These categories included: cardiovascular disease, cardiovascular system development and function, cell death, cellular growth and proliferation, cell morphology, cell signaling, and immune response. As shown in Table 5.5, GOMiner analysis of the microarray results of the two cell types identified 6 major biological categories that are pertinent to vascular biology and pathophysiology: oxidative stress, cell adhesion, angiogenesis, apoptosis, and cell proliferation.

There were 30 shear-sensitive genes identified in the oxidative stress category. These genes appear to be p47phox-dependent since all of them changed significantly in only one cell type. Another category of interest is cell adhesion in which we found 25 genes. p47phox-independent genes which changed significantly and in the same way in both cell types included Rhob and Edil3. Other genes, such as CTGF and Alcam may be p47phox-dependent since they were down-regulated by OS in only MAE-WT. Eighteen genes were identified as having a function in apoptosis. Fourteen genes had roles in cell proliferation. Of these genes, the majority of them changed in only one cell type, indicating their possible dependence on p47phox and p47phox-based NADPH oxidases.

(a)

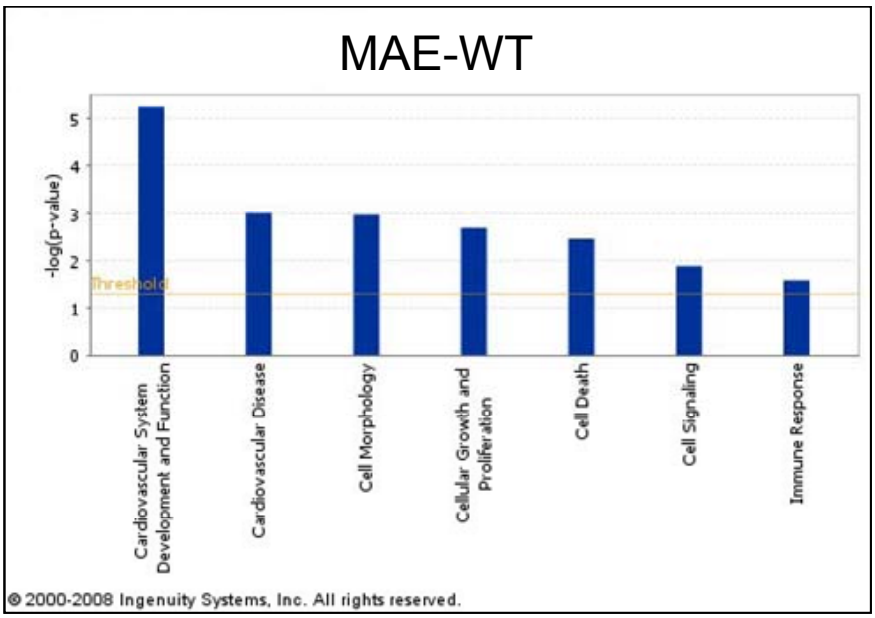

(b)

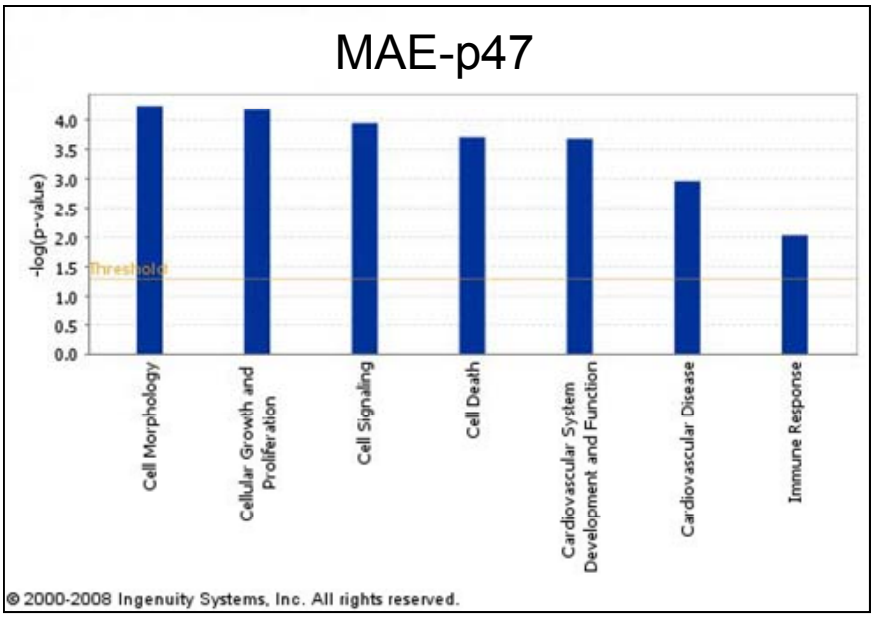

Figure 4.11. Microarray results were analyzed by Ingenuity Pathways Analysis. IPA identified several categories of biological functions represented by the shear-sensitive genes in (a) MAE-WT and (b) MAE-p47.

Table 5.5. Gene Ontology categorization of genes changing significantly by OS in either MAE-WT or MAE-p47

		MAE-WT		MAE-p47	
Accession No.	**Gene Description**	**O/L**	**p-value**	**O/L**	**p-value**
Oxidative Stress					
NM_010728	lysyl oxidase (Lox)	0.50	0.00	--	--
NM_010476	hydroxysteroid (17-beta) dehydrogenase 7 (Hsd17b7)	0.51	0.01	--	--
NM_010941	NAD(P) dependent steroid dehydrogenase-like (Nsdhl)	0.56	0.02	--	--
NM_020010	cytochrome P450, family 51 (Cyp51)	0.57	0.01	--	--
NM_172769	sterol-C5-desaturase homolog (Sc5d)	0.59	0.02	--	--
NM_009128	stearoyl-Coenzyme A desaturase 2 (Scd2)	0.62	0.00	--	--
NM_177282	microtubule associated monoxygenase, calponin and LIM domain 2 (Mical2)	0.62	0.01	--	--
NM_028454	transmembrane 7 superfamily member 2 (Tm7sf2)	0.63	0.00	--	--
NM_016780	integrin beta 3 (Itgb3)	0.64	0.00	--	--
NM_199476	ribonucleotide reductase M2 B (TP53 inducible) (Rrm2b)	0.65	0.01	--	--
NM_010271	glycerol-3-phosphate dehydrogenase 1 (soluble) (Gpd1)	0.66	0.00	--	--
NM_019699	fatty acid desaturase 2 (Fads2)	0.66	0.03	--	--
NM_029688	sulfiredoxin 1 homolog (S. cerevisiae) (Srxn1)	1.58	0.03	--	--
NM_028002	dihydrouridine synthase 4-like (S. cerevisiae) (Dus4l)	1.61	0.01	--	--
NM_023066	aspartate-beta-hydroxylase (Asph)	1.61	0.01	--	--
NM_018881	flavin containing monooxygenase 2 (Fmo2)	1.79	0.01	--	--
NM_008706	NAD(P)H dehydrogenase, quinone 1 (Nqo1)	--	--	0.39	0.14
NM_010403	hydroxyacid oxidase 1, liver (Hao1)	--	--	0.47	0.07
NM_007436	aldehyde dehydrogenase family 3, subfamily A1 (Aldh3a1)	--	--	0.56	0.14
NM_001042513	thioredoxin reductase 1 (Txnrd1)	--	--	0.58	0.11
NM_153162	thioredoxin reductase 3 (Txnrd3)	--	--	0.60	0.11
NM_010344	glutathione reductase 1 (Gsr)	--	--	0.61	0.08
NM_013777	aldo-keto reductase family 1, member C12 (Akr1c12)	--	--	0.63	0.09
NM_011303	dehydrogenase/reductase (SDR family) member 3 (Dhrs3)	--	--	0.65	0.09
NM_011285	retinitis pigmentosa GTPase regulator (Rpgr)	--	--	1.53	0.13
NM_019823	cytochrome P450, family 2, subfamily d, polypeptide 22 (Cyp2d22)	--	--	1.56	0.17
NM_009104	ribonucleotide reductase M2 (Rrm2)	--	--	1.61	0.06
NM_153543	aldehyde dehydrogenase 1 family, member L2 (Aldh1l2)	--	--	1.68	0.08
NM_011150	lectin, galactoside-binding, soluble, 3 binding protein (Lgals3bp)	--	--	1.98	0.17
NM_133832	retinol dehydrogenase 10 (all-trans) (Rdh10)	--	--	2.13	0.11
Cell Adhesion					
NM_007483	ras homolog gene family, member B (Rhob)	0.35	0.00	0.50	0.00
NM_001037987	EGF-like repeats and discoidin I-like domains 3 (Edil3)	0.53	0.00	0.36	0.01
NM_010217	connective tissue growth factor (Ctgf)	0.46	0.01	--	--
NM_007743	collagen, type I, alpha 2 (Col1a2)	0.46	0.03	--	--
NM_007735	collagen, type IV, alpha 4 (Col4a4)	0.50	0.03	--	--
NM_178615	RGM domain family, member B (Rgmb)	0.59	0.03	--	--
NM_008396	integrin alpha 2 (Itga2)	0.60	0.02	--	--
NM_022410	myosin, heavy polypeptide 9, non-muscle (Myh9)	0.64	0.01	--	--
NM_016780	integrin beta 3 (Itgb3)	0.64	0.00	--	--
NM_001033954	calcitonin/calcitonin-related polypeptide, alpha (Calca)	1.59	0.03	--	--
NM_009655	activated leukocyte cell adhesion molecule (Alcam)	2.97	0.03	--	--
NM_010112	Embryonal Fyn-associated substrate (Efs)	--	--	0.36	0.01
NM_008397	integrin alpha 6 (Itga6)	--	--	0.37	0.01
NM_010577	integrin alpha 5 (fibronectin receptor alpha) (Itga5)	--	--	0.46	0.00
NM_011518	spleen tyrosine kinase (Syk)	--	--	0.52	0.03
NM_018764	protocadherin 7 (Pcdh7)	--	--	0.52	0.02
NM_178685	protocadherin 20 (Pcdh20)	--	--	0.52	0.01
XM_001003344	protocadherin 9 (Pcdh9)	--	--	0.54	0.03
NM_011607	tenascin C (Tnc)	--	--	0.57	0.00
NM_013565	integrin alpha 3 (Itga3)	--	--	0.62	0.00
NM_133167	parvin, beta (Parvb)	--	--	0.63	0.00
NR_001592	H19 fetal liver mRNA (H19)	--	--	0.65	0.02
NM_010135	enabled homolog (Drosophila) (Enah)	--	--	0.65	0.01
NM_010820	multiple PDZ domain protein (Mpdz)	--	--	0.66	0.01
NM_146151	testis-specific kinase 2 (Tesk2)	--	--	1.56	0.01
Angiogenesis					
NM_007483	ras homolog gene family, member B (Rhob)	0.35	0.00	0.50	0.00
NM_010929	Notch gene homolog 4 (Drosophila) (Notch4)	0.44	0.00	--	--
NM_010217	connective tissue growth factor (Ctgf)	0.46	0.01	--	--
NM_009154	semaphorin 5A (Sema5a)	0.59	0.00	--	--
NM_022410	myosin, heavy polypeptide 9, non-muscle (Myh9)	0.64	0.01	--	--
NM_008486	alanyl (membrane) aminopeptidase (Anpep)	--	--	0.54	0.00
NM_010228	FMS-like tyrosine kinase 1 (Flt1)	--	--	1.74	0.00

Table 5.5. continued

		MAE-WT		MAE-p47	
Accession No.	**Gene Description**	**O/L**	**p-value**	**O/L**	**p-value**
Apoptosis					
NM_007483	ras homolog gene family, member B (Rhob)	0.35	0.00	0.50	0.00
NM_011738	tyrosine 3-monooxygenase (Ywhah)	0.65	0.01	0.64	0.01
NM_021389	SH3-domain kinase binding protein 1 (Sh3kbp1)	0.45	0.00	--	--
XM_619639	tensin 1 (Tns1)	0.55	0.00	--	--
NM_028778	NUAK family, SNF1-like kinase, 2 (Nuak2)	0.58	0.01	--	--
NM_028778	NUAK family, SNF1-like kinase, 2 (Nuak2)	0.58	0.01	--	--
NM_019827	glycogen synthase kinase 3 beta (Gsk3b)	0.60	0.00	--	--
NM_011052	programmed cell death 6 interacting protein (Pdcd6ip)	0.60	0.01	--	--
NM_146001	huntingtin interacting protein 1 (Hip1)	0.62	0.01	--	--
NM_018807	pleiomorphic adenoma gene-like 2 (Plagl2)	0.64	0.01	--	--
NM_011018	sequestosome 1 (Sqstm1)	2.33	0.03	--	--
NM_177343	calcium/calmodulin-dependent protein kinase ID (Camk1d)	--	--	0.45	0.00
NM_153552	THO complex 1 (Thoc1)	--	--	0.51	0.03
NM_009289	STE20-like kinase (yeast) (Slk)	--	--	0.55	0.01
NM_008380	inhibin beta-A (Inhba)	--	--	0.57	0.00
NM_011535	T-box 3 (Tbx3)	--	--	0.58	0.00
NM_080287	engulfment and cell motility 2, ced-12 homolog (C. elegans) (Elmo2)	--	--	0.63	0.03
NM_146151	testis-specific kinase 2 (Tesk2)	--	--	1.56	0.01
Proliferation					
NM_007553	bone morphogenetic protein 2 (Bmp2)	0.37	0.01	0.35	0.00
NM_019827	glycogen synthase kinase 3 beta (Gsk3b)	0.60	0.00	--	--
NM_007561	bone morphogenic protein receptor, type II (serine/threonine kinase) (Bmpr2)	0.65	0.00	--	--
NM_011158	protein kinase, cAMP dependent regulatory, type II beta (Prkar2b)	1.61	0.01	--	--
NM_011518	spleen tyrosine kinase (Syk)	--	--	0.52	0.03
NM_011670	ubiquitin carboxy-terminal hydrolase L1 (Uchl1)	--	--	0.55	0.00
NM_011535	T-box 3 (Tbx3)	--	--	0.58	0.00
XM_897426	rhotekin 2 (Plekhk1)	--	--	0.58	0.02
NM_001042513	thioredoxin reductase 1 (Txnrd1)	--	--	0.58	0.02
NM_016900	caveolin 2 (Cav2)	--	--	0.60	0.03
NM_007616	caveolin, caveolae protein 1 (Cav1)	--	--	0.63	0.01
NM_145136	myocardin (Myocd)	--	--	0.64	0.00
NM_008783	RIKEN cDNA 4833414E09 gene (Pbx1)	--	--	0.65	0.00
NM_013584	leukemia inhibitory factor receptor (Lifr)	--	--	1.86	0.01

Verification of Microarray Results By Quantitative PCR

To verify the results of our microarray analyses, we chose genes that either have been previously identified as shear-responsive or had potentially interesting roles in atherogenesis and appeared to be p47phox-dependent. We were able to corroborate some of our microarray results by quantitative PCR (qPCR) analysis of our primary MAEC samples, as shown in Figure 4.12. We confirmed that Klf2 was dramatically down-regulated by OS in both MAE-WT and MAE-p47 by both microarray analysis (or gene chip) and qPCR. We also showed that eNOS was down-regulated by OS in both MAE-WT and MAE-p47, though the microarray fold change was not significant while the qPCR results were significant. Angiopoietin 2 (Ang2) has been shown to be shear-responsive in other endothelial cells; however, our microarray results and qPCR analysis indicate that MAEC are not shear-responsive under our particular *in vitro* conditions. Jam2 was confirmed to be a shear-sensitive gene in only the wild-type cells, being down-regulated by almost 2-fold in MAE-WT. This indicates that its shear response may be p47phox-dependent. A similar pattern was found for Bmpr2. It was significantly down-regulated by OS in only MAE-WT, indicating that its shear response also may be p47phox-dependent.

In order to be able to investigate a larger number of genes and determine their functional roles, we chose to also use the immortalized MAEC cell lines. We were able to validate some of our microarray results with these cells. Shown in Figure 4.13 are qPCR results using the immortalized cells. Klf2, as expected, was dramatically down-regulated by OS in both iMAE-WT and iMAE-p47 by both MA and qPCR. Also, we confirmed the results for junctional adhesion molecule 2 (Jam2). Jam2 was down-regulated by OS in iMAE-WT but not in iMAE-p47 which supported the microarray results. This indicates that Jam2 may be shear-sensitive and p47phox-dependent.

Verification of Microarray Results by Immunoblotting

We next validated microarray results of selected genes at the protein level by Western blot analysis. We analyzed protein expression changes for Klf2 and total eNOS. As has been reported in other endothelial cells, Klf2 was dramatically down-regulated by OS in both iMAE-WT and iMAE-p47. Total eNOS was also down-regulated by OS in both iMAE-WT and iMAE-p47. While the change was not dramatic, it was consistent. We also probed for Bmpr2. We showed that while OS down-regulated Bmpr2 in iMAE-WT, it did not change the expression of Bmpr2 in iMAE-p47. This corroborates the mRNA expression changes, as demonstrated in primary MAEC, and further suggests that this gene's shear response is p47phox-dependent.

Bone Morphogenetic Protein 4

We validated microarray results for Bmp4 at the mRNA levels using both primary cells and immortalized cells. As shown in Figure 4.15(a), microarray analysis suggested that Bmp4 mRNA levels did not change in response to OS in either MAE-WT or MAE-p47. We validated this with both primary cells and immortalized cells. However, at the protein level, we did see that OS increased the expression of the mature form of Bmp4 by Western analysis. This was true only in iMAE-WT. Protein expression of Bmp4 did not appear to respond to OS in iMAE-p47. These results are shown in Figure 4.15(b).

We further used an *in vivo* partial ligation model to look at Bmp4's shear response. In this model, the internal carotid, external carotid, and occipital arteries are ligated on the left side of the animal only, as illustrated in Figure 4.16(a). This decreases flow and shear stress on the ligated side while increasing flow and shear stress on the non-ligated side. One day following partial ligation, we looked at Bmp4 expression near the ligated area where flow was decreased using en face imaging. As shown in Figure 4.16(b), Bmp4 protein expression was increased on the ligated, low flow side, in wild-type animals. However, no change in Bmp4 expression was observed in p47phox$^{-/-}$

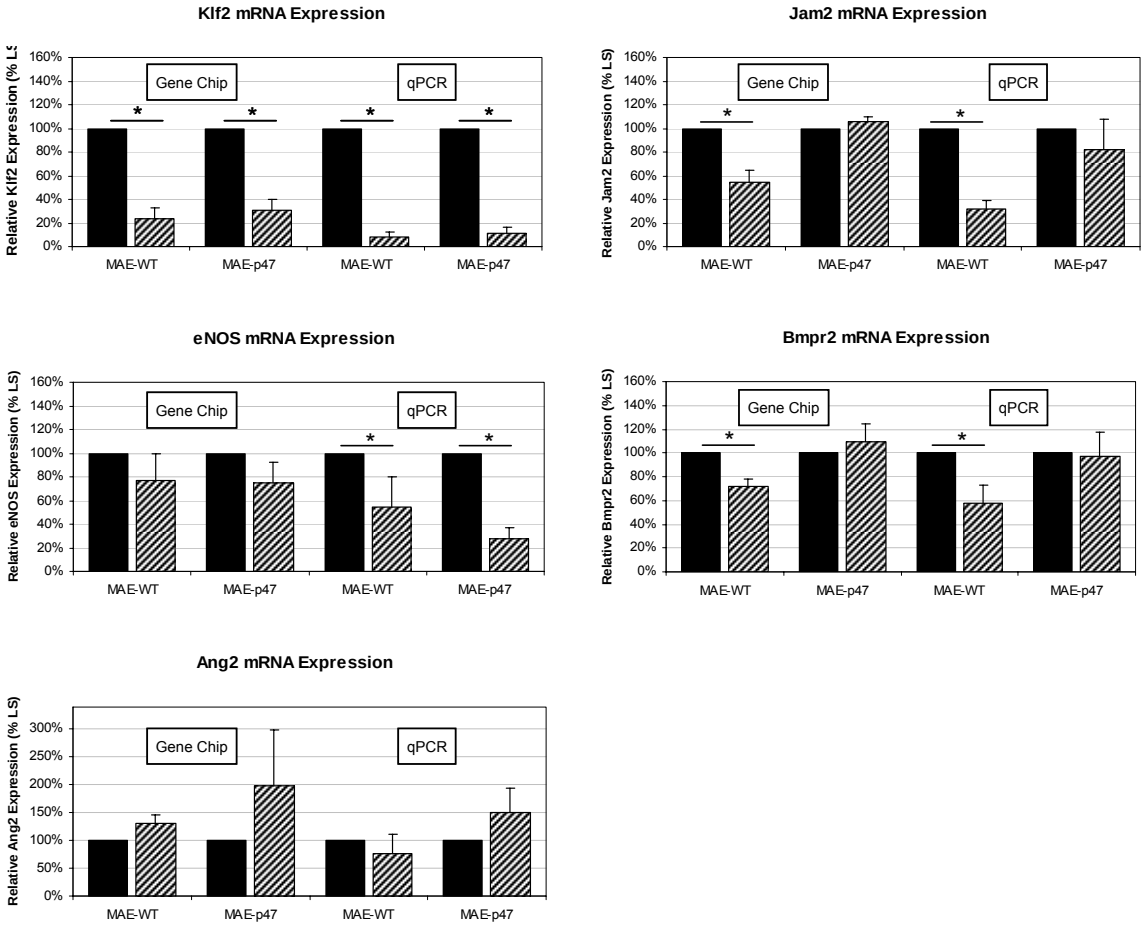

Figure 4.12. qPCR validation of microarray results using primary MAEC. Following microarray analysis, gene expression changes were validated with primary cell samples for several genes, including Klf2, eNOS, Ang2, Jam2, and Bmpr2. Microarray results are shown on the left of each graph and the corresponding quantitative PCR results are shown on the right of each graph for both cell types MAE-WT and MAE-p47. Statistical significance was determined by a Student's t-test where * indicates p-value ≤ 0.05, n = 3-4.

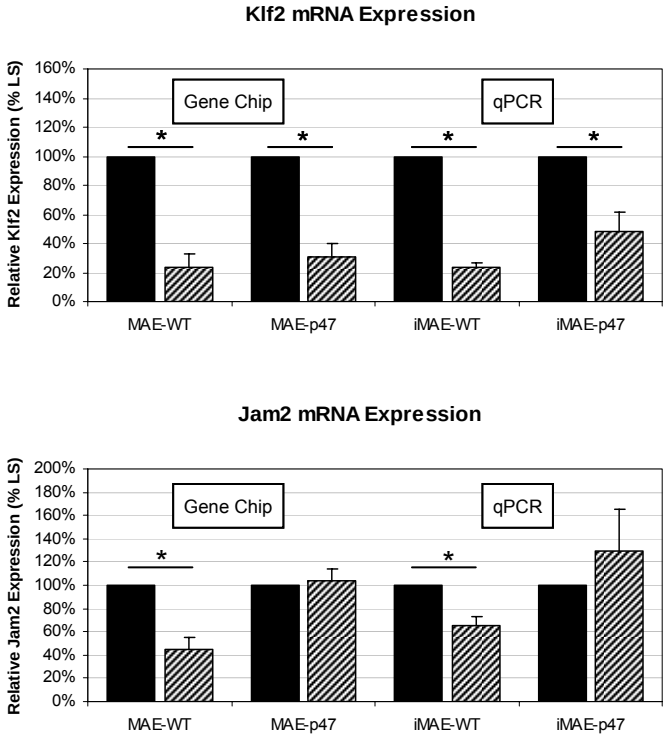

Figure 4.13. qPCR validation of microarray results using immortalized MAEC. Following microarray analysis, gene expression changes were validated with immortalized cell samples for genes, including Klf2 and Jam2. Microarray results are shown on the left of each graph and the corresponding quantitative PCR results are shown on the right of each graph. Statistical significance was determined by a Student's t-test where * indicates p-value ≤ 0.05, n = 3-4 for gene chip and n = 6-8 for qPCR.

(a)

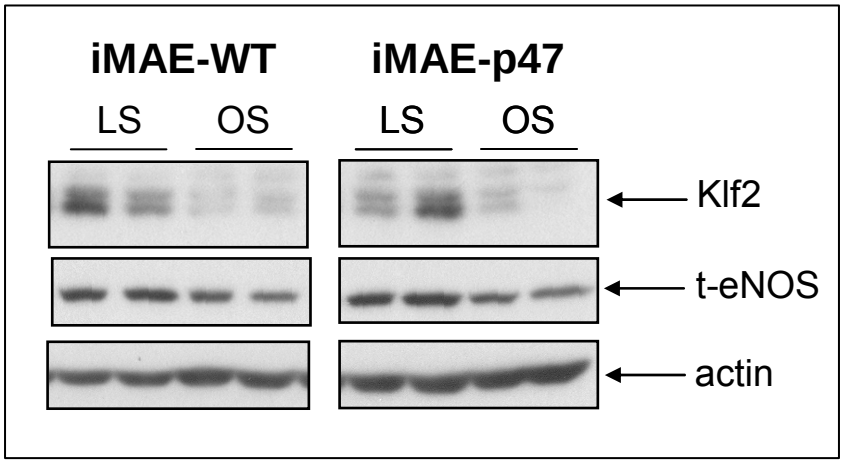

(b)

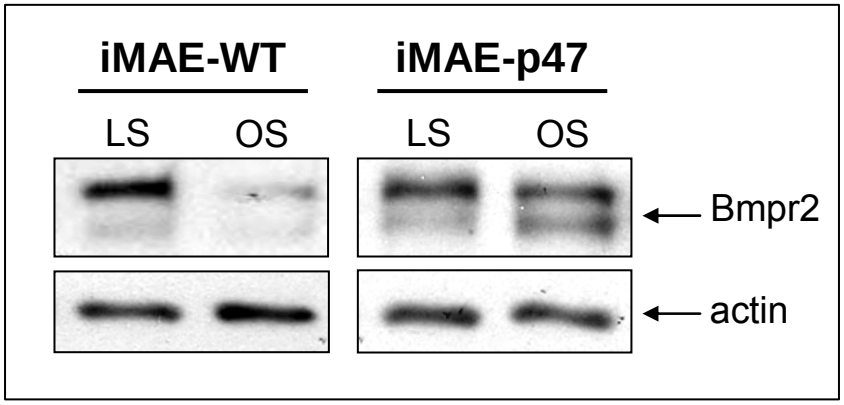

Figure 4.14. Protein validation of microarray results using immortalized MAEC. (a) Cell lysates obtained from iMAE-WT and iMAE-p47 exposed to either laminar (LS) or oscillatory shear (OS) conditions were analyzed by Western blot using antibodies for total eNOS (t-eNOS), Kruppel-like factor 2 (Klf2), and β-actin (used as a loading control). (Contributed by Chih-Wen Ni.) (b) Cell lysates obtained from iMAE-WT and iMAE-p47 exposed to either LS or OS conditions were analyzed by Western blot using antibodies for bone morphogenic receptor 2 (Bmpr2) and β-actin (used as a loading control). (Contributed in part by Dr. HyukSang Kwon.)

(a)

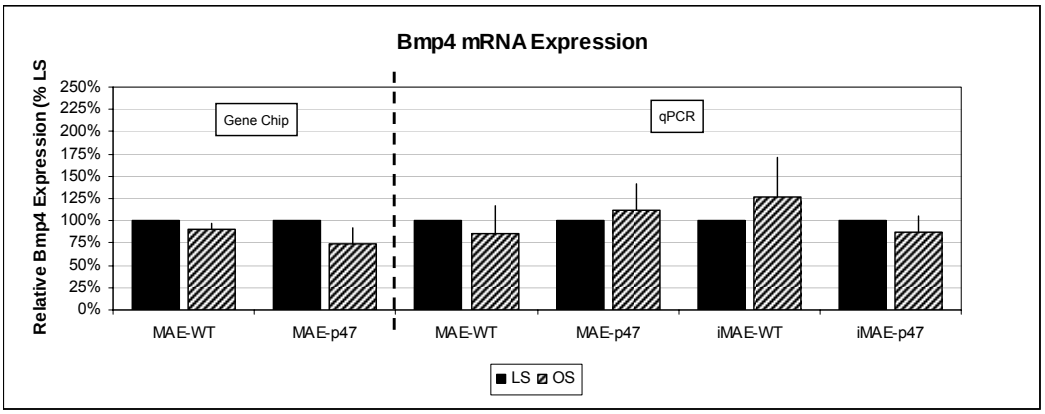

(b)

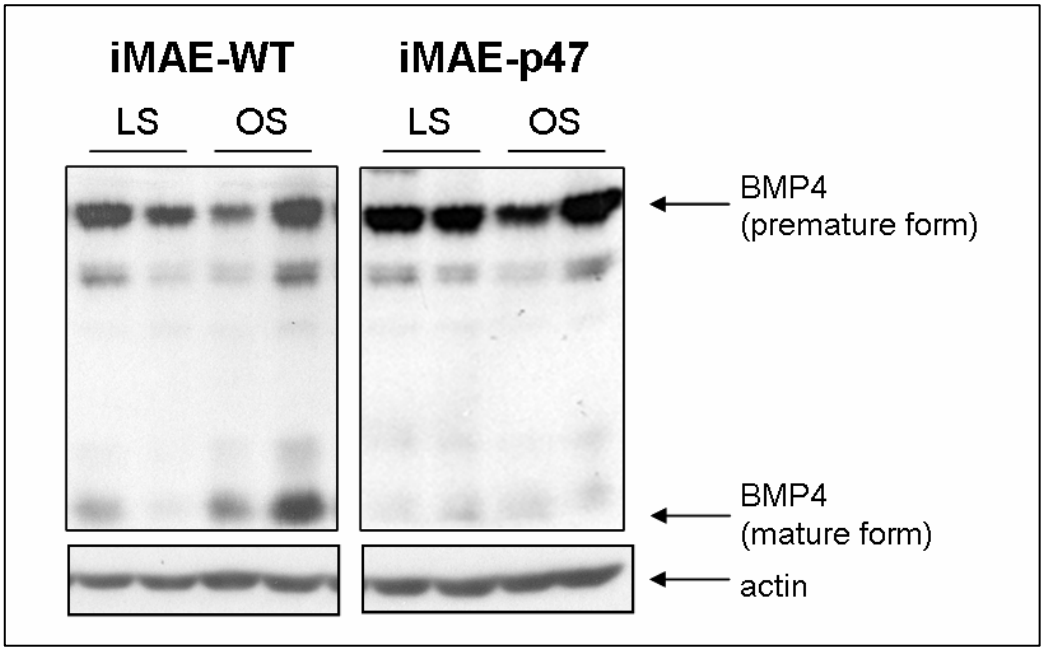

Figure 4.15. OS upregulates Bmp4 at the protein level. Bmp4 mRNA levels were not shear-responsive according to the microarray analysis. This was confirmed in both primary cells and immortalized cells, as shown in (a). However, the mature form of Bmp4 is upregulated by OS in iMAE-WT but not in iMAE-p47, as shown by Western blot analysis in (b). (Contributed in part by Chih-Wen Ni.)

(a)

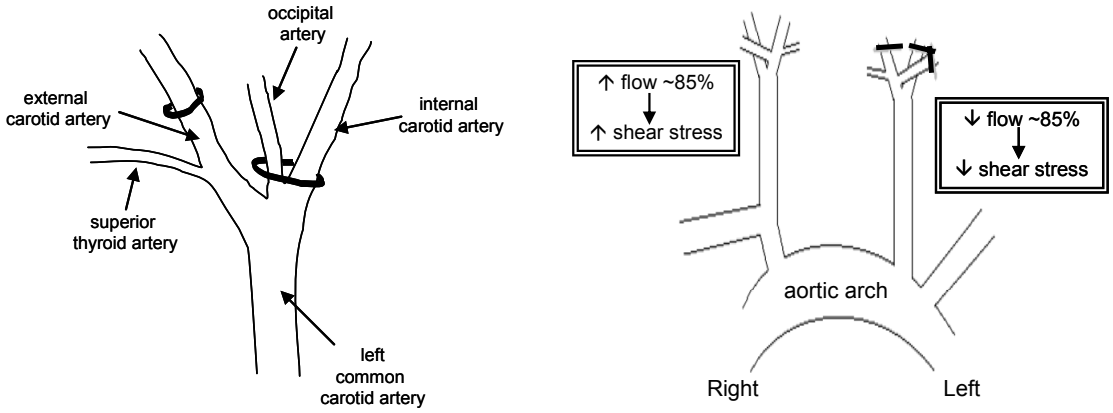

(b)

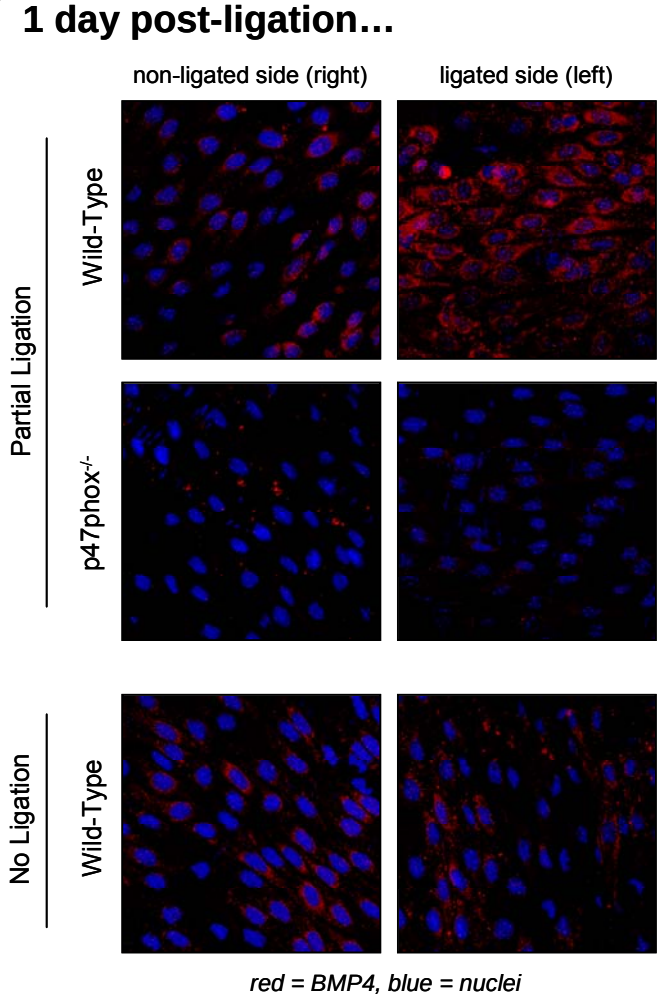

Figure 4.16. Bmp4 expression in a carotid partial ligation model. Wild-type and p47phox$^{-/-}$ mice underwent partial ligation. The external carotid, internal carotid, and occipital arteries were ligated on the left side only. One day following the procedure, the mice were euthanized. The vascular was perfused and fixed with formalin. Aortas were incubated with an antibody towards Bmp4. En face images of the endothelial surface upstream but proximal to the ligation were taken using a Zeiss LSM 510 confocal microscope. Expression of Bmp4 was increased on the ligated side, or low-flow side, in wild-type animals. This response was not observed in p47phox$^{-/-}$ animals. En face images of non-ligated sham controls were included. (Contributed by Dr. Doug Nam.)

animals. While this needs to be investigated further, these initial results corroborate our *in vitro* data and suggest that Bmp4's shear response is p47phox-dependent.

Discussion

The major and novel finding of this study is the identification of genes that were regulated by shear stress in NADPH oxidase-dependent and –independent manners. These findings provide us with insights into which mechanosensitive genes are regulated by the p47phox-based NADPH oxidases.

Increased vascular production of ROS, including superoxide and H_2O_2, commonly occurs in hypertension, atherosclerosis, aging, hypercholesterolemia, and diabetes. [24, 26, 92] ROS have been intimately linked to atherogenesis via inflammatory responses that result from disturbed flow conditions. [41, 88, 91] We have previously shown that OS stimulates ROS production in endothelial cells, while LS reduces ROS compared to static controls. OS stimulation of ROS leads to ICAM1 expression and monocyte adhesion, early and critical atherogenic events. [47] Evidence showing a role for p47phox-based NADPH oxidases in OS-induced ROS production and inflammatory responses has come from studies using endothelial cells in conjunction with the NADPH oxidase inhibitor apocynin or ROS chelators.

Some shear responses remain unchanged in MAE-p47 cells in comparison to MAE-WT. For example, both cell types show similar cell shape alignment in the direction of unidirectional LS, while both cell types do not align in response to bi-directional OS (Figures 4.7 and 4.8). While many of the shear-sensitive genes identified in MAE-WT showed different trends in MAE-p47 cells, 22 genes changed the same in both cell types, suggesting that either these genes are upstream of the p47phox-based NADPH oxidases or they are involved in an entirely independent pathway. One example of a p47phox-independent gene is Klf2. Klf2 is a transcription factor that has been

shown to be a shear-sensitive gene. It is upregulated by laminar shear and is thought to have a protective role in atherogenesis. We showed that Klf2 is shear-sensitive but p47phox-independent. It was significantly down-regulated by OS in both MAE-WT and MAE-p47 by microarray analysis and qPCR as well as in both iMAE-WT and iMAE-p47 by qPCR and Western blot.

Microarray analysis identified genes involved in oxidation and the oxidant response, shown in Table 5.5. Some interesting genes include lysyl oxidase (Lox) and NQO1. Lysyl oxidase is an enzyme that helps the cross-link collagen fibers. It has been reported to be induced by laminar shear stress and downregulated by high LDL levels, implicating a possible protective role in cardiovascular disease. [93, 94] While its shear response is known, its possible regulation by p47phox-based NADPH oxidases is unique and warrants further study. NQO1 is a cytosolic flavoenzyme that is classified as a detoxification enzyme. [95] This gene is known to have an antioxidant response element (ARE) in its promoter region. Its expression was downregulated by 0.39-fold in MAE-p47 while its expression tended to increase, but not significantly, in MAE-WT.

Gene ontology resources also helped identify genes in our analysis that are involved in cell adhesion. Some of these genes were regulated similarly in both cell types, suggesting that they are not sensitive to the p47phox-based NADPH oxidases. However, several genes, including Jam2 and Alcam, appear to be regulated differently among the two cell types suggesting that they are sensitive to the p47phox-based NADPH oxidases to some extent. These genes may play critical roles in endothelial permeability or monocyte adhesion to endothelial cells under shear stress conditions. Jam2 is a component of tight junctions in endothelial cells and may help regulate transendothelial migration of leukocytes. [96, 97] We were able to verify by PCR in an immortalized cell line that it was down-regulated by OS in iMAE-WT but did not change in response to shear in iMAE-p47. Further studies at the protein level and *in vivo* must

be conducted before any further conclusions are drawn. Nonetheless, this is the first report that it is a shear-sensitive gene and that its shear response is p47phox-dependent.

We have shown previously that Bmp4 is a mechanosensitive gene. [47, 54, 98] We unexpectedly did not see Bmp4 mRNA levels changing in response to OS in our microarray analysis. We confirmed this by quantitative PCR in both primary and immortalized MAEC, which can be seen in Figure 4.15(a). However, Bmp4 protein levels were shear-responsive. As shown in Figure 4.15(b), OS up-regulated the mature form of Bmp4 in iMAE-WT. OS had no effect on the mature form of Bmp4 in iMAE-p47, indicating that its shear response may be p47phox-dependent. We examined this gene even further using an *in vivo* partial ligation model. In this model, the external carotid, internal carotid, and occipital arteries are ligated on the left side only, leaving the superior thyroid artery patent. The ligation decreases flow, and hence shear, on the left side and increases flow, and hence shear, on the right side. With this model, we see increased Bmp4 expression on the ligated, or low-flow, side one day following ligation. This was true only in wild-type mice. There was no change in Bmp4 expression after ligation of p47phox$^{-/-}$ mice. This corroborates our in vitro data, showing that Bmp4's shear response is p47phox-dependent. These are early results and warrant further investigation.

An interesting observation with our microarray analysis was that more genes were shear-responsive in MAE-p47 than in MAE-WT. Figure 4.9 summarizes the number of genes changing in response to shear in both cell types; almost twice as many genes change in MAE-p47 than in MAE-WT. While this difference may be due to a technical bias from the arrays themselves or analysis or due to difference in cell purities, it may also indicate a significant impact of p47phox on overall transcription. While speculative, it may be that p47phox participates on some level in deacetylation of histones or transcription factors, inhibiting DNA transcription. [99] This is a very interesting hypothesis which warrants further investigation.

In summary, we have identified several genes that are sensitive to both shear and the p47phox-based NADPH oxidases. Future studies, identifying the functional roles of unexpected genes could provide important novel clues into the understanding of mechanotransduction as well as the atherogenic mechanisms regulated by shear stress and reactive oxygen species.

CHAPTER FIVE:

DISCUSSION AND FUTURE DIRECTIONS

Atherosclerosis occurs preferentially at branches and curves in arteries exposed to disturbed flow while sparing straight portions of arteries exposed to undisturbed flow. *In vivo* and *in vitro* studies have implicated NADPH oxidases in atherosclerosis and hypertension. Shear stress stimulates ROS production in endothelial cells from a variety of sources, including NADPH oxidases which are regulated in part by the p47phox subunit. Studies have shown that this regulatory subunit, in particular, is critical in the development of atherosclerosis as well as vessel remodeling and hypertension. [35, 38, 40, 48] Here, we examined the hypothesis that unidirectional laminar shear (LS) and ocillatory shear (OS) would differentially regulate gene expression profiles in p47phox-dependent and -independent manners, and that these genes would provide novel molecular targets in understanding endothelial cell biology and vascular disease.

The p47phox subunit of the NADPH oxidase can act as an important regulator of certain Nox isoforms, including Nox1 and Nox2 which may be responsible for shear-induced superoxide production. In order to isolate p47phox-dependent shear responses, we took advantage of the p47phox$^{-/-}$ transgenic mouse model which lacks a functional p47phox subunit. We developed a method to isolate murine aortic endothelial cells using enzymatic digestion and cell sorting. These cells were characterized as expressing typical endothelial markers, including VE-cadherin, PECAM1, and eNOS, and aligning in the direction of flow. This was a challenging project since the initial cell yield is low and the cells do not readily proliferate in culture. There is still room for investigation into how to optimally culture and expand these cells for experimental use. Nonetheless, we successfully isolated small populations of primary murine aortic endothelial cells from both wild-type C57BL/6 mice (MAE-WT) and p47phox$^{-/-}$ mice (MAE-p47).

Furthermore, we were able to establish an immortalized cell line from each of these cell types, iMAE-WT and iMAE-p47.

We carried out microarray studies using Affymetrix Mouse Genome 430 2.0 Arrays with almost 40,000 transcripts on MAE-WT and MAE-p47 that were exposed to atheroprotective LS or atherogenic OS for 24 hours. In comparison to LS, OS significantly changed the expression of 187 and 298 genes in MAE-WT and MAE-p47, respectively. Of those, 23 genes showed similar gene expression patterns in both cell types while 462 genes showed different gene expression patterns in the two cell types, demonstrating a considerable role for p47phox-based NADPH oxidases in shear-dependent gene expression.

Microarray analysis identified a large group of genes whose shear response is potentially regulated by p47phox, either through ROS production via the NADPH oxidases it regulates or through other, heretofore unidentified intracellular protein interactions. This large data set is simply the beginning of numerous investigations as each of these targets may be involved in the advancement of or protection from cardiovascular disease. Changes in expression of several genes, including Klf2, Jam2, and eNOS, were confirmed by quantitative PCR and/or immunoblotting using both primary cells and immortalized cells. Jam2 is particular novel since this is the first report to demonstrate its shear sensitivity as well as its p47phox-dependent shear response. Jam2 is an adhesion molecule involved in tight junctions between endothelial cells that may play a role in transendothelial leukocyte migration. While this has been studied in the context of venous endothelial cells, it is possible that it also functions in arterial endothelial cells. Since subintimal migration of monocytes is one of the first key steps in atherogenesis, and this occurs largely in areas of unsteady, oscillating shear stress, Jam2 would be an interesting target to continue studying.

Taken together, our studies have identified a set of shear- and p47phox-sensitive genes, including unexpected and novel targets, that may play critical roles in vascular cell biology and pathobiology.

REFERENCES

1. *Heart Disease and Stroke Statistics - 2008 Update*. 2008, American Heart Association.
2. *Number of Americans with Diabetes Continues to Increase*. 2005, Centers for Disease Control.
3. *US Obesity Trends 1985-2006*. 2008 [cited 2008 April 10]; Available from: http://www.cdc.gov/nccdphp/dnpa/obesity/trend/maps/index.htm.
4. Napoli, C., et al., *Fatty streak formation occurs in human fetal aortas and is greatly enhanced by maternal hypercholesterolemia. Intimal accumulation of low density lipoprotein and its oxidation precede monocyte recruitment into early atherosclerotic lesions.* J Clin Invest, 1997. **100**(11): p. 2680-90.
5. Davies, P.F., *Flow-mediated endothelial mechanotransduction.* Physiol Rev, 1995. **75**(3): p. 519-60.
6. Ross, R., *Atherosclerosis--an inflammatory disease.* N Engl J Med, 1999. **340**(2): p. 115-26.
7. Ross, R., *The pathogenesis of atherosclerosis--an update.* N Engl J Med, 1986. **314**(8): p. 488-500.
8. Glagov, S., et al., *Compensatory enlargement of human atherosclerotic coronary arteries.* N Engl J Med, 1987. **316**(22): p. 1371-5.
9. Enos, W.F., R.H. Holmes, and J. Beyer, *Landmark article, July 18, 1953: Coronary disease among United States soldiers killed in action in Korea. Preliminary report. By William F. Enos, Robert H. Holmes and James Beyer.* JAMA, 1986. **256**(20): p. 2859-62.
10. Spain, D.M., *Atherosclerosis.* Sci Am, 1966. **215**(2): p. 48-56.
11. Papadaki, M. and S.G. Eskin, *Effects of fluid shear stress on gene regulation of vascular cells.* Biotechnol Prog, 1997. **13**(3): p. 209-21.
12. Fung, Y., *Biomechanics: circulation*. 2nd ed. 1996, New York: Springer-Verlag.
13. Frangos, S.G., V. Gahtan, and B. Sumpio, *Localization of atherosclerosis: role of hemodynamics.* Arch Surg, 1999. **134**(10): p. 1142-9.
14. Glagov, S., et al., *Micro-architecture and composition of artery walls: relationship to location, diameter and the distribution of mechanical stress.* J Hypertens Suppl, 1992. **10**(6): p. S101-4.
15. Barbee, K.A., P.F. Davies, and R. Lal, *Shear stress-induced reorganization of the surface topography of living endothelial cells imaged by atomic force microscopy.* Circ Res, 1994. **74**(1): p. 163-71.
16. Helmlinger, G., et al., *Effects of pulsatile flow on cultured vascular endothelial cell morphology.* J Biomech Eng, 1991. **113**(2): p. 123-31.
17. Levesque, M.J. and R.M. Nerem, *The elongation and orientation of cultured endothelial cells in response to shear stress.* J Biomech Eng, 1985. **107**(4): p. 341-7.
18. Chen, K.D., et al., *Mechanotransduction in response to shear stress. Roles of receptor tyrosine kinases, integrins, and Shc.* J Biol Chem, 1999. **274**(26): p. 18393-400.

19. Ohno, M., et al., *Fluid shear stress induces endothelial transforming growth factor beta-1 transcription and production. Modulation by potassium channel blockade.* J Clin Invest, 1995. **95**(3): p. 1363-9.
20. Okamoto, T., et al., *Caveolins, a family of scaffolding proteins for organizing "preassembled signaling complexes" at the plasma membrane.* J Biol Chem, 1998. **273**(10): p. 5419-22.
21. Park, H., et al., *Caveolin-1 regulates shear stress-dependent activation of extracellular signal-regulated kinase.* Am J Physiol Heart Circ Physiol, 2000. **278**(4): p. H1285-93.
22. Shyy, J.Y. and S. Chien, *Role of integrins in endothelial mechanosensing of shear stress.* Circ Res, 2002. **91**(9): p. 769-75.
23. Tzima, E., et al., *A mechanosensory complex that mediates the endothelial cell response to fluid shear stress.* Nature, 2005. **437**(7057): p. 426-31.
24. Cai, H. and D.G. Harrison, *Endothelial dysfunction in cardiovascular diseases: the role of oxidant stress.* Circ Res, 2000. **87**(10): p. 840-4.
25. Rueckschloss, U., N. Duerrschmidt, and H. Morawietz, *NADPH oxidase in endothelial cells: impact on atherosclerosis.* Antioxid Redox Signal, 2003. **5**(2): p. 171-80.
26. Li, J.M. and A.M. Shah, *Endothelial cell superoxide generation: regulation and relevance for cardiovascular pathophysiology.* Am J Physiol Regul Integr Comp Physiol, 2004. **287**(5): p. R1014-30.
27. Berry, C.E. and J.M. Hare, *Xanthine oxidoreductase and cardiovascular disease: molecular mechanisms and pathophysiological implications.* J Physiol, 2004. **555**(Pt 3): p. 589-606.
28. McNally, J.S., et al., *Role of xanthine oxidoreductase and NAD(P)H oxidase in endothelial superoxide production in response to oscillatory shear stress.* Am J Physiol Heart Circ Physiol, 2003. **285**(6): p. H2290-7.
29. Landmesser, U., et al., *Oxidation of tetrahydrobiopterin leads to uncoupling of endothelial cell nitric oxide synthase in hypertension.* J Clin Invest, 2003. **111**(8): p. 1201-9.
30. Kuzkaya, N., et al., *Interactions of peroxynitrite, tetrahydrobiopterin, ascorbic acid, and thiols: implications for uncoupling endothelial nitric-oxide synthase.* J Biol Chem, 2003. **278**(25): p. 22546-54.
31. Mochizuki, S., et al., *Exogenous NO suppresses flow-induced endothelium-derived NO production because of depletion of tetrahydrobiopterin.* Am J Physiol Heart Circ Physiol, 2005. **288**(2): p. H553-8.
32. Schmidt, T.S. and N.J. Alp, *Mechanisms for the role of tetrahydrobiopterin in endothelial function and vascular disease.* Clin Sci (Lond), 2007. **113**(2): p. 47-63.
33. Rossi, F. and M. Zatti, *Biochemical aspects of phagocytosis in polymorphonuclear leucocytes. NADH and NADPH oxidation by the granules of resting and phagocytizing cells.* Experientia, 1964. **20**(1): p. 21-3.
34. Babior, B.M., *The leukocyte NADPH oxidase.* Isr Med Assoc J, 2002. **4**(11): p. 1023-4.
35. Landmesser, U., et al., *Role of p47(phox) in vascular oxidative stress and hypertension caused by angiotensin II.* Hypertension, 2002. **40**(4): p. 511-5.

36. Bedard, K. and K.H. Krause, *The NOX family of ROS-generating NADPH oxidases: physiology and pathophysiology.* Physiol Rev, 2007. **87**(1): p. 245-313.
37. Clark, R.A., et al., *Genetic variants of chronic granulomatous disease: prevalence of deficiencies of two cytosolic components of the NADPH oxidase system.* N Engl J Med, 1989. **321**(10): p. 647-52.
38. Barry-Lane, P.A., et al., *p47phox is required for atherosclerotic lesion progression in ApoE(-/-) mice.* J Clin Invest, 2001. **108**(10): p. 1513-22.
39. Hsich, E., et al., *Vascular effects following homozygous disruption of p47(phox) : An essential component of NADPH oxidase.* Circulation, 2000. **101**(11): p. 1234-6.
40. Vendrov, A.E., et al., *Atherosclerosis is attenuated by limiting superoxide generation in both macrophages and vessel wall cells.* Arterioscler Thromb Vasc Biol, 2007. **27**(12): p. 2714-21.
41. De Keulenaer, G.W., et al., *Oscillatory and steady laminar shear stress differentially affect human endothelial redox state: role of a superoxide-producing NADH oxidase.* Circ Res, 1998. **82**(10): p. 1094-101.
42. Hwang, J., et al., *Pulsatile versus oscillatory shear stress regulates NADPH oxidase subunit expression: implication for native LDL oxidation.* Circ Res, 2003. **93**(12): p. 1225-32.
43. Chen, X.L., et al., *Laminar flow induction of antioxidant response element-mediated genes in endothelial cells. A novel anti-inflammatory mechanism.* J Biol Chem, 2003. **278**(2): p. 703-11.
44. Hosoya, T., et al., *Differential responses of the Nrf2-Keap1 system to laminar and oscillatory shear stresses in endothelial cells.* J Biol Chem, 2005. **280**(29): p. 27244-50.
45. Ungvari, Z., M.S. Wolin, and A. Csiszar, *Mechanosensitive production of reactive oxygen species in endothelial and smooth muscle cells: role in microvascular remodeling?* Antioxid Redox Signal, 2006. **8**(7-8): p. 1121-9.
46. Silacci, P., et al., *Flow pulsatility is a critical determinant of oxidative stress in endothelial cells.* Hypertension, 2001. **38**(5): p. 1162-6.
47. Sorescu, G.P., et al., *Bone morphogenic protein 4 produced in endothelial cells by oscillatory shear stress induces monocyte adhesion by stimulating reactive oxygen species production from a nox1-based NADPH oxidase.* Circ Res, 2004. **95**(8): p. 773-9.
48. Castier, Y., et al., *p47phox-dependent NADPH oxidase regulates flow-induced vascular remodeling.* Circ Res, 2005. **97**(6): p. 533-40.
49. Frangos, J.A., et al., *Flow effects on prostacyclin production by cultured human endothelial cells.* Science, 1985. **227**(4693): p. 1477-9.
50. Dewey, C.F., Jr., et al., *The dynamic response of vascular endothelial cells to fluid shear stress.* J Biomech Eng, 1981. **103**(3): p. 177-85.
51. Go, Y.M., et al., *In vitro system to study role of blood flow on nitric oxide production and cell signaling in endothelial cells.* Methods Enzymol, 1999. **301**: p. 513-22.
52. Boo, Y.C., et al., *Shear stress stimulates phosphorylation of endothelial nitric-oxide synthase at Ser1179 by Akt-independent mechanisms: role of protein kinase A.* J Biol Chem, 2002. **277**(5): p. 3388-96.

53. Hwang, J., et al., *Oscillatory shear stress stimulates endothelial production of O2- from p47phox-dependent NAD(P)H oxidases, leading to monocyte adhesion.* J Biol Chem, 2003. **278**(47): p. 47291-8.
54. Sorescu, G.P., et al., *Bone morphogenic protein 4 produced in endothelial cells by oscillatory shear stress stimulates an inflammatory response.* J Biol Chem, 2003. **278**(33): p. 31128-35.
55. Hansson, G.K., *Advanced Information: Gene Modification in Mice*. 2007, The Nobel Assembly at Karolinska Institute.
56. Jackson, S.H., J.I. Gallin, and S.M. Holland, *The p47phox mouse knock-out model of chronic granulomatous disease.* J Exp Med, 1995. **182**(3): p. 751-8.
57. *Entrez Gene: Ncf1 netrophil cytosolic factor 1 (Mus musculus).* 2008 [cited 2008 April 11]; Available from: http://www.ncbi.nlm.nih.gov/sites/entrez?db=gene&cmd=Retrieve&dopt=full_report&list_uids=17969.
58. Daugherty, A., *Mouse models of atherosclerosis.* Am J Med Sci, 2002. **323**(1): p. 3-10.
59. Lake-Bruse, K.D. and C.D. Sigmund, *Transgenic and knockout mice to study the renin-angiotensin system and other interacting vasoactive pathways.* Curr Hypertens Rep, 2000. **2**(2): p. 211-6.
60. Huang, H., J. McIntosh, and D.G. Hoyt, *An efficient, nonenzymatic method for isolation and culture of murine aortic endothelial cells and their response to inflammatory stimuli.* In Vitro Cell Dev Biol Anim, 2003. **39**(1-2): p. 43-50.
61. Kevil, C.G. and D.C. Bullard, *In vitro culture and characterization of gene targeted mouse endothelium.* Acta Physiol Scand, 2001. **173**(1): p. 151-7.
62. Kevil, C.G., et al., *Intercellular adhesion molecule-1 (ICAM-1) regulates endothelial cell motility through a nitric oxide-dependent pathway.* J Biol Chem, 2004. **279**(18): p. 19230-8.
63. Kevil, C.G., R.P. Patel, and D.C. Bullard, *Essential role of ICAM-1 in mediating monocyte adhesion to aortic endothelial cells.* Am J Physiol Cell Physiol, 2001. **281**(5): p. C1442-7.
64. Kevil, C.G., et al., *Regulation of endothelial glutathione by ICAM-1: implications for inflammation.* FASEB J, 2004. **18**(11): p. 1321-3.
65. Kobayashi, M., et al., *A simple method of isolating mouse aortic endothelial cells.* J Atheroscler Thromb, 2005. **12**(3): p. 138-42.
66. Lincoln, D.W., 2nd, et al., *Isolation of murine aortic endothelial cells in culture and the effects of sex steroids on their growth.* In Vitro Cell Dev Biol Anim, 2003. **39**(3-4): p. 140-5.
67. Magid, R., et al., *Optimization of isolation and functional characterization of primary murine aortic endothelial cells.* Endothelium, 2003. **10**(2): p. 103-9.
68. Balconi, G., R. Spagnuolo, and E. Dejana, *Development of endothelial cell lines from embryonic stem cells: A tool for studying genetically manipulated endothelial cells in vitro.* Arterioscler Thromb Vasc Biol, 2000. **20**(6): p. 1443-51.
69. Hansen-Smith, F.M., et al., *Griffonia simplicifolia I: fluorescent tracer for microcirculatory vessels in nonperfused thin muscles and sectioned muscle.* Microvasc Res, 1988. **36**(3): p. 199-215.

70. BTI. *BTI Lipoproteins/Proteins*. 2008 [cited 2008 April 29, 2008]; Available from: http://www.btiinc.com/page/cata4.html#DIL.
71. Minami, T. and W.C. Aird, *Endothelial cell gene regulation.* Trends Cardiovasc Med, 2005. **15**(5): p. 174-84.
72. Rajotte, D., et al., *Molecular heterogeneity of the vascular endothelium revealed by in vivo phage display.* J Clin Invest, 1998. **102**(2): p. 430-7.
73. Spanel-Borowski, K., A.M. Ricken, and W.F. Patton, *Cytokeratin-positive and cytokeratin-negative cultured endothelial cells from bovine aorta and vena cava.* Differentiation, 1994. **57**(3): p. 225-34.
74. DeLeve, L.D., et al., *Rat liver sinusoidal endothelial cell phenotype is maintained by paracrine and autocrine regulation.* Am J Physiol Gastrointest Liver Physiol, 2004. **287**(4): p. G757-63.
75. Weinberg, N., et al., *Lineage tracing evidence for in vitro dedifferentiation but rare proliferation of mouse pancreatic beta-cells.* Diabetes, 2007. **56**(5): p. 1299-304.
76. Giddens, D.P., C.K. Zarins, and S. Glagov, *The role of fluid mechanics in the localization and detection of atherosclerosis.* J Biomech Eng, 1993. **115**(4B): p. 588-94.
77. Brooks, A.R., P.I. Lelkes, and G.M. Rubanyi, *Gene expression profiling of human aortic endothelial cells exposed to disturbed flow and steady laminar flow.* Physiol Genomics, 2002. **9**(1): p. 27-41.
78. Chen, B.P., et al., *DNA microarray analysis of gene expression in endothelial cells in response to 24-h shear stress.* Physiol Genomics, 2001. **7**(1): p. 55-63.
79. Dai, G., et al., *Distinct endothelial phenotypes evoked by arterial waveforms derived from atherosclerosis-susceptible and -resistant regions of human vasculature.* Proc Natl Acad Sci U S A, 2004. **101**(41): p. 14871-6.
80. Garcia-Cardena, G., et al., *Biomechanical activation of vascular endothelium as a determinant of its functional phenotype.* Proc Natl Acad Sci U S A, 2001. **98**(8): p. 4478-85.
81. McCormick, S.M., et al., *DNA microarray reveals changes in gene expression of shear stressed human umbilical vein endothelial cells.* Proc Natl Acad Sci U S A, 2001. **98**(16): p. 8955-60.
82. Ohura, N., et al., *Global analysis of shear stress-responsive genes in vascular endothelial cells.* J Atheroscler Thromb, 2003. **10**(5): p. 304-13.
83. Parmar, K.M., et al., *Integration of flow-dependent endothelial phenotypes by Kruppel-like factor 2.* J Clin Invest, 2006. **116**(1): p. 49-58.
84. Passerini, A.G., et al., *Coexisting proinflammatory and antioxidative endothelial transcription profiles in a disturbed flow region of the adult porcine aorta.* Proc Natl Acad Sci U S A, 2004. **101**(8): p. 2482-7.
85. Warabi, E., et al., *Effect on endothelial cell gene expression of shear stress, oxygen concentration, and low-density lipoprotein as studied by a novel flow cell culture system.* Free Radic Biol Med, 2004. **37**(5): p. 682-94.
86. Lum, H. and K.A. Roebuck, *Oxidant stress and endothelial cell dysfunction.* Am J Physiol Cell Physiol, 2001. **280**(4): p. C719-41.

87. Jo, H., H. Song, and A. Mowbray, *Role of NADPH oxidases in disturbed flow- and BMP4- induced inflammation and atherosclerosis.* Antioxid Redox Signal, 2006. **8**(9-10): p. 1609-19.
88. Griendling, K.K., D. Sorescu, and M. Ushio-Fukai, *NAD(P)H oxidase: role in cardiovascular biology and disease.* Circ Res, 2000. **86**(5): p. 494-501.
89. Lassegue, B. and R.E. Clempus, *Vascular NAD(P)H oxidases: specific features, expression, and regulation.* Am J Physiol Regul Integr Comp Physiol, 2003. **285**(2): p. R277-97.
90. Takeya, R., et al., *Novel human homologues of p47phox and p67phox participate in activation of superoxide-producing NADPH oxidases.* J Biol Chem, 2003. **278**(27): p. 25234-46.
91. Go, Y.M., et al., *Evidence for peroxynitrite as a signaling molecule in flow-dependent activation of c-Jun NH(2)-terminal kinase.* Am J Physiol, 1999. **277**(4 Pt 2): p. H1647-53.
92. Stocker, R. and J.F. Keaney, Jr., *Role of oxidative modifications in atherosclerosis.* Physiol Rev, 2004. **84**(4): p. 1381-478.
93. Ando, J., et al., *Differential display and cloning of shear stress-responsive messenger RNAs in human endothelial cells.* Biochem Biophys Res Commun, 1996. **225**(2): p. 347-51.
94. Rodriguez, C., et al., *Low density lipoproteins downregulate lysyl oxidase in vascular endothelial cells and the arterial wall.* Arterioscler Thromb Vasc Biol, 2002. **22**(9): p. 1409-14.
95. Siegel, D., J. Ryder, and D. Ross, *NAD(P)H: quinone oxidoreductase 1 expression in human bone marrow endothelial cells.* Toxicol Lett, 2001. **125**(1-3): p. 93-8.
96. Aurrand-Lions, M., et al., *Junctional adhesion molecules and interendothelial junctions.* Cells Tissues Organs, 2002. **172**(3): p. 152-60.
97. Johnson-Leger, C.A., et al., *Junctional adhesion molecule-2 (JAM-2) promotes lymphocyte transendothelial migration.* Blood, 2002. **100**(7): p. 2479-86.
98. Chang, K., et al., *Bone morphogenic protein antagonists are coexpressed with bone morphogenic protein 4 in endothelial cells exposed to unstable flow in vitro in mouse aortas and in human coronary arteries: role of bone morphogenic protein antagonists in inflammation and atherosclerosis.* Circulation, 2007. **116**(11): p. 1258-66.
99. Chen, W., M. Bacanamwo, and D.G. Harrison, *Activation of p300 histone acetyl-transferase activity is an early endothelial response to laminar shear stress and is essential for stimulation of eNOS mRNA transcription.* J Biol Chem, 2008.

VITA

Michelle Christine Sykes

Michelle Christine Sykes was born on March 15, 1978 in Jacksonville, Florida. She lived there and attended Stanton College Preparatory School, graduating as valedictorian in 1996. She then moved to Atlanta, Georgia and attended the Georgia Institute of Technology to study aerospace engineering. During this time, she gained research experience under the mentorship of Dr. P.K. Yeung. She graduated with highest honors in 2000. That same year, she began her graduate studies in bioengineering under the mentorship of Dr. Hanjoong Jo. With his support, she was accepted by and matriculated at the Medical College of Georgia in 2002 in order to pursue a joint M.D./Ph.D. degree. After completion of two years of medical school, Michelle returned to the Georgia Institute of Technology under Dr. Hanjoong Jo in order to continue her studies and research in bioengineering. She is anticipating graduation and will return to the Medical College of Georgia in order to complete her medical degree by 2010, after which she plans to enter a residency for further clinical training.